Ca^{2+} Activated Cl^- Channel ANO6 and Voltage Gated Proton Channel H_v1 in Dendritic Cell Functions

Dissertation

der Mathematisch-Naturwissenschaftlichen Fakultät

der Eberhard Karls Universität Tübingen

zur Erlangung des Grades eines

Doktors der Naturwissenschaften

(Dr. rer. nat.)

vorgelegt von

Kalina Szteyn

aus Olsztyn / Polen

Tübingen

2012

Tag der mündlichen Qualifikation:	05.09.2012
Dekan:	Prof. Dr. Wolfgang Rosenstiel
1. Berichterstatter:	Prof. Dr. Michael Duszenko
2. Berichterstatter:	Prof. Dr. Med. Florian Lang

The present study was performed in the Institute of Physiology I, Eberhard Karls University Tübingen under the supervision of Prof. Dr. Med. Florian Lang and Prof. Dr. Michael Duszenko from the Institute of Biochemistry.

I would like to thank Prof. Dr. Med. Florian Lang for scientific and financial support of the Physiology Institute and for giving me a chance for an intellectual growth and learning new techniques that will be the foundation of my future scientific career.

I thank Prof. Dr. Michael Duszenko for warm welcome to the Department of Biochemistry, for supervision, advice and help with the project.

Special thanks go to Dr. Ekaterina Shumilina whose friendship and mentoring made this project a very special experience. Her optimism and support helped me through all the ups and downs of this research project and her very Zen out look on life was an amazing stimulus for personal and scientific growth.

I thank the whole ‘Cell Physiology of Dendritic and Mast Cell’ research group. It was a pleasure to work with all of you ,specially my dear friends Evi Shmid, Wenting Yang and Meerim Nurbaeva, who provided friendly and cheerful work environment. In addition I would like to thank Prof. Dr. Stephan Huber for sharing his Patch Clamp expertise.

With all of my heart I thank my parents, without their unconditional love and support non of this would be possible.

TABLE OF CONTENT

ABBREVIATIONS 6
LIST OF TABLES 8
LIST OF FIGURES 8
ABSTRACT 10
ABSTRACT (German) 11
I. INTRODUCTION 13
I.I Dendritic cells 13
I.II Ca^{2+} dependent DC functions 14
Activation and maturation of DCs 14
Migration of DCs 17
Immunological synapse 21
I.III Ca^{2+} homeostasis in DCs 22
Ca^{2+} release mechanisms 23
Ca^{2+} entry mechanisms 23
Transient receptor potential channels 24
Purinergic receptors 24
Ion channels regulating Ca^{2+} entry 25
Ca^{2+} signal termination 26
I.III Calcium activated chloride channels (CaCCs) 26
CLCA 27
Tweety 27
Bestrophins 27
Anoctamins 28
I.IV Antigen uptake, processing and presentation in DCs 30
I.V H_v1 proton channel 32
II. MATERIALS AND METHODS 35
II.I Materials 35
II.I.I Equipment 35
II.I.II Chemicals and Reagents 37
II.I.III Solutions 39
II.I.IV Animals 41
II.II Methods 42
II.II.I Cell Culture 42

II.II.II Intracellular Calcium Imaging 42
II.II.III Whole-cell patch clamp 44
II.II.III.I Calcium Activated Chloride Channels 44
II.II.III.II Proton Channels 45
II.II.III.III NADPH oxidase electron currents 45
II.II.IV Migration Assay 46
II.II.V Cytokine Production 46
II.II.VI ROS Production 46
II.II.VII Western Blot 47
II.II.VIII RT-PCR 47
II.II.IX ANO6 silencing 48
II.II.X Statistic 49
III. RESULTS 50
III.I Calcium activated chloride channels in dendritic cells 50
III.I.I Ca^{2+}-activated Cl^- channel (CaCC) currents in mouse DCs 50
III.I.II Store-operated Ca^{2+} entry is suppressed by Cl^- channel inhibitors in DCs 53
III.I.III Migration of DCs is highly dependent on CaCC activity 56
III.I.IV CaCCs control cytokine secretion of DCs 57
III.I.V Expression of mRNA of Anoctamin family of proteins in dendritic cells 57
III.I.VI Knock-down of ANO6 reveals that it accounts for CaCC conductances in DCs 58
III.I.VII Migration of DCs is dependent on ANO6 activity 59
III.II Proton channels 60
III.II.I Proton currents in DCs 60
III.II.II Lipopolisaccharide regulation of proton currents in DCs 63
III.II.III Lipopolisaccharide regulation of NOX2 electron currents in DCs 65
IV. DISCUSSION 67
IV.I Calcium activated chloride channels 67
IV.II Proton channels in dendritic cells 71
REFERENCES 75
Curriculum Vitae 81
Publications: 83
Declaration 84
Contributions 84

ABBREVIATIONS

$[Ca^{2+}]_i$ - intracellular Ca^{2+} concentration

2APB - 2-aminoethoxydiphenylborate

5-TH - 5-hydroxytryptamine,serotonin

ADPR – ADP-ribose

AE2 - Cl^-/HCO_3^- exchanger

APC – antigen presenting cells

cADPR – cyclic ADP-ribose

CRAC - Ca^{2+} release activated Ca^{2+} channels

DAG - diacylglycerol

DCs – dendritic cells

DPC - diphenylamine-2-carboxylate

FRT – Fisher Rat Thyroid

H_2O_2 – hydrogen peroxide

HSC - hematopoietic stem cells

Ii – invariant chains

IL- interleukin

IP_3 - inositol 1,4,5 triphosphate

IP_3R - inositol 1,4,5 triphosphate receptor

LPS – lipopolosaccharide

MDPs - macrophage/DCs progenitors

mGluR - matabotropic glutamate receptor

MHC - major histocompatibility complex

NAADP - nicotinic acid adenine dinucleotide phasphate

NFA – niflumic acid

NFAT - nuclear factor of activated T cells

NHE – Na^+/H^+ exchanger

ORCC – outward rectifying Cl^- currents

P2R – purinergic receptors

PGN – peptidoglycan

PIP_2 - phosphatidylinositol-(4,5)- bisphosphate

PLC – phospholipase C

RyR – ryanodine receptor

SOCE – store operated Ca^{2+} entry

TLR – toll like receptor

TRP- transient receptor potential channels

TRPM2 - transient receptor potential melastatin 2 channels

TRPV1 - transient receptor potential channels vanilloid 1

VGLUT – glutamate-specific vesicular glutamate transporter

LIST OF TABLES

Materials and Methods

Table 1: RT-PCR Primers sequences..... 48

LIST OF FIGURES

Introduction

Fig. 1: Ca^{2+}signaling inducing maturation of dendritic cells (DCs). 17
Fig. 2: Transport processes contributing to the polar differentiation of a migrating DC. 20
Fig. 3: The main molecules and transporters thought to participate in charge compensation and pH regulation during the respiratory burst. 33

Material and Methods

Fig. 4: Molecular structure of Fura-2 and graphic representation of Fura-2-Ca^{2+}complex..... 43
Fig. 5: Fluorescence excitation spectra of Fura-2 in solutions containing 0-39.8µM of free Ca^{2+} 43

Results

Fig. 6: Cl^- currents are activated by IP_3 in DCs. 51
Fig. 7: Cl^- currents are activated by ionomycin-induced Ca^{2+} increase in DCs. 52
Fig. 8: Cl^- currents are activated by CCL21 in DCs. 54
Fig. 9: Inhibition of Ca^{2+}-activated Cl^- channels attenuates the store-operated Ca^{2+} entry in DCs. 55
Fig. 10: Dendritic cells migration was strongly inhibited by treatment with CaCC channels blockers. 56
Fig. 11: Production of cytokines showes sensitivity to Cl^- channels blockers 57
Fig. 12: Expression of Anoctamins in mouse DCs. 58
Fig. 13 : Knockdown of ANO6 inhibits CaCC currents in DCs. 58
Fig. 14: Chemokine-induced DC migration is inhibited by knock-down of ANO6..... 59
Fig. 15: Proton currents in DCs. 60
Fig 16: Analysis of G/V relationship and τ of activation of proton currents in DCs. ... 61
Fig 17: Analysis of Hv1 channel tail currents. 62
Fig. 18: LPS matured DCs show proton currents inhibition and decreased ROS production. 64

Fig. 19: Acute LPS treatment stimulated enhanced Hv1 gating and NOX2 electron currents. 65

Discussion

Fig. 20: Graphic representation of possible mechanisms by which activity of ANO6 regulate migration of DCs. 70
Fig. 21: Acute and long term LPS regulation of Hv1 and NOX2 in DCs. 74

ABSTRACT

Dendritic cells (DCs) belong to the family of antigen presenting cells, located at the center of immunological responses, which decide on induction of tolerance or specific immunity. A whole variety of DC functions, for example their activation, migration and maturation, is regulated by Ca^{2+} signaling. Intracellular Ca^{2+} levels are tightly regulated through various mechanisms, which include diverse ion channels that control membrane potential sustaining or decreasing the driving force for Ca^{2+}. The first aim of the present investigation was to determine whether DCs express functional Ca^{2+} activated Cl^- channels, their molecular identity and a possible role in DC functions. In whole cell patch clamp experiments on mouse bone marrow-derived DCs, increase in intracellular Ca^{2+} levels induced by intracellular IP_3, extracellular ionomycin in the presence of Ca^{2+} or by ligation of the chemokine receptor CCR7 resulted in the activation of the outwardly rectifying Cl^- channels (CaCCs). Anoctamine 6 (ANO6) was identified as the molecule responsible for the formation of CaCCs in DCs, as demonstrated by the whole cell patch clamp experiments in DCs upon ANO6 knock down by siRNA. Furthermore, when ANO6 was silenced, DC migration efficiency significantly decreased suggesting that the activity of ANO6 plays a major role in the regulation of DC migration.

Another crucial function of DCs is their ability to uptake and process antigens during phagocytosis. The NADPH oxidase NOX2 regulated phagocytosis is a major mechanism that accounts for the highly controlled protein degradation in phagolysosomes. Continuous activity of NOX2 requires pH and charge compensation, both of which are provided in other cell types by the work H_v1 proton channel. In the present study on mouse bone marrow-derived DCs functional expression of Hv1 channel was demonstrated. LPS was shown to regulate H_v1 in a bimodal way, with acute, PKC dependent induction of the enhanced gating mode of the channel, followed by a strong inhibition of Hv1 currents in LPS (24 h) matured cells. Those H_v1 responses were paralleled with correspondent changes in NOX2 activity: acute NOX2 stimulation by LPS as measured by LPS induced electron currents and impaired NOX2 activity in LPS (24 h) matured DCs, as assessed by a decreased ROS production. Therefore, Hv1 functions as a regulator of NOX2 dependent phagocytosis in DCs.

ABSTRACT

Dendritische Zellen (DCs) gehören zu den Antigen-präsentierenden Zellen und stehen im Zentrum der Immunantwort. Sie entscheiden zwischen der Induktion von Immun-Toleranz oder der Ausprägung spezifischer Immunität. Eine Reihe unterschiedlicher Funktionen von DCs, wie ihre Aktivierung, Migration und Reifung wird durch Ca^{2+}-Signale reguliert. Intrazelluläre Ca^{2+}-Level werden eng durch verschiedene Mechanismen kontrolliert, die die Aktivität verschiedener Ionenkanäle einschließt. Letztere determinieren das Membranpotenzial oder modulieren die elektrochemische Triebkraft für die Transmembran-Ca^{2+}-Flüsse.

Als erstes Ziel der vorliegenden Arbeit sollte geklärt werden, inwieweit DCs Ca^{2+}-aktivierte Cl^--Kanäle funktionell exprimieren. Bei einer vorliegenden Expression dieser Kanäle sollte die molekulare Identität und mögliche Funktion dieser Kanäle definiert werden.

In Ganzzell Patch Clamp-Experimenten an DCs, die aus Mausknochenmark gewonnen wurden (mBMD-DCs), ließen sich durch Erhöhung der zytoplasmatischen freien Ca^{2+}-Konzentration mittels intrazelluläres IP_3, Ca^{2+}-Permeabilisierung der Plasmamembran durch Ionomycin oder Ligation des Chemokin-Rezeptors CCR7 auswärts gleichrichtende Cl^--Kanäle (CaCCs) aktivieren.

Anoctamine 6 (ANO6) konnte als dasjenige Molekül identifiziert werden, das die CaCCs in DCs bildet. Dies wurde durch Ganzzell Patch Clamp-Ableitungen nach ANO6-Knock down in siRNA-Experimenten nachgewiesen. Silencing von ANO6 verminderte zudem die DC-Migrationseffizienz signifikant, was darauf hindeutet, dass die Aktivität von ANO6 eine wichtige Rolle bei der Regulation der DC-Migration spielt.

Die Fähigkeit der Aufnahme und Prozessierung von Antigenen während der Phagozytose stellt eine weitere, wesentliche Funktion von DCs dar. Die Phagozytose, die durch die NADPH-Oxidase NOX2 reguliert wird, ist wiederum ein entscheidender initialer Prozess für die spätere hoch-kontrollierte Protein-Degradation im Phagolysosom. Die fortlaufende Aktivität der NOX2 kann nur bei ständiger pH und Ladungskompensation stattfinden. Für beide Prozesse wurden in andern Zelltypen Hv1 Protonen-Kanäle verantwortlich gemacht. Die vorliegende Arbeit konnte in mBMD-DCs die funktionelle Expression von H_v1-Kanälen nachweisen. Es zeigte sich, dass Lipopolysaccharid (LPS) H_v1-Kanäle in

einer bimodalen Weise reguliert: einem, nach akuter LPS-Stimulation erhöhten Gating des Kanals, das Protein Kinase C (PKC)-abhängig war, folgte eine starke Inhibition der H_v1-Ströme in LPS (24 h)-gereiften DCs. Diese Hv1-Antworten wurden begleitet von entsprechenden Änderungen der NOX2-Aktivität: LPS induzierte akut eine NOX2-Stimulation, die als LPS-induzierter Elektronen-Strom nachweisbar war. In LPS (24 h)-gereiften DCs dagegen war die NOX2-Aktivität abgeschwächt, wie eine verminderte ROS-Produktion zeigte. Draus lässt sich schließen, dass H_v1 in DCs die NOX2-abhängige Phagozytose als initialen Schritt der Antigen-Prozessierung reguliert.

I. INTRODUCTION

I.I Dendritic cells

Dendritic cells (DCs), for which discovery Ralph Steinman was awarded 2011 Nobel Prize, were first identified in mouse lymphoid organs (125). DCs belong to the family of antigen presenting cells (APC), which also includes macrophages and B cells. DCs are highly specialized cells designed to capture, process and present antigens to naïve T cells in the T cell zones of lymphoid organs. The interaction of DCs with T cells can lead to tolerance or different types of immune responses.

DC development starts from hematopoietic stem cells (HSCs). The earliest self-renewing HSCs in the adult bone marrow give rise to series of precursors that farther progress into specialized cellular lineages. First defined precursors of DCs are HSC derived progenitors with myeloid restricted differentiation potential (39). Those progress, in bone marrow, into common myeloid progenitors, followed by granulocyte-macrophage precursors and macrophage/DC progenitors (MDPs) (39). Still in bone marrow, MDPs differentiate into monocytes and common DC precursors, which then can give, rise to plasmacytoid DCs or precursors of classical (conventional, myeloid) DCs that are found in bone marrow, blood and spleen (39). Monocytes, which are precursors for macrophages, can also function as DC precursors (120). The division of DCs into subtypes is based on their location and specialized function in immune system. When we take under consideration the localization of DCs, two groups of cells emerge: migratory and lymphoid-tissue-resident DCs (120). The migratory DCs patrol peripheral tissues and after identification of danger signals migrate to lymphatic organs via afferent lymphatic and high endothelial venules (39). Usually the migratory cells manifest mature phenotype on reaching destined lymphoid organ (120). DCs that reside in lymphoid organs capture and present antigens found in the lymphoid organ itself and demonstrate the immature phenotype till activation by antigen uptake. The resident DCs present the majority of DCs in thymus and spleen (120). In mouse lymphoid tissue DCs can be divided into $CD8^+$, that express high levels of CD8α on the cell surface, produce large amounts of interleukin (IL)-12 and polarize nave $CD4^+$ T cells towards Th1 phenotype (97). In contrast, $CD8^-$ population induces Th2 responses, also presents higher endocytic and phagocytic abilities, even though $CD8^+$ population is the one capable of internalization of apoptotic cells (6, 97). Another distinctive population of DCs

constitute of plasmacytoid DCs (pDCs), also known as the natural interferon producing cells. pDCs are located in all mouse lymphoid organs and are considered as the front-line of viral immunity on account of their potential to produce extremely high amounts of type I interferon (6, 133). In addition, $B220^{+}$ pDC are involved in the maintenance of T cell tolerance by stimulation of regulatory T cell differentiation, which then can block the activation of naïve T cells in the IL-10 dependent mechanism (6).

I.II Ca^{2+} dependent DC functions

Activation and maturation of DCs

The reprogramming of DCs from immature to mature phenotype starts with recognition of hazardous stimuli, including microbial products that can activate DCs via toll like receptors (TLR), NOD, RIG-I and Mda-5 receptors (124). Furthermore, lymphocytes and neutrophils can trigger DC maturation through activation of CD40 or lymphotoxin αβ receptors (124). Additionally, stimulation can be induced by endogenous ligands like uric acid, histamine and ATP. Also, cytokines including TNF, interferons and IL-10 and immune complexes acting via FcR have capability to instigate maturation in DCs (124). The most commonly used method for an activation of DCs is stimulation of TLRs. TLRs are pattern-recognition receptors that identify highly conserved motifs of microbial membrane components like lipids, lipoproteins and proteins (58). Additionally, TLR isoforms expressed exclusively in the intracellular vesicles such as ER, endosomes, lysosomes and endolysosomes are capable of identification of pathogenic nucleic acids (58). The conequence of DC exposure to peptidoglycan (PGN, Gram-positive bacterial cell wall component), which is a TLR2 ligand, or lipopolosaccharide (LPS, Gram-positive bacteria outer membrane element), a TLR4 ligand, is tyrosine phorphorylation of PLCγ2 (2). The switching on of PLC signaling leads to hydrolysis of phosphatidylinositol- (4,5)-bisphosphate (PIP_2) into inositol-1, 4,5-triphosphate (IP_3) and diacylglycerol (DAG). IP_3 binds to its receptors in ER, generating Ca^{2+} release from the stores, which causes activation of Ca^{2+} release, activated Ca^{2+} (CRAC) channels and additional Ca^{2+} influx from extracellular environment. Because Ca^{2+} entry would cause depolarization of the membrane, decreasing the driving force for Ca^{2+} influx, other ion

channels, like voltage-gated K^+ (K_v) channels in DCs are required to maintain Ca^{2+} flux. When DCs are treated with K_v channel blockers, LPS induced increase in intracellular Ca^{2+} concentration $[Ca^{2+}]_i$ was significantly decreased, showing that the polarization of the cell membrane by K_v activity is necessary for effective Ca^{2+} entry (82). Induction of Ca^{2+} signal downstream from TLR4 is CD14 dependent, as Ca^{2+} levels, in DCs derived from CD14 knockout mouse, show no reacton on the LPS stimulation (144). CD14 is a surface protein that controls endosomal signalling and is responsible for TLR4 endocytosis (144). CD14 was the first recognized pattern recognition receptor (PRR) that binds directly to LPS and chaperones those molecules to TLR4 signaling complex (144).

Human DCs show a different pattern of the Ca^{2+} signal behaviour. Immature human monocyte-derived DCs display large rhythmic oscillations of $[Ca^{2+}]$ and exposure to LPS does not change those oscillations and it does not cause the increase in $[Ca^{2+}]$ (136). Ca^{2+} responsible for oscillations originate from both, IP_3 induced release from the intracellular stores and influx of Ca^{2+} from extracellular environment. Those high frequency oscillations are characteristic for immature human DCs, since they are not observed in cells matured by ligation of the TLR (136). Additionally, low levels of CD14 expression in human DCs may be responsible for differences in LPS triggered responses between human and mouse DCs.

When DCs mature they loose their endocytic capabilities, however, they up regulate expression of quite a few ‘maturation’ markers: major histocompatibility complex II (MHC II), costimulatory molecules (CD80, CD86, CD40) and specific cytokines (IL-6, IL-10, IL-12, TNFα). All of those modifications show Ca^{2+} dependence, when we consider the fact that SKF-96365, a CRAC channels blocker, attenuates all previously mentioned phenotipical changes linked to the maturation of DCs (82, 141). Comparable maturation crippling effects have been observed with K_v channel blockers (82, 87, 141). Further evidence of Ca^{2+} involvement in upregulation of maturation markers, MHCII and CD86, has emerged from study of TRPV1 Ca^{2+}-permeable channels in DCs, TRPV1 activation with capsaicin promotes upregulation of formerly mentioned molecules (12). Synaptotagmin VII is a Ca^{2+} sensing molecule that regulates lysosomal exocytosis. During LPS-induced DC activation, synaptotagmin VII abundance is increased in the cell membrane, and DCs isolated

from synaptotagmin VII knockout mouse exhibit delayed translocation of MHCII (13). Further evidence regarding the role of Ca^{2+} in the maturation process has been brought by examining this process both *in vitro* and *in vivo* in TRPM2-deficient mice. In both cases, maturation has been heavily dependent on Ca^{2+} entry through TRPM2 channels, when determined by surface expression of maturation markers CD80, CD86 and MHC II (129).

Till date, not many Ca^{2+} sensing mechanisms have been identified in DCs. Ca^{2+} signal, associated with LPS stimulation, switches on the calcineurin-dependent NFAT (nuclear factor of activated T cells) nuclear translocation and stimulates transcription of genes coding cytokine, like IL-2 (144).

Quite opposite situation can be observed in human monocyte derived DCs. Their constant Ca^{2+} oscillations in immature state promote NFAT nuclear location, that puts this transcription factor in control over immature phenotype pool genes, whereas the termination of the Ca^{2+} oscillations, by LPS or 2-aminoethoxydiphenylborate (2-APB), endorses NFAT cytoplasmic location (136). Another well defined Ca^{2+} dependent signaling pathway involves the activation of NF-κB transcription factor, which controls plethora of genes responsible for DC maturation (72). Ca^{2+}/calmodulin kinase phosphorylates IκB molecule, which at phosphorylated state dissociates from NF-κB, allowing NF-κB transport to the nucleus (72) (Fig.1).

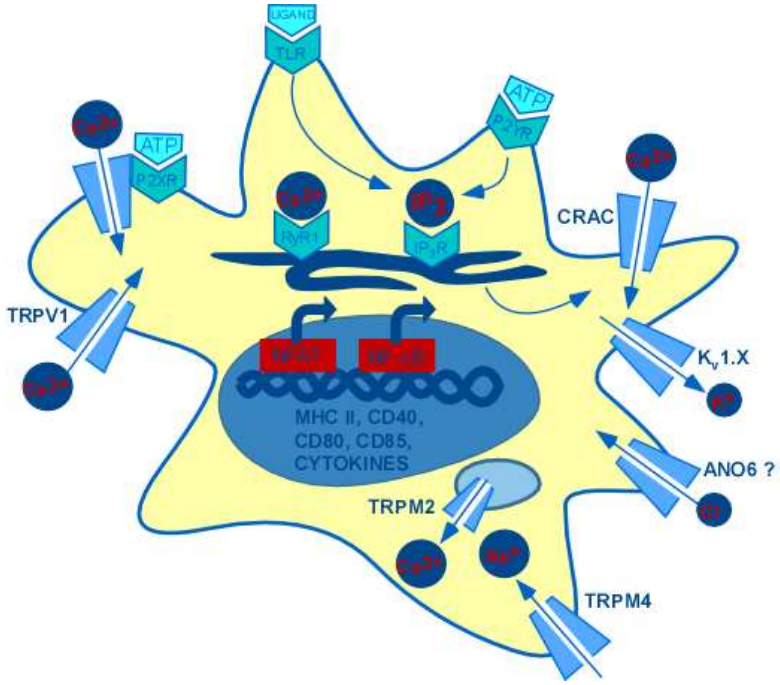

Fig. 1: Ca^{2+}signaling inducing maturation of dendritic cells (DCs).

Danger signals like ligands of Toll-like receptors (TLRs) stimulate in concert with modifying factors such as extracellular ATP the generation of Ca^{2+} signals via Ca^{2+} release from intracellular stores and subsequent capacitative Ca^{2+} entry through Ca^{2+} release-activated Ca^{2+} (CRAC) channels. CRAC-generated Ca^{2+}-entry depolarizes the membrane, resulting in inactivation of the inwardly-rectifying CRAC channels. The Ca^{2+} entry through CRAC channels is a function of cell membrane potential and is thus modified by hyperpolarizing voltage-gated Kv and depolarizing transient receptor potential (TRP) melastatin channels TRPM4, which are nonselective cation channels. In addition, in human DCs a rise in extracellular K^+ concentration by inflammatory necrotic cell death or by T cell K^+ channel activity at immunological synapses stimulates Ca^{2+} entry through voltage-gated L-type (Cav1.2) Ca^{2+} channels. Finally, high extracellular ATP concentrations induce Ca Ca^{2+} entry via ionotropic P2X purinoceptors. The Ca^{2+} signals, in turn, activate transcription factors such as nuclear factor of activated T cells (NFAT) or nuclear factor-κB (NF-κB). CaMKII, Ca^{2+}/calmodulin-dependent kinase II; IP3, inositol trisphosphate; IP3R, inositol-trisphosphate receptor; MHC II, major histocompatibility complex class II; P2YR, metabotropic purinoceptor; RyR, ryanodine receptor. [Adapted from (122)]

Migration of DCs

In complexity of DC life cycle migration entails: ability to exit bone marrow, recruitment to target tissues, the capacity to access lymph vessels to travel to draining lymph nodes or back to the blood (3). DCs travel towards chemotactic agents, like endogenous chemokines or exogenous microbial chemoattractants (eg. *N*-formylmethionyl-leucyl-phenylalanine, fMLP) (129). In DCs, G-protein coupled receptors play the role of chemotactic sensors. The initial response of a cell to chemoattractants is to polarize along its longitudinal axis and to extend protrusions, in case of DCs, lamellipodium, in direction of migration. Polarization of the cells means that the molecular processes differ between leading and rear end of the cell. There is an accumulation of NHE1 and Cl^-/HCO_3^- exchanger (AE2) in the leading edge of lamellipodium, where these transporters regulate internal and external pH

levels. That is particularly needed, because lack of mitochondria in the lamellipodium mobilizes lactic acid metabolism, causing rise in proton production (127). In DCs, we also observe LPS up regulated expression of NHE1 though the phosphoinositide 3-kinase (PI3K) signaling (106), which plays an important role in the microenviromental osmotic balance, as entry of Na^+ at the leading end and exit of KCl at the rear end, inducing local volume changes (127). Furthermore, slight alkalization of the lamellipodial environment promotes the reorganization of actin filaments and influences the rate of cell motion (127).

In DCs, binding of chemoatractants to the respective receptor, for instance chemokines CCL21 to CCR7 or CXCL12 to CXCR4, activates the classical PLC pathway, causing IP_3 sensitive release of Ca^{2+} from the stores, followed by Ca^{2+} entry through CRAC channels. When Ca^{2+} entry is blocked by inhibition of CRAC channels or when blocking Kv channels induces depolarization of the membrane, CCL21 promoted migration is significantly impaired (82, 141). CD38 is an ectoenzyme that generates cyclic ADP ribose (cADPR) and ADP ribose (ADPR) from NAD^+ and in acidic environment it can also generate $NAADPH^+$ (118). While IP_3 is the best characterized Ca^{2+} mobilizing metabolite, few additional second messangers have been identified: cADPR, ADPR and $NAADPH^+$ (118). cADPR can mobilize Ca^{2+} from the stores by ligation of RyR and ADPR controls cation entry through TRPM2 channels or other ADPR-gated channels (101). By using 8-bromo-ADPR, a substance that restricts ADPR dependent cation influx, it has been demonstrated that chemotaxis dependent on activation of CCR7 and CXCR4 rely on Ca^{2+} entry through TRPM2 or another ADPR-gated cation channel (101). Few years down the road and the role of TRPM2 in DC chemotaxis has been clarified. TRPM2 are expressed exclusively in the endolysosomal vesicles and TRPM2-deficient DCs show severely compromised chemokine dependent directional migration due to suppresion of TRPM2 dependent Ca^{2+} release and secondary modification in store operated Ca2+ entry (SOCE) (129). DCs deficient in both TRPM2 and IP_3 receptors loose the ability to perform chemotaxis entirely (129).

Next worth mentioning Ca^{2+} entry mechanism, which is switched on during migration, is the activation of TRPV1 channels. The accumulation of protons at the glycocalyx space of the lamellipodium surface causes TRPV1 activation, as these

channels are pH sensitive (127). Corresponding evidence from mouse deficient in TRPV1 has showed that administration of capsaicin, TRPV1 activator, triggered *in vivo* DC migration to the draining lymph nodes in wild type animals, but DCs in TRPV1 knockout mice stayed indifferent to that stimulation (12).

Yet another chemotactic signal, that DCs respond to, is nucleotides. Presence of increased concentration of ATP in the extracellular environment is a signal for immune system that there is tissue damage. DC responses evoked by ATP involve two different P2 receptors (P2R) (54). P2XR are ligand-gated ion channels permeable for Ca^{2+}, Na^{+} and K^{+} (54). On the other hand, P2YR interact, at the cytoplasmic side of the cell membrane, with G-proteins coupled to PLC, which activity mobilizes Ca^{2+} from the stores (54). Ligation of P2R was also connected to increased actin polymerization and the same, improved migration capacity of DCs (54). Moreover, $P2Y^{-/-}$ mice brought further evidence regarding P2YR role in DC migration. In $P2Y^{-/-}$ animals reduced allergic airway inflammation has been observed due to impaired migration of myeloid DCs (88).

Despite the fact that Ca^{2+} signal is essential for proper migration, Ca^{2+} overload has quite an opposite effect, which is why the termination of Ca^{2+} signal is as important as Ca^{2+} initiation. TRPM4 is a Ca^{2+}-activated non-selective cation channel, and when active floods the cell with Na^{+}. This influx of Na^{+} results in membrane depolarization that limits driving force for Ca^{2+} and activity of CRAC channels (9). The absence of TRPM4, causes Ca^{2+} overload, decreases the activity of PLC-β2, as demonstrated by lower Ca^{2+} release from the stores, and significant deficiency in DC migration (9).

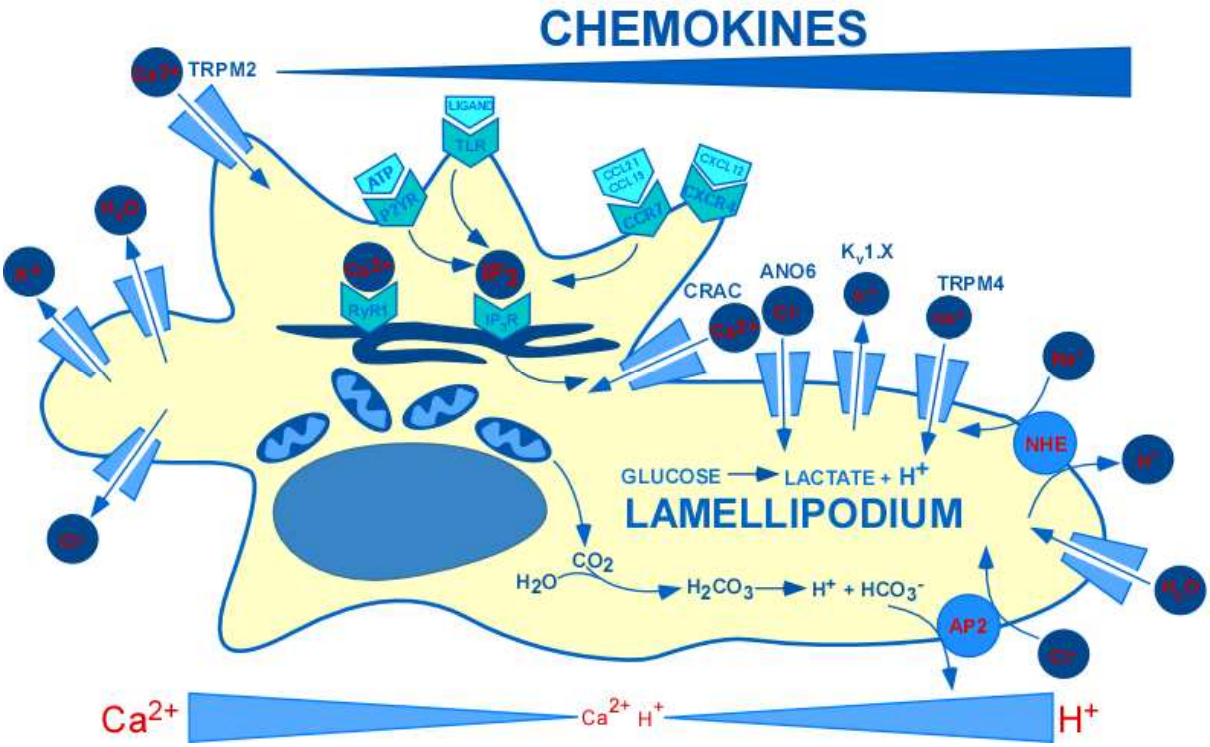

Fig. 2: Transport processes contributing to the polar differentiation of a migrating DC.

DCs polarize, forming a protruding lamellipodium and a retracting cell rear. Extracellular gradients of chemokines are detected by an unequal ligation of chemokine receptors (CXCR4 and CCR7) distributed around the DC. Ligation of CXCR4 or CCR7 induces IP3 -mediated Ca^{2+} release from the stores and subsequent Ca^{2+} entry through store-operated CRAC channels. CRAC-generated Ca^{2+} entry is enhanced by activation of voltage-gated $K_v1.x$ K^+ channels and suppressed by activation of Ca^{2+}-activated TRPM4 nonselective cation channels. The Ca^{2+} sensitivity of the latter provides a negative feedback loop preventing Ca^{2+} overload. In addition, ligation of CXCR4 and CCR7 induces Ca^{2+} entry and release via stimulation of the exoenzyme CD38 and the transformation of nicotinamide adenine dinucleotide (NAD^+) into cyclic adenosine diphosphate ribose (cyclicADPribose) and ADPribose. Local extracellular acidification is induced by Na^+/H^+ antiport at the lamillepodium. In DCs, LPS stimulates the Na^+ /H^+ antiport via phosphoinositide 3-kinase (PI3K). (Adapted from (122))

When *E.coli* supernatants have been introduced in proximity of DCs, with the use of micropipette, within few seconds Ca^{2+} flux and rapid cytoskeleton reorganization in lamellipodium have been observed (109). Further Ca^{2+} dependent reorganization of cytoskeletal elements involve cysteine protease calpain, which role in cell motility is partly associated with formation or disassembly of adhesion sites (20). Inhibition of calpain is accompanied by enhanced accumulation of actin filaments, which lead to stabilization of podosome turnover, reduction in velocity of the cell locomotion and impaired transmigration across an endothelial monolayer (20). At least one more element should be included into the Ca^{2+} dependent migration machinery, Ca^{2+}-regulated phospholipid-binding proteins, namely annexins. Annexins are thought to be the bridge between Ca^{2+} signal and actin dynamic at membrane contact sites. Expression of annexin isoforms I, II, IV, V and VI has been detected in human DCs, and the evidence from annexin-I deficient mice has confirmed its active role in DC migration (51).

Immunological synapse

The immunological synapse is a term used to describe tight connection between T cells and DCs (or other APCs). This highly organized and dynamic structure acts as a platform for bidirectional cell-to-cell flow of information exchanged by the means of direct secretion (32). The synapse involves the cross-talk between receptor signaling, cytoskeletal reorganization and direct transport of cell surface receptors and other molecular messengers (52). T cell receptor (TCR): MHC interaction is in the center of the synapse and that first cell-to-cell contact is a stop signal for a T cell, which then terminates migration and forces stable positional contact with the APC (52). The formation of mature synapse takes minutes but afterwards this cellular arrangement can be stable for hours (32). The formation of contact zone between alloreactive $CD8^+$ T cells and DCs is followed by an increase in $[Ca^{2+}]_i$ in DCs (37). However, conflicting reports have been published about Ca^{2+} signal during $CD4^+$ T cell and DC interaction. Gardella et al. have shown that $CD4^+$ T cell contact with DCs results in a Ca^{2+} response in T cells but not in DCs (37), whereas Montes and colleagues have shown transient Ca^{2+} signals in both cells forming the synapse (85). Nevertheless, this T cell and DC communication promoted Ca^{2+} signal has a potential to trigger all Ca^{2+} dependent phenomena like exocytosis in both cell types.

During T cell recognition of antigen presented on MHC, DCs secrete several cytokines including IL-1β and IL-18 (36-38). The exocytosis of these cytokines is a Ca^{2+} dependent on account of being potentiated by the Ca^{2+} ionophore ionomycin and BayK 8644, a L-type Ca^{2+} channel agonist and inhibited by nifidipine, inhere mentioned channel blocker (36, 37). Moreover, STIM1 and Orai1 in T cells and STIM2 and Orai2 in DCs are recruited to the forming immunological synapse (8, 73).

Interestingly, in addition to typical signaling molecules of immune system like cytokines, classical neurotransmitters including serotonin (5-hydroxytryptamine, 5-TH) and glutamate are released by DCs, at the sites of the immunological synapses by the Ca^{2+} dependent exocytosis (95). 5-TH can modify the rate of T cell proliferation and differentiation by decreasing the levels of cAMP (95). DCs have ability to uptake 5-TH secreted by other cells like: activated platelets, degranulating

mast cells, and sympathetic neurons and, most importantly, activated T cells (95). Because of their frequent contact with both, activated and naïve T cells, DCs are able to use 5-TH produced by active T cells to induce tolerance and adaptive immune responses in naïve T cells (95).

Glutamate serves as a major excitatory neurotransmitter in the central nervous system but there is also growing evidence that it plays a role as an immunomodulator (19). Upon maturation, DCs release glutamate through cystine/glutamate antiporter X_c^- system (96). In the early stages of T cell – DC interaction glutamate binds constitutively to matabotropic glutamate receptor 5 (mGlu5R) on T cells (the receptor being not expressed on DCs, which excludes autocrine mechanism) (96). mGlu5R is positively coupled to adenylate cyclase in T cells and causes impaired IL-6 production asmeasured in the cell medium from T cell – DC co culture (96). This lower interleukin secretion, in consequence, decreases T cell proliferation (96). However, after 24 – 48 hours of T cell – DC interaction, T cells start expressing mGlu1R, which signaling stimulates the secretion of TNF-α, IL-2, IL-10 and INF-γ through ERK pathway (96). Furthermore, DCs express VGLUT1 and 2 and other components involved in neurotransmitter exocytosis through SNARE complex formation, as well as synaptotagmin-I, a Ca^{2+} sensor for glutamate release (1). Additionally, ionomycin and SDF-1α (a physiological stimulus in astrocytes) trigger both an increase in $[Ca^{2+}]_i$ and glutamate release demonstrating that DCs are capable of fast glutamate release in a Ca^{2+} dependent manner (1).

I.III Ca^{2+} homeostasis in DCs

Ca^{2+} is one of the most universal signal transduction molecules. It is able to alter local electrostatic fields evoking changes in protein charge and conformation, and same modifying protein-protein interactions. In resting mammalian cells $[Ca^{2+}]_i$ remains in 50-150 nM range and cells invest a lot of energy to maintain their Ca^{2+} homeostasis, dealing with 20 000 fold chemical gradient across the cell membrane (48). The management of $[Ca^{2+}]_i$ requires balance between influx, release and clearing mechanisms.

Ca^{2+} release mechanisms

The release of Ca^{2+} from intracellular stores can be achieved by stimulation of inositol 1,4,5 triphosphate (IP_3) and ryanodine (RyR) receptors expressed on the ER membrane surface (15). In DCs tyrosine phosphorylation of PLC-γ2 leads to hydrolysis of PIP_2 into DAG and IP_3, stimulation of IP_3 receptor and Ca^{2+} release from the intracellular stores (2). DCs express so called 'skeletal' isoform of RyR1 coupled with $Ca_v1.2$ subunit of L-type Ca^{2+} channels, which activation depends on the presence of extracellular Ca^{2+} and is sensitive to ryanodine and nifidipine (94, 135). RyR can also be activated by adenine-based metabolites, cyclic ADP-ribose (cADPR) and nicotinic acid adenine dinucleotide phasphate (NAADP) (70). Quite recently, TRPM2 has been recognized as another important channel responsible for Ca^{2+} release from endolysosomal compartments in DCs (129). TRPM2 forms a Ca^{2+} permeable nonspecific cation channel that contains a Nudix-like region that binds and hydrolyses ADP-ribose (ADPR) to ribose 5-phosphate and AMP (129). ADPR binding to the channel induces Na^+ and Ca^{2+} influx into the cell (129). TRPM2 gating by ADPR is further promoted by NAADP, cADPR, H_2O_2, and Ca^{2+}, whereas AMP and permeating protons enforce channel inhibition (129). In DCs, TRPM2 expression is restricted to endolysosomal vesicles and TRPM2 deficient DCs show impaired maturation and migration profile due to impaired Ca^{2+} release which caused further perturbation in Ca^{2+} influx through store-operated Ca^{2+} (SOC) channels (129).

Ca^{2+} entry mechanisms

When Ca^{2+} release from the intracellular stores causes the drop in free Ca^{2+} concentration in ER, below resting values ~400-600 µM, Ca^{2+} release-activated Ca^{2+} (CRAC) channels, a major player in Ca^{2+} entry in immune cells, are activated (48). CRAC channels are composed of: a pore subunit, a four transmembrane domain protein named ORAI (isoforms 1-3) and its "guardian", ER-resident Ca^{2+} sensing, single transmembrane stromal interaction molecule (STIM; isoforms 1 and 2) (48). CRAC in DCs is primary composed of STIM2 and ORAI2 subunits (8).

In cardiac and skeletal muscle dihydropyridine receptor (DHPR) L-type Ca^{2+} channels sense changes in membrane potential and activate Ca^{2+} release from ER through RyR1 (135). RyR1 presence in mouse DCs is well established and the expression of $Ca_v1.2$ cardiac subunit of (DHPR) L-type Ca^{2+} channel has been shown in human immature DCs (135). DCs respond to the depolarizing stimulus (100mM KCl) with significant increase of $[Ca^{2+}]_i$, which is blunted by cell pre-treatment with 10µM nifidipine or 500µM ryanodine, strongly suggesting that similar to striated muscle, Ca^{2+} release in DCs occurs through RyR1, and is functionally coupled with DHPR L-type Ca^{2+} channels (135).

Transient receptor potential channels

Transient receptor potential (TRP) super family of cation channels respond to numerous stimuli like light, sound, temperature, pH, touch etc (134). With exception of TRPM4 and TRPM5, which are the only two members of the super family that are permeable exclusively for monovalent cations, the rest of TRP channels are Ca^{2+} permeable (134).

TRPV1 is a thermo sensitive channel specifically activated by temperatures > 43˚C in sensory neurons (12). In DCs TRPV1 does not play a role as a heat receptor, since both $TRPV1^{+/+}$ and $TRPV1^{-/-}$ DCs show no differences in the heat induced maturation (12). On the other hand, capsaicin, a TRPV1 ligand that has been shown to engage in the perception of pain in neurons (12), induces maturation of $TRPV1^{+/+}$ but not $TRPV1^{-/-}$ DCs demonstrating that TRPV1 transmits immunological inflammatory signals (12).

Purinergic receptors

ATP is a small solute bearing from two to four negative charges depending on pH and Ca^{2+} and Mg^{2+} concentration (28). ATP is present at high concentrations intracellularly (5-10 mM) and, in the resting conditions, at very low (1-10 nM) extracellular concentrations, making it very potent extracellular messenger (28). DCs express multiple P2Y ($P2Y_1$, $P2Y_2$, $P2Y_4$, $P2Y_6$, $P2Y_{11}$ and $P2Y_{14}$) and P2X ($P2X_1$, $P2X_4$ and $P2X_7$) receptors (28). Acute stimulation, transient stimulation of DCs with ATP or UTP causes typical P2R responses like phosphatidyl inositol breakdown, release of $Ca^{2+}$from intracellular stores, Ca^{2+}influx across the plasma membrane, and

even the opening of the $P2X_7$ large conductance pore if a high ATP concentration is used (28). Nucleotides have a potency to activate two types of responses in DCs. The chronic, low concentration (10-250 µM) exposure triggers a process of DC maturation as shown by increased expression of the classical maturation markers (CD54, CD80, CD83 and CD86) as well as decreased endocytosis and enhanced ability to stimulate Th_2 lymphocytes (28). On the other hand, when DCs are exposed to acute, high concentration (500 µM -1 mM) of nucleotides, they started secreting increased amounts of pro-inflammatory cytokines, especially IL-1β and if the high ATP conditions continue, cell death occurs (28). Additionally, $G_{i/o}$protein-coupled P2YR agonists turn out to be a potent chemotactic stimuli for immature DCs and ligation of those receptors is accompanied by increase in $[Ca^{2+}]_i$ and actin polymerization (54). Mature DCs lose their sensitivity towards ATP, which allow them to migrate from ATP-rich inflammatory, injury sites to draining lymph nodes in order to initiate immune responses (54).

Ion channels regulating Ca^{2+} entry

To maintain Ca^{2+} entry, mechanisms that would counteract the membrane depolarization caused by Ca^{2+} influx are needed. This is usually achieved by K^+ efflux of Cl^- influx into the cell. DCs express voltage gated K_v 1.3 and 1.5 channels that have been shown to maintain cell membrane negative potential providing the necessary electrical driving force to sustain Ca^{2+} entry through CRAC channels (71). On the other hand, Na^+ influx would have an opposite effect – membrane depolarization, decreased driving force for Ca^{2+} and inhibition of CRAC channels. TRPM4 is a Ca^{2+} activated nonselective cation channel, which under physiological conditions allows massive entry of Na^+, causing membrane depolarization, the same decreasing the driving force for influx of Ca^{2+} through CRAC channels (9). Expression of fully functional TRPM4 channels has been shown in mouse DCs and its role in prevention of Ca^{2+} overload is important for successful DC migration (9).

Ca^{2+} signal termination

Because Ca^{2+} is such a powerful second messenger, a delicate balance between induction of Ca^{2+} signal and its termination needs to be kept, as Ca^{2+} overload leads to apoptosis and cell death. The termination of Ca^{2+} signal depends on Ca^{2+} transport back into intracellular compartments and extrusion across the cell membrane. ATPase pumps are designed to transport Ca^{2+} against chemical gradient into ER – SERCA pumps or across membrane – PMCA (71). SERCA exchanges protons for two and PMCA for one Ca^{2+} for every hydrolysed ATP.

A second mechanism involves Na^+/Ca^{2+} exchangers, which have much higher turnover rate than pumps. Mouse DCs express functional K^+ - independent (NCX 1-3) and K^+- dependent (NCKX 1, 3-5) exchangers (123). The direction of ion transport through exchangers depends on dominant electrochemical driving force, which depends on the intra and extra-cellular Na^+ and Ca^{2+} concentrations as well as on the cell membrane potential (71). NCXs exchange three Na^+ for one Ca^{2+}, whereas NCKXs transport K^+ in the same direction as Ca^{2+}, in the four Na^+ for one Ca^{2+} and one K^+ ratio (71). Regulation of Ca^{2+} signal in DCs is very sensitive to the activity of Na^+/Ca^{2+} exchangers (122).

In addition, previously mentioned TRPM4 channels, when activated, allowed massive influx of Na^+ that 'breaks' the membrane potential and terminates the Ca^{2+} signal (9).

I.III Calcium activated chloride channels (CaCCs)

In the regulation of Ca^{2+} homeostasis in DCs, Cl^- channels might play an important role. One family of Cl^- channels, Ca^{2+}-activated Cl^- channels (CaCCs) were first described in 1883, as endogenous channels in *Xenopus* oocytes that are activated by $[Ca^{2+}]_i$ increase upon fertilization (83). Activation of CaCCs causes cell membrane depolarization and prevents additional sperm entry (83). CaCCs have been shown to play various roles in numerous cell types. In epithelium they are responsible for secretion (64), in neurons (4) and cardiac muscle for membrane excitability (43), also they seem to play role in olfactory transduction (81), regulation of vascular tone (5) and photoreception (68). Several molecular candidates have

been proposed including CLCA, tweety, bestrophins and anostamins, which current characteristics most closely resemble the ones described in *Xenopus* oocytes (46).

CLCA

The CLCA family has been cloned from a bovine cDNA expression library screened with use of antibody generated against the protein that behaved like CaCC when incorporated into artificial bilayers (46). Even though transfection of various cell types with cDNA encoding for members of CLCAs has induced Ca^{2+}-dependent currents, those molecules are no longer considered as serious candidates for CaCCs. One of the reasons is that they resemble adhesion proteins and some are soluble, secreted proteins. Furthermore, the structure – function analysis has not provided and evidence that CLCA is actually an ion channel (46). In addition there are clear differences in Ca^{2+} sensitivity, voltage dependence and pharmacology between CLCA and native CaCC currents (46) and many cells that express native CaCCs do not express CLCAs (98). That is why CLCA proteins have been proposed to be CaCC modulators rather than channels themselves (14).

Tweety

Two proteins encoded by human genes *hTTHY2* and *hTTHY3* have been suggested as the molecular basis for Ca^{2+}-regulated maxi Cl^- channels (260 pS), which may correspond to the Cl^- channels found in spinal neurons and skeletal muscle (46), but is very unlikely that those channels are responsible for the classical native CaCC currents. First, the single channel conductance of Tweety is way too big - 260pS compared to 8-40 pS (dependent on cell type) of the native CaCCs, second, they are not expresses in acinar cells of secretory glands (46).

Bestrophins

It has been proposed that bestrophin 1 (Best1) forms CaCC in the basorateral membrane of retinal pigment epithelial (RPE) cells and is responsible for the generation of so-called light peak in the electrooculogram, but several facts point against such a role of those proteins (63). The most important evidence has been brought from Best1 deficient mouse, which still presents CaCC currents (78). However co expression of bestrophins and voltage gated Ca^{2+} channels in RPE cell line and HEK293 cells have been shown to change properties of the former (63). Recently, it has been shown that, in both native and Best1 over expressing cells,

Best1 is predominantly localized in ER where it interacts with STIM1 (10). Moreover, $P2Y_2$ receptor induced transient increase in $[Ca^{2+}]_i$ is more pronounced in HEK293 cells over expressing human Best1 (10). Furthermore, lack of Best1 in respiratory epithelial cells of the mBest1 knockout mice, causes expansion of ER cisterns and induces Ca^{2+} deposit (10). Best1 is, therefore, responsible for Ca^{2+} handling of ER stores and plays a role as a counterion channel to balance transient membrane potential changes on the ER membrane occurring through IP_3 induced Ca^{2+} release and store refill (10). There is few further differences between classical CaCC and Best1, including different voltage-dependent kinetics, Best1 activation by cell swelling in the absence of Ca^{2+}, not observed in native CaCCs, and Ca^{2+} affinity of Best1 ten times higher than CaCCs (63). All those arguments exclude bestrophins as the candidate molecules forming CaCCs.

Anoctamins

Anoctamins have taken their name from the play of words, AN as anion selective channels with eight (OCT) transmembrane regions (142). In the time span of couple months, three independent groups have reported anoctamine 1 (ANO1), also known as TMEM16A, to form CaCCs. Each of the laboratories has taken on a different approach, Yand et al. have chosen ANO1 from a bioinformatic screen designed to identify channels and transporters like genes with multiple transmembrane domains (142). Upon cotransfection of HEK293 cells with endothelin receptor, which ligation elevates $[Ca^{2+}]_i$, ANO1 has been shown to mediate endothelin induced Cl^- currents (142). The interest, of the Caputo group, in ANO1 has evolved from the microarray analysis of the membrane proteins that were up regulated in airway epithelial cells that underwent long term stimulation with IL-4 (21). Silencing of ANO1 in the CFPAC-1 and CFBe41o- cells with high endogenous CaCC currents has greatly reduced purynergic receptor and ionomycin induced currents (21). The Schroeder laboratory has identified ANO1 during cDNA library (prepared from size fractioned RNA of Xenopus oocyte) screen in the axolotl oocyte expression system, in which no native CaCC currents had been detected (117). Currents detected by all three groups exhibit the pharmacological profile of the endogenous Xenopus oocyte CaCCs (NFA > DIDS > NPPB >DPC) (46), furthermore, ANO1 knockout mice show deficiency in the Ca^{2+}- dependent Cl^- transport in number of tissues, which supports the evidence that ANO1 is a major component of CaCCs (65).

Mammalian ANO family consist of ten members and it does not show any obvious homology to other known ion channels (65). ANO1 forms a tertiary structure with eight predicted transmembrane helices, both NH_2- and COOH terminus located intracellularly and the pore formed by the 5^{th} and 6^{th} transmembrane regions with re-entrant membrane loop in between (65). The overall homology between the members of ANO family is moderate but the putative pore region is highly conserved (65). ANO1 and ANO2 share 60% of amino acid identity, while the rest of the family demonstrates similarity of 30% or below, suggesting diversity in their function (65). In the mouse and human cell types that have been examined till date at least two if not more members of ANO family are expressed in parallel, with ANO6 being the most abundant isoform (65). Even though the scientific community agrees that ANO1 and 2 function as CaCCs, conflicting reports have been published considering generation of Cl^- currents by other members of ANO family. In the FTR cells overexpression of ANO6 and ANO7 has produced Ca^{2+} activated Cl^- conductance, even though they exhibit different Ca^{2+} sensitivity and time of activation in comparison to ANO1 (114). Furthermore, recent report has shown that endogenous ANO6, in A549 airway epithelial cells and in Jurkat lymphocytes, is a major contributor to outwardly rectifying Cl^- currents (ORCC) activated by membrane depolarization (79). Further activation of ANO6/ORCC could be induced by cAMP in cooperation with cystic fibrosis transmembrane conductance regulator (CFTR) (79). Conflicting results have shown that over expression of ANO3-7 in HEK293 cells, do not generate Cl^- conductance and confocal imaging has reflected their intracellular location (31). It is also worth mentioning that ANO9 and 10 suppress basal Cl^- conductance and that co expression of ANO1 with ANO9 in FRT cells has caused significant inhibition of Ca^{2+} activated Cl^- currents (114).

Regardless of the clear evidence of Ca^{2+} dependence, neither E-F hand like Ca^{2+} binding site nor IQ-domain CaM binding domain, have been recognized in the structure of ANO1 (46). A string of negatively charged glutamic acid residues in the first intracellular loop could form a Ca^{2+} binding packet but its role remains unclear (131). While the phosphorylation by protein kinases is not required for ANO1 activation, cytosolic ATP and interaction with calmodulin are necessary for full channel activity (131).

The whole-cell CaCC currents are similar in various cell types. They are characterized by initial outward rectification, which with time develops into more linear current-voltage relationship (46). Furthermore, the current –voltage relationship depends on the intracellular Ca^{2+} concentration: below 1µM, the currents are outwardly rectifying and exhibit time dependent activation and deactivation, but at higher intracellular Ca^{2+}concentrations the currents manifest a linear I-V relationship and a time-independent kinetic (46).

The aim of our study was to determine if DCs express functional Ca^{2+} activated Cl^- channels, what physiological signals may contribute to their regulation and the role of those channels in DC function.

I.IV Antigen uptake, processing and presentation in DCs

Internalization of extracellular material is an essential process for eukaryotic cells. Depending on the receptors involved and the particle size, the endocytic pathways are divided into: clathrin-mediated endocytosis, micropinocytosis, caveolae-mediated endocytosis and phagocytosis (17). By internalizing elements within their microenvironment, DCs play a major role in immune system by inducing tolerance or immunity. The decision about the immunological outcome depends essentially on the signal transduction pathway triggered during internalization (16). DCs perform different types of receptor mediated endocytosis and micropinocytosis, but large pathogens are internalized by process of phagocytosis, which is exclusive for neutrophils, macrophages and DCs (17). TLR activation transiently increases the ability if DCs to uptake soluble antigens, immune complexes and phagocytosable forms of antigen (138). DC maturation with TLR ligands causes lost of phagocytosis dependent on actin remodelling and macropinocytosis but the clathrin-dependent endocytosis continues (138). The process of phagocytosis starts with internalization of the pathogen and formation of intracellular single membrane organelle – phagosome (110). The ligation of phagosome with lysosomes leads to formation of fully mature digestive organelle – phagolysosome (110). During progression of phagocytosis, TLR2 and TLR4 that initially were at the plasma membrane accumulate in the phagosomal vesicles. In case of TLR4, the initiaton of endocytosis after LPS binding requires another pattern recognition receptor, CD14 that chaperones LPS molecules to TLR4 signaling complex (144). The presence of TLRs

in the phagosomal cargo significantly influences the presentation of processed antigens on the MHC II and phagocytosis is the most effective route to deliver antigens to MHCII reach compartments (16). MHCII molecules are synthesized in ER, where they associate with the cytoplasmic domain of invariant chains (Ii) and, therefore, are directed to phagosomal pathway, where they bind the peptides from processed antigens (16). Even though all cargos are delivered to the same phagolysosomal compartments, only the vesicles containing TLR ligand complexes have an ability to 'upgrade' the compartments to efficiently process and present antigens on the MHC class II molecules (17). The hydrolytic environment of mature phagolysosomes is required not only for the antigen processing but also for the modulation of the MHCII invariant chains by a series of proteolytic steps, which only take place in the phagosomes that engage the TLR signaling (17).

Partial antigen degradation needs to be tightly controlled to preserve the ~1kDa peptides that are loaded on the MHCII molecules and finally, presented to naïve T cells (112). In phagolysosomes protein degradation is controlled by large family of proteases, which optimal proteolytic activity is in acidic pH (pH 5.5 to 6.5) environment (23). In DCs, recruitment of NADPH oxidase NOX2 to the early phagosomes and NOX2 activity, plays a major role in the control of the proteolytic power of the 'lysosomal proteases' responsible for antigen degradation (107, 112). NOX2 is a multicomponent enzyme, that is inactive in resting cells but assembles at the phagosomal sites in the stimulus dependent manner (119). The enzyme consists of the cytosolic subunits: p47*phox*, p67*phox*, p40*phox*, rac1 or 2 and membrane heterodimers p22*phox*, p91*phox*, which contain the electron transport chain (119). DCs express NOX2 at the relatively low levels (~5% of the level found in neutrophils) and the mechanisms by which the enzyme controles the phagosomal proteolysis are not quite clear. The first proposed theory revolves around the idea that the electrons transported by NOX2 into the phagosomal lumen, generate superoxide anions that further dismutate to produce hydrogen peroxide and other ROS (112). ROS production consumes a grand amount of protons causing alkalization of phagosomal lumen and decreased activity of proteases, the same preserving antigen derived peptides (112). This study has been nicely supported by the fact that DCs isolated from NOX2 deficient mice have shown phagosomal acidification, increased antigen degradation and defective cross presentation to the $CD8^+$ T cells (112). The second

proposed mechanism has explored the idea that NOX2 activity decreases the phagosomal proteolysis through the redox modulation of local cysteine cathepsins (107). The real time analysis of phagosomal environment has shown that the acidification of those compartments is unaffected, however both the activity of local cysteine cathepsins and the ability of DC phagosomes to reduce disulphides is compromised by NOX2 activity (107). No matter which theory we consider the undeniable fact is that NOX2 activity is mandatory for the proper handling of antigens in DCs.

I.V Hv1 proton channel

NOX2 activity is electrogenic and can cause +200mV depolarization in less than 20 ms, which would shut off its activity (25). Another variable that regulates NADPH oxidase activity is pH that needs to be maintained in the range between 7.0 – 7.5 for the optimal NOX2 working conditions (25). Matching proton flux stoichiometrically with electron flux would prevent membrane depolarization and drastic pH changes on either side of the membrane (25). A perfect candidate that has the ability to perform both of those actions simultaneously is a voltage gated proton channel – Hv1, a product of *Hvcn1* gene.

Other candidate molecules, like Na^+/H^+ antiport is electroneutral and even though it regulates the intracellular pH, its activity does not allowed for the charge compensation (25), also the CO_2 diffusion does not generate charge and the inhibition of H^+-ATPase did not influence ROS production in neutrophils or macrophages (25). The strong arguments supporting the role of Hv1 in the charge compensation during respiratory burst come from Hvcn1 knockout leukocytes that show 75% decrease in the NOX2 activity (25). This supported previous experiments, with use pharmacologicals like Zn^{2+}, showing that the effects on those substances on the NADPH activity was mostly due to its inhibition of proton channels (24).

Regardless of the fact that Hv1 takes care of the bulk of the charge compensation in neutrophils in other cells there might be a bigger contribution of other electrogenic molecules (Fig. 3). Proposed candidates include ClC-3 Cl^-/H^+ antiporter (69), CLIC Cl channel (84) , TRPV1 nonselective cation channel (113),

SK2 and SK4 Ca^{2+}- activated K^+ channels (59) and $K_v1.3$ delayed rectifier K^+ channels (35).

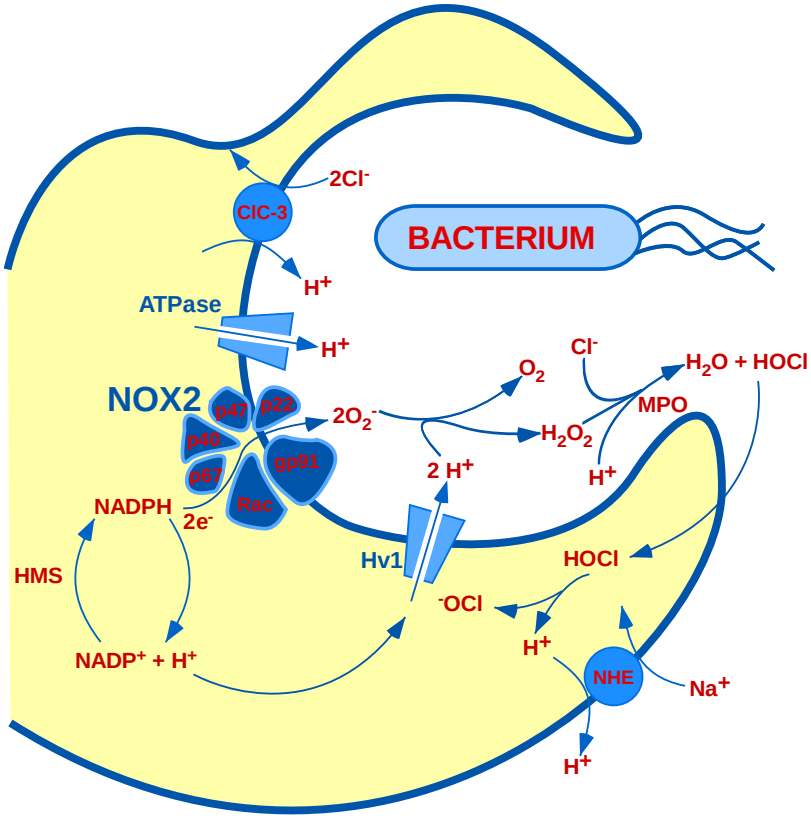

Fig. 3: The main molecules and transporters thought to participate in charge compensation and pH regulation during the respiratory burst.

A phagocyte is depicted engulfing a bacterium into a nascent phagosome, which will proceed to close and become intracellular. NADPH oxidase assembles preferentially in the phagosomal membrane and begins to function before the phagocytic cup has sealed. Charge compensation is required wherever the enzyme is located. The entire system is driven by NADPH oxidase activity. Electrons from cytoplasmic NADPH are translocated across a redox chain to reduce O_2 to superoxide anion (O_2^{-}•) inside the phagosome or extracellularly during respiratory burst in the early stages of phagocytosis. The electrogenic activity can be measured directly as electron current (Fig 19. For each electron removed from the cell, approximately one proton is left behind. Thus NADPH oxidase activity tends to depolarize the membrane, decrease pH_i, and increase pH_o or $pH_{phagosome}$. NADPH is regenerated continuously by the hexose monophosphate shunt (HMS) during the respiratory burst. ClC-3, which is shown to move H^+ into the phagosome and Cl^- out, as is expected to occur at depolarized potentials that exist during the respiratory burst. In endosomes lacking NOX activity, ClC-3 is thought to operate in the reverse direction, removing H^+ and injecting Cl^- into the interior to compensate for electrogenic H^+-ATPase activity. HOCl reacts rapidly with phagosomal constituents but is membrane permeable and also reacts with cytoplasmic contents such as taurine or glutathione. For present purposes, HOCl shuttles protons out of the phagosome. Note that the H^+ in any compartment are equivalent; e.g., protons derived from HOCl dissociation are not preferentially removed by Na^+/H^+ antiport. (Adapted from (25))

The Hv1 protein closely resembles the first four membrane-spanning regions of other voltage-gated ion channels, S1-S4, known as the voltage sensing domain but lack the S5-S6, which in other channels form the pore domain (24). Hv1 has a 'perfect' selectivity for protons, as permeation of no other ions has been ever detected (92). The perfect selectivity mechanisms involve: titratable amino acid residue in the permeation pathway that imparts proton selectivity or water molecules 'frozen' in the narrow pore that conduct protons excluding other ions (92). Recently aspartate 112 residue has been recognized as the selectivity filter (92). When

Asp112 is substituted by other amino acids, the channel loses its selectivity or does not conduct at all (92). The only amino acid swap that preserves the proton-selectivity includes glutamate, showing that acidic group is needed at the selectivity filter (92). Another feature that distinguishes Hv1 from other channels is their pH dependent gating. Increase of extracellular pH (pH_o) or decrease of intracellular pH (pH_i) shifts the voltage threshold of activation ($V_{threshold}$) 40 mV towards more negative voltages (24). Because of ~+20mV offset, the empirical formula establishes $V_{threshold} = 20 – 40 (pH_o – pH_i)$, this formula holds over all physiological pH values, manifesting that the gating is designed to assure the outward proton flux – acid extrusion from the cell (25). The most potent inhibitor of Hv1 is Zn^{2+}, which effects resemble the action of divalent cations on other voltage-gated channels (24). Exposure to Zn^{2+} shifts the conductance-voltage (*g-V*) relationship toward more positive voltages, however, those effects are much less pronounced at low pH_o, suggesting the competition between Zn^{2+} and H^+ (25). Another interesting characteristic of Hv1 is an extreme temperature sensitivity of this channel. Temperature increase influences gating kinetics, both activation and deactivation are much faster at high temperatures, with the temperature coefficient Q_{10} = 6-9, also H^+ conductance greatly increases with Q_{10} ≥ 2 (26). When phagocytic cells are treated with phorbol myristate acetate (PMA), an activator of NADPH and PKC, significant changes in Hv1 behaviour have been observed, indicating altered gating. The so called, ‘enhanced gating mode’ modifies four features in the proton channel properties: 1) increases the likelihood of channel opening; 2) the channel opens faster and closes more slowly; 3) increases maximal proton conductance (g_{Hmax}) and 4) shifts the proton *g-V* relationship 40mV towards more negative potentials (90). The mutation of Thr^{29} in the intracellular N-terminus causes the loss of PKC responses; strongly suggesting that phosphorylation of that residue by PKCδ is responsible for the enhanced gating mode of Hv1 channel (90).

The goal of our study was to determine if dendritic cells express functional voltage-gated proton channels and to detect their regulation and impact on dendritic cell functions.

II. MATERIALS AND METHODS

II.I Materials

II.I.I Equipment

Cell Culture

Equipment	Company
Centrifuge RotiFix 32	Hettich Zentrifugen, Tuttlingen, Germany
Eppendorf cups 1.5 ml	Eppendorf AG, Hamburg, Germany
Eppendorf pipettes 1000 µl, 100 µl, 10 µl	Eppendorf AG, Hamburg, Germany
Heraeus Incubator	Thermo Electron Corporation, Dreieich, Germany
Needles BD Microlance™ 3, 0.55x25 mm	Becton Dickinson Labware, Franklin Lakes, USA
Neubauer counting chamber	Brand, Wertheim, Germany
Pipetus® pipetting aid	Hirschmann Laborgeräte, Eberstadt, Germany
PP-Test tubes 15, 50 ml	Greiner bio-one, Frickenhausen, Germany
Stripette® 5, 10, 25 ml	Corning Incorporated, Corning NY, USA
Syringe BD 10 ml, Luer-Lok™ Tip	Becton Dickinson Labware, Franklin Lakes, USA
Tissue Culture Dishes 60x15 mm	Becton Dickinson Labware, Franklin Lakes, USA
Vortex Genie	Scientific Industries, Bohemia NY, USA

Calcium Immaging

Equipment	Company
Camera Proxitronic	Proxitronic, Bensheim, Germany
Centrifuge RotiFix 32	Hettich Zentrifugen, Tuttlingen, Germany
Discofix® Stopcock for Infusion Therapy	B. Braun, Melsungen, Germany
Filter Set for Fura-2	AHF Analysentechnik AG, Tübingen, Germany
Filter tips 10, 100, 1000µl	Biozym Scientific, Hess. Oldendorf, Germany
Filter wheel	Sutter Instrument Company, Novato, USA
Infusion Regulator Dosi-Flow 10	Dahlhausen, Köln/Sürth, Germany
Lambda 10-2	Sutter Instrument Company, Novato, USA
Lamp XBO 75	Leistungselektronik Jena GmbH, Jena, Germany
Metafluor software	Universal Imaging, Downingtown, USA
Microscope Axiovert 100	Zeiss, Oberkochen, Germany
Microscope cover glasses round,	Karl Hecht KG, Sondheim, Germany
30mm diameter, 0.13-0.16 mm	
Neutral densitiy filters 10, 20, 40, 60%	AHF Analysentechnik AG, Tübingen, Germany
Objective fluar 40x/1.3 oil	Carl Zeiss, Oberkochen, Germany
Syringe BD 10 ml, Luer-Lok™ Tip	Becton Dickinson Labware, Franklin Lakes, USA
Syringe BD Perfusion™ 50 ml	Becton Dickinson Labware, Franklin Lakes, USA
Tissue Culture Dishes 35x10 mm	Becton Dickinson Labware, Franklin Lakes, USA
Winged Needle Infusion Set Butterfly®-21	Hospira Venisystems, Donegal Town, Ireland

Patch Clamp

Equipment	Company
Borosilicate glass filaments	Harvard Apparatus, March-Hugstetten, Germany
DMZ puller	Zeitz, Augsburg, Germany
EPC-9 amplifier	Heka, Lambrecht, Germany
ITC-16 Interface	Instrutech, Port Washington, N.Y., USA
Microscope Axiovert 100	Zeiss, Oberkochen, Germany
MS314 electrical micromanipulator	MW, Märzhäuser, Wetzlar, Germany
Pulse software	Heka, Lambrecht, Germany

FACS

Equipment	Company
FACS Calibur	Becton Dickinson, Heidelberg, Germany
FACS tubes, 1.3 ml, PP, round bottom	Greiner bio-one, Frickenhausen, Germany

Migration and Cytokine Production

Equipment	Company
Magellan™ software	Tecan Group Ltd., Männedorf, Switzerland
Multi well plates; 24, 96 well	Corning Inc., Corning NY, USA
Sunrise™ Microplate Reader	Tecan Trading AG, Switzerland

Immunoblotting

Equipment	Company
Agarose gel electrophoresis chamber	BioRad, München, Germany
Centrifuge 5415R	Eppendorf, Hamburg, Germany
Densitometer Quantity One	BioRad, München, Germany
Gel tips	Alpha Laboratories, Hampshire, UK
Kodak film	Sigma, Hannover, Germany
Nitrocellulose membrane	Millipore,

RT – PCR

Equipment	Company
Densitometer	BioRad, München, Germany
LightCycler System	Roche Diagnostics, Mannheim, Germany
Mastercycler®	Eppendorf AG, Hamburg, Germany

II.I.II Chemicals and Reagents

Cell Culture

Substance	Company
Foetal Bovine Serum (FBS)	GIBCO, Carlsbad, Germany
GMCSF mouse recombinant	Peprotech/Tebu, Cölbe, Germany
L-Glutamine	GIBCO, Carlsbad, Germany
Lipopolysaccharide E.coli (LPS)	Sigma, Taufkirchen, Germany
MEM Non-Essential Amino Acids	Invitrogen, Karlsruhe, Germany
Penicillin-Streptomycin	Invitrogen, Karlsruhe, Germany
Phosphate buffered saline (PBS)	GIBCO, Carlsbad, Germany
RPMI 1640	GIBCO, Carlsbad, Germany
Trypan blue solution 0,4%	Sigma, Taufkirchen, Germany
β-mercaptoethanol	Invitrogen, Karlsruhe, Germany

Intracellular Calcium Imaging and Patch Clamp

Substance	Company
AO1	Sygnature Chemicals Services Ltd., UK
$C_2H_6O_3S$	Sigma, St.Luis, US
$CaCl_2$	Carl Roth, Karlsruhe, Germany
CsCl	Sigma, Taufkirchen, Germany
Digallic Acid	Sigma, Taufkirchen, Germany
Diphenyleneiodonium chloride (DPI)	Sigma, St.Luis, US
D-myo-inositol-1,4,5-triphosphate (IP3)	Enzo, Life Sciences, Germany
Ethylene glycol tetraacetic acid (EGTA)	Sigma, Taufkirchen, Germany
Fura-2 AM	Invitrogen, Karlsruhe, Germany
GFX	Calbiochem, , Darmstadt, Germany
Glucose	Carl Roth, Karlsruhe, Germany
HCl	Sigma, Taufkirchen, Germany
HEPES	Sigma, Taufkirchen, Germany
Immersol 518F	Carl Zeiss, Göttingen, Germany
Ionomycin	Sigma, Taufkirchen, Germany
KCl	Carl Roth, Karlsruhe, Germany
MES	Applichem, Darmstadt, Germany
MgATP	Sigma, Taufkirchen, Germany
$MgCl_2$ x 6 H_2O	Sigma, Taufkirchen, Germany
$MgSO_4$ x 7 H_2O	Sigma, Taufkirchen, Germany
Na_2HPO_4 x 2 H_2O	Sigma, Taufkirchen, Germany
NaCl	Sigma, Taufkirchen, Germany
NaOH	Sigma, Taufkirchen, Germany
Niflumic Acis	Sigma, Taufkirchen, Germany
N-methyl-D-glucamine (NMDG)	Sigma, Steinheim, Germany
Poly-L-Lysine	Sigma, Taufkirchen, Germany
Silicone grease	Carl Roth, Karlsruhe, Germany
Tannic Acid	Sigma, Taufkirchen, Germany
Tetraethylammonium chloride (TEACl)	Sigma, Taufkirchen, Germany
Tetramethylammonium hydroxide (TMA)	Sigma, St.Luis, US
Thapsigargin	Molecular Probes, Leiden, The Netherlands
Tricine	Sigma, St.Luis, US

FACS and Migration Assay

Reagent	Company
CCL21	Peprotech/Tebu, Cölbe, Germany
APC-conjugated anti-mouse CD11c,clone HL3	BD Pharmingen, Heidelberg, Germany
2',7'-dichlorodihydrofluorescein diacetate (DCFDA)	Sigma, St.Luis, US

Cytokine Production

Kit	Company
Mouse IL-2 ELISA Set	BD Pharmingen, Heidelberg, Germany
Mouse IL-6 ELISA Set	BD Pharmingen, Heidelberg, Germany

RT-PCR

Reagent / Kit	Company
10 x reaction buffer	Biolabs, Frankfurt, Germany
Agarose	Sigma, Taufkirchen, Germany
DEPC water	Ambion, Darmstadt, Germany
dNTP mix	Promega, Mannheim, Germany
Ethanol 99.7%	VWR, Darmstadt, Germany
Ethidium bromide	Sigma, Taufkirchen, Germany
Master Sybr Green I Mix	Roche, Mannheim, Germany
M-MuLV reverse transcriptase	Biolabs, Frankfurt, Germany
Murine MRPS9 Kit	Search LC, Heidelberg, Germany
Primer mix	Search LC, Heidelberg, Germany
puReTaq Ready-To-Go PCR bead	Amersham Biosciences, Freiburg, Germany
QIAshredder	Qiagen, Hilden, Germany
Recombinant RNase inhibitor	Roche, Mannheim, Germany
RLT lysis buffer	Qiagen, Hilden, Germany
Rnase-free Dnase Set	Qiagen, Hilden, Germany
Rneasy Mini Kit	Qiagen, Hilden, Germany

Immunoblotting

Reagent	Company
Acrylamide/bisacrylamide	Carl Roth, Karlsruhe, Germany
BenchMark prestained protein ladder	Invitrogen, California, USA
Cell lysis buffer	Pierce, Bonn, Germany
ECL Detection reagent	GE Healthcare, München, Germany
Glycine	Sigma, Taufkirchen, Germany
Loading buffer (4x)	Carl Roth, Karlsruhe, Germany
Milk powder	Carl Roth, Karlsruhe, Germany
Ponceau S	Sigma, Taufkirchen, Germany
Protease inhibitor	Sigma, Taufkirchen, Germany
Sodium dodecyl sulfate (SDS)	Sigma, Hannover, Germany
TEMED	Carl Roth, Karlsruhe, Germany
Triethanolamine-buffered saline (TBS)	Sigma, Taufkirchen, Germany
Tween-20	Böhringer Ingelheim, Mannheim, Germany

II.I.III Solutions

Intracellular Calcium Imaging

Standard Ringer

NaCl	125 mM
KCl	5 mM
$MgSO_4$ x 7 H_2O	1.2 mM
HEPES	32.2 mM
Na_2HPO_4 x 2 H_2O	2 mM
Glucose	5 mM
$CaCl_2$ x 2 H_2O	2 mM

[NaOH; pH 7.4]

Ca^{2+}- free Ringer

NaCl	125 mM
KCl	5 mM
$MgSO_4$ x 7 H_2O	1.2 mM
HEPES	32.2 mM
Na_2HPO_4 x 2 H_2O	2 mM
Glucose	5 mM
EGTA	0.5 mM

[NaOH; pH 7.4]

Patch Clamp - Bath Solutions

Standard Ringer

NaCl	145 mM
KCl	5 mM
$MgCl_2$	2 mM
$CaCl_2$	2 mM
HEPES	10 mM
Glucose	20 mM

[NaOH; pH 7.4]

NMDG-based solution

NaCl	145 mM
KCl	5 mM
$MgCl_2$	2 mM
$CaCl_2$	2 mM
HEPES	10 mM
Glucose	20 mM

[NaOH; pH 7.4]

e^- solution

CsCl	75 mM
CsOH	50 mM
TEACl	10 mM
$MgCl_2$	1 mM
HEPES	50 mM
Glucose	5.5 mM

[CsOH; pH 7.1]

$TMASO_3$ 6.0pH solution

$(CH_3)_2SO_3$	80 mM
MES	100 mM
Glucose	20 mM

[TMAOH; pH 6.0]

$TMASO_3$ 7.0pH solution

$(CH_3)_2SO_3$	80 mM
HEPES	100 mM
Glucose	20 mM

[TMAOH; pH 7.0]

$TMASO_3$ 8.0pH solution

$(CH_3)_2SO_3$	80 mM
Tricine	100 mM
Glucose	20 mM

[TMAOH; pH 8.0]

Patch Clamp – Pipette Solutions

$TMASO_3$ 6.0pH solution

$(CH_3)_2SO_3$	80 mM
MES	100 mM
Glucose	20 mM
[TMAOH; pH 6.0]	

$TMASO_3$ 7.0pH solution

$(CH_3)_2SO_3$	80 mM
HEPES	100 mM
Glucose	20 mM
[TMAOH; pH 7.0]	

$TMASO_3$ 8.0pH solution

$(CH_3)_2SO_3$	80 mM
Tricine	100 mM
Glucose	20 mM
[TMAOH; pH 8.0]	

e^- solution

CsCl	75 mM
CsOH	50 mM
TEACl	10 mM
$MgCl_2$	1 mM
Mg-ATP	1 mM
HEPES	50 mM
NADPH	8 mM
[CsOH; pH 7.6]	

CsCl based solution

CsCl	120 mM
NaCl	35 mM
EGTA	10 mM
Mg-ATP	1 mM
HEPES	10 mM
IP_3	40 µM
[CsOH; pH 7.2]	

NMDG based solution

NMDG-Cl	180 mM
EGTA	1 mM
Mg-ATP	1 mM
HEPES	10 mM
[CsOH; pH 7.2]	

FACS

FACS Buffer

PBS

0.1 % heat-inactivated FBS

Cytokine Production

ELISA

Coating buffer

0.2 M sodium phosphate pH 6.5

Assay diluent

1x PBS

heat-inactivated FBS 10 %

Stop Solution

2 M H_2SO_4

Immunoblotting

Running buffer	
Tris	25 mM
Glycine	250 mM
SDS	0,1 %

Transfer buffer	
Tris	25 mM
Glycine	192 mM
Methanol	20 %
[HCl; pH 8.3]	

Wash buffer (TBS-T)	
Tris	50mM
NaCl	150mM
Tween-20	0.05 %
[HCl; pH 7.5]	

II.I.IV Animals

The mice (C57BL/6,129/Sv) were obtained from Charles River, Sulzfeld, Germany. Alternatively, any wild type mice bred in the Institute of Physiology were used because a comparison between cells from wild type and knock out animals was not performed.

II.II Methods

II.II.I Cell Culture

Bone marrow derived DC cultures were prepared according to established protocol (55) with slight modifications. After removing all the muscle tissues from femurs and tibias, both ends of the bone were cut with scissors and bone marrow cells were flushed out from bone cavities with use of PBS-filled syringe and 27-gauge needle. Cells were washed twice with RPMI 1640, by centrifuging at 1500 rpm for 5 min at 4℃. The supernatant was discharged and the cells were resuspended in complete cell culture medium for the 2nd wash. In the next step, cells were counted with use of a Neubauer counting chamber and seeded out at density 2 x 10^6 cells per 60mm x 15mm dish in 10ml of RPMI 1640 substituted with 10% FCS, 1% penicillin/streptomycin, 1% glutamate, 1% non-essential amino acids and 0.05 % β-mercaptoethanol. In the final step GM-CSF (35ng/ml) was added to the cell culture medium.

Cells were cultured for 7 days. On 3rd day, 10ml of fresh cell medium was added to each dish. On 6th day, 10ml of cell medium was removed and exchanged for fresh medium of the same volume. Experiments were performed on DCs at days 7th through 11th.

II.II.II Intracellular Calcium Imaging

The intracellular calcium concentration $[Ca^{2+}]_i$ measurements were performed in the dark room with use of the set up composed of the following elements: oil-immersion inverted phase-contrast microscope, a camera, a fluorescent lamp, a filter wheel with different excitation filters, a shutter element, a perfusion system inserted into a measuring chamber, a water bath, and a pump to allow a continuous exchange of the bath solutions. During experiments cells were continuously superfused with solutions at 37˚C.

Prior to measurements, DCs were incubated with 2μM Fura-2-acetylomethyl (Fura-2-AM) at 37˚C, 5% CO_2 for 30 minutes. Fura-2-AM is a ratiomeric indicator dye, which at low concentrations allows to accurately measure $[Ca^{2+}]_i$ (Fig. 4). The acetylomethyl (AM) groups allow for cell permeation and after crossing the cell membrane AM groups are cleaved by cellular esterases. Fura-2 , pentacarboxylate

calcium indicator, is reconstructed and is free to form Fura-2 – Ca^{2+} complexes (140).

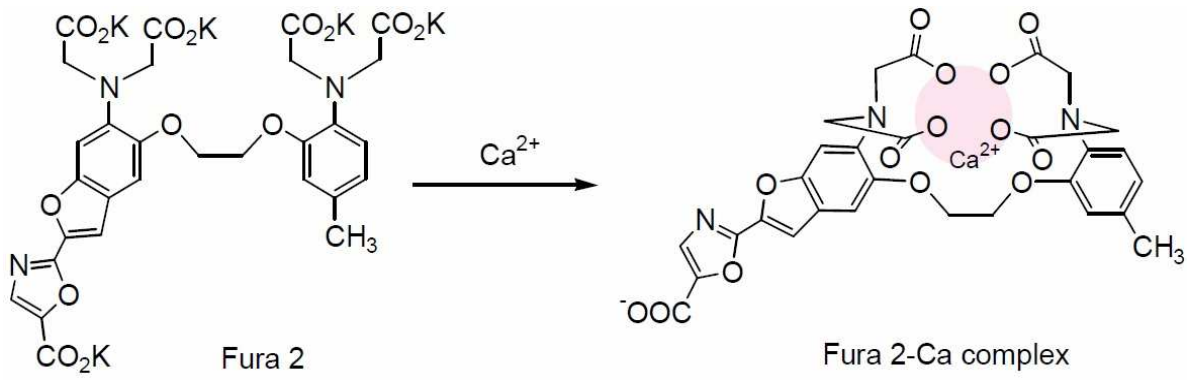

Fig. 4: Molecular structure of Fura-2 and graphic representation of Fura-2-Ca^{2+}complex

(source: www.invitrogen.com)

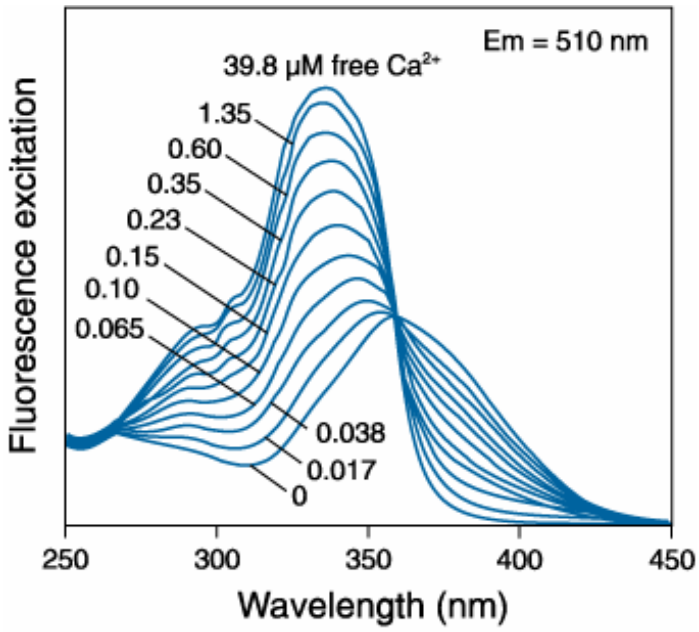

Fig. 5: Fluorescence excitation spectra of Fura-2 in solutions containing 0-39.8µM of free Ca^{2+}

(source: www.invitrogen.com)

During $[Ca^{2+}]_i$ measurements, cells were excited alternatively at 340 and 380nm and the intensity of fluorescent emission was recorded at 505nm. Data acquisition was performed every 6-10 seconds by Metafluor computer software and then exported to Excel data sheet for further analysis. The alterations in the levels of $[Ca^{2+}]_i$ were analyzed as a function of two variables: amplitude of $[Ca^{2+}]_i$ change as peak, and the speed at which that change occurred as slope. Because the calibration of Fura-2 ratiomeric measurements was shown to be highly unreliable (145), we use the ratio values for data analysis.

II.II.III Whole-cell patch clamp

Patch clamp experiments were performed at room temperature in voltage-clamp, fast-whole-cell mode according to Hamill et al. (44). The cells were continuously superfused through a flow system inserted into the dish. The bath was grounded via a bridge filled with NaCl Ringer solution. Borosilicate glass pipettes (1-3 MΩ tip resistance; GC 150 TF-10, Clark Medical Instruments, Pangbourne, UK) manufactured by a microprocessor-driven DMZ puller (Zeitz, Augsburg, Germany) were used in combination with a MS314 electrical micromanipulator (MW, Märzhäuser, Wetzlar, Germany). The currents were recorded by an EPC-9 amplifier (Heka, Lambrecht, Germany) using Pulse software (Heka) and an ITC-16 Interface (Instrutech, Port Washington, N.Y., USA). The currents were recorded with an acquisition frequency of 10 kHz and 3 kHz low-pass filtered. The liquid junction potential ΔE between the pipette and the bath solutions and between the salt bridge and the bath solutions were estimated as described earlier (11). Data were corrected for the estimated ΔE values.

II.II.III.I Calcium Activated Chloride Channels

DCs were superfused with a 'NaCl bath solution' containing: 145 mM/l NaCl, 5 mM/l KCl, 2 mM/l $CaCl_2$, 2 mM $MgCl_2$, 20 mM/l glucose, 10 mM/l HEPES/NaOH, pH 7.4. To study the Ca^{2+} sensitivity of the measured current a 'NaCl, 0 Ca^{2+} bath solution' was used, which contained 10 mM EGTA and 0 $CaCl_2$. In other experiments extracellular Na^+ was substituted by $NMDG^+$ and the 'NMDG-Cl' bath solution contained: 145 mM/l NMDG-Cl, 2 mM/l $MgCl_2$, 2 mM/l $CaCl_2$, 20 mM/l glucose, 10 mM/l HEPES/NMDG, pH 7.4. To determine the Cl^- permeability of the outward current all chloride salts were isoosmotically replaced by respective gluconate salts ('Na-gluconate bath solution' or 'NMDG-gluconate bath solution'). In order to induce the Ca^{2+}-activated Cl^- currents, ionomycin (1 µM, Calbiochem, Germany) was applied in 'NMDG-Cl' bath. To prove the Ca^{2+} sensitivity of ionomycin-induced currents 'NMDG-Cl, 0 Ca^{2+} bath solution' was used, which contained 10 mM EGTA and 0 $CaCl_2$.

The patch clamp pipettes were filled with either 'CsCl pipette solution' containing: 120 mM/l CsCl, 35 mM/l NaCl, 1 mM/l MgATP, 10 mM/l EGTA, 40 µM/l D-*myo*-

inositol-1,4,5-triphosphate (Enzo, Life Sciences), 10 mM/l HEPES/CsOH, pH 7.2; or 'NMDG-Cl pipette solution' containing: 180 mM/l NMDG-Cl, 1 mM/l Mg-ATP, 1 mM/l EGTA, 10 mM/l HEPES, pH 7.2.

Where indicated tannic acid (10 µM, Sigma), AO1 (20 µM, Sygnature Chemical Services Ltd, Nottingham, UK), niflumic acid (300 µM, Sigma) or digallic acid (100 µM, Santa Cruz) were added to the bath solution.

Protocol: Currents were elicited by 200 ms square wave voltage pulses from -50 to +50 mV in 10 mV steps delivered from a holding potential of -30 mV.

II.II.III.II Proton Channels

NaCl Ringer bath solution contained (in mM): 145 NaCl, 5 KCl, 2 $CaCl_2$, 2 $MgCl_2$, 10 HEPES, (pH 7.4, NaOH). $TMASO_3$ bath solution contained (in mM): 80 $(CH_3)_2SO_3$, 100 MES (pH 6.0) / 100 HEPES (pH 7.0) / 100 TRICINE (pH 8.0), 2 $MgCl_2$, 1 EGTA.

Where indicated bath solutions were supplemented with 1µg/ml LPS (Enzo Life Sciences, Germany), GFX (10 nM, Calbiochem, Germany), Zn^{2+} (50 µM, Sigma-Aldrich, Germany), DPI (10 µM, Sigma-Aldrich, Germany).

The patch clamp pipettes were filled with either $TMASO_3$ solution containing (in mM): 80 $(CH_3)_2SO_3$, 100 MES (pH6.0) / 100 HEPES (pH 7.0) / 100 TRICINE (pH 8.0), 2 $MgCl_2$, 1 EGTA or CsCl pipette solution contained (in mM): 145 CsCl, 10 HEPES, 2 $MgCl_2$, 2 Mg-ATP, 1 EGTA.

Protocol: Depolarizing pulses lasting 4s between -80 and + 80 mV in 20mV steps, were applied from the holding potential of -80 mV.

II.II.III.III NADPH oxidase electron currents

The bath solution contained in (mM): 75 CsCl, 50 CsOH, 50 HEPES, 10 tetraethyl ammonium chloride (TEACl), 1 MgCl2, 0.1% glucose (pH 7.1 CsOH). Pipette solution for electron currents measurements contained in (mM): 75 CsCl, 50 CsOH, 50 HEPES, 10 TEACl, 1 $MgCl_2$, 1 MgATP, 8 NADPH, (pH 7.6).

Protocol: The constant current measurement was performed at the holding potential 0 mV.

II.II.IV Migration Assay

For migration assays transwell inserts and BD BioCoatTM MatrigelTM Invasion Chambers were used with a pore diameter size of 8 µm. The transwells were placed in a 24-well cell culture plate containing cell culture medium (500 µl) with or without either CXCL12 (50 ng/ml, Peprotech, for immature DCs) or CCL21 (25 ng/ml, Peprotech, for mature DCs) in the lower chamber. The upper chambers were filled with 500 µl cell culture medium containing immature or LPS (1 µg/ml, 24 h) -matured DCs either untreated or treated with one of Cl^- channel blockers for 24 h: AO1 (20 µM, Sygnature Chemical Services Ltd, Nottingham, UK) or niflumic acid (300 µM, Sigma) in a concentration of 5 x 10^4 cells/ml. The chamber was placed in a 5% CO_2 37℃ incubator for 3h. In the following step, the transwells were placed in 4% PFA for over night incubation in 4˚C, to allow the cells to fix on the membrane. Unattached cells were gently removed with cotton swab, the membrane was then mended on a slide and stained with ProLong® Gold antifade reagent with DAPI (Invitrogen). Cells from five representative areas of each membrane were counted.

II.II.V Cytokine Production

IL-6 and IL-2 concentrations in culture supernatants from DCs treated with LPS (1 µg/ml, 24 h) (for IL-6 measurements) or LPS (1 µg/ml, 18 h) and thapsigargin (50 nM, 18 h) (for IL-2 measurements) in the absence or in the presence of AO1 (20 µM, Sygnature Chemical Services Ltd, Nottingham, UK) or niflumic acid (300 µM, Sigma) were determined by using OptEIA ELISA kit (BD Pharmingen) according to the manufacturer's protocol.

II.II.VI ROS Production

ROS production in DCs was determined with use of 2',7'-dichlorodihydrofluorescein diacetate (DCFDA, Sigma-Aldrich, Germany). Cells were collected and washed once with RPMI and resuspended in fresh medium at 1x10^6/ml

density. DCs were stained with DC marker CD11c antibody (1:1000 dilution, BD Biosciences) and incubated for 1h at 37˚C. After 30 min of incubation with CD11c antibody, DCFDA was added at the final concentration of 10 µM and the cells were incubated for another 30 min. Cells were washed twice with ice-cold PBS and resuspended in FACS buffer (PBS supplemented with 0,1% FCS) and the fluorescence was analyzed by flow cytometry. The CD11c intensity was measured at FL4 and DCFDA intensity was detected at FL1. Only cells positive for both markers were analyzed.

II.II.VII Western Blot

Protein lysates were separated by SDS page 10% gel electrophoresis and transferred onto nitrocellulose membrane. Membrane containing the immobilized proteins was incubated for 1 hour at room temperature with 10% non fat milk in Tris-buffered saline-0.1% Tween 20 (TBS-T), followed by overnight incubation (4˚C) with ANO6 primary antibody (1:300 dilution in 5% non fat milk in TBS-T; Davids, Regensburg), rabbit polyclonal Hv1 (1:200, 36 kDa, Alomone Labs, Israel), rabbit monoclonal NOX2 (1:1000, 60 kDa, Epitomics, USA) or rabbit monoclonal GAPDH (1:1000, 36 kDa, Cell Signaling, USA). The following day membrane was washed 3 times in TBS-T and incubated for 1 h at room temperature with anti-rabbit (Cell Signalling) secondary antibody and washed again in TBS-T. For detection, membrane was blotted with ECL reagent (Amersham, Freiburg, Germany), exposed to X-ray film (GE Healthcare) and developed.

II.II.VIII RT-PCR

Total RNA was extracted from mouse DCs in Trizol (Peqlab, Erlangen, Germany) according to the manufacturer’s instructions. After DNAse digestion reverse transcription of total RNA was performed using random hexamers (Roche Diagnostics, Penzberg, Germany) and SuperScriptII reverse transcriptase (Invitrogen, Carlsbad, CA, USA). Polymerase chain reaction (PCR) amplification of the respective genes were set up in a total volume of 20 µl using 40 ng of cDNA, 500 nM forward and reverse primer and 2 x iTaq Fast SYBR Green (Bio-Rad, Hercules, CA, USA) according to the manufacturer's protocol. Cycling conditions were as follows: initial denaturation at 95℃ for 2 min, fo llowed by 40 cycles of 95℃ for 15 s,

55℃ for 15 s and 68℃ for 20 s. For the amplificat ion the following primers were used (5`->3`orientation):

Table 1: RT-PCR Primers sequences

Name	Forward sequence	Reverse sequence
HVCN1	TGCAAAGGAGTGCTGCAAACTA	TGCAAAGGAGTGCTGCAAACTA
ANO1	AGGAATATGAGGGCAACCTG	CGACACCATGGATTTTGGTA
ANO2	ATCCAGCCACCGTCTTCTT	ATCCAGCCACCGTCTTCTT
ANO3	TGATAAAAGAAACACATTTGAAAAGAA	AAACATGATATCGGGGCTTG
ANO4	TGGCTTCATTTTTGCTGTTCT	CCTGCTTATTTGTTTATCGATCC
ANO5	CAGGGACCACAGTGACCTTT	CAGGCGGTATATGAGGATGG
ANO6	GTATGAGGCCCAGTGCAATC	TTCCCACAGGTGGTAAATGG
ANO7	TTGGAATCCGAAATGAGGAG	GAGCTCCTGTGCCAGCTC
ANO8	CTTGGAGGACCAGCCAATC	TGAACTGGAAACACCTGCTG
ANO9	CAGAGCCCCACATTGACC	CTGGGAACTCTCATCATCCTG
ANO10	CTGATTGTGGTGGCCGTAG	TGGCAAATGCGAGTATGAAC
TATA	CAAGCTGGAGGTGATCATCG	CCACAGTGCTCTTGAATTCG

Specificity of the PCR product was confirmed by analysis of melting curves. Real-time PCR amplifications were performed on a CFX96 Real Time System (Bio-Rad). All experiments were done in duplicates. Amplification of housekeeping gene Tbp (TATA binding protein) was performed to standardize the amount of sample RNA. Relative quantification of gene expression was achieved with the ΔΔCt method (where Ct is threshold cycle) as described previously (102). In addition, PCR products were analysed by agarose gel electroporesis.

II.II.IX ANO6 silencing

Specific siRNA sequences for ANO6 (CCUCCAUCAUCAGCUUUAUAAUUAU, Invitrogen) and negative control (Silencer ® GAPDH siRNA, Ambion, USA) were synthesized and annealed by the manufacturer. siRNA transfection was carried out using the GeneSilencer siRNA transfection reagent (Genlantis, San Diego, CA,USA). 2 x 10^6 cells were washed and plated in 6-well plates in 2 ml of serum-free RPMI 1640. The ANO6 siRNA and the negative control (1000 ng/ml) were incubated with GeneSilencer reagent following the manufacturer's protocol. Transfection mixture was then added to the wells and incubated overnight. The efficiency of silencing was assessed with RT-PCR.

II.II.X Statistic

Data are provided as means ± SE, *n* represents the number of independent experiments. All data were tested for significance using Student's unpaired or paired two-tailed *t*-test or ANOVA and only results with $p < 0.05$ were considered statistically significant.

III. RESULTS

III.I Calcium activated chloride channels in dendritic cells

III.I.I Ca^{2+}-activated Cl^- channel (CaCC) currents in mouse DCs

In whole-cell patch clamp experiments we studied Ca^{2+}-dependent conductances in mouse bone marrow-derived dendritic cells (DCs) in response to an elevation of cytosolic Ca^{2+} ($[Ca^{2+}]_i$). We first permeabilized the cells with the CsCl-based pipette solution with high Ca^{2+} buffering capacity (10 mM EGTA) containing IP_3 (40 µM) in order to trigger Ca^{2+} release from the intracellular stores and the subsequent entry of extracellular Ca^{2+} through the store-operated Ca^{2+} (SOC) channels in the plasma membrane. With this pipette solution we observed a fast activation (within 1-2 min following membrane disruption) of outwardly rectifying current with a slope outward conductance of 0.37 ± 0.03nS and the reversal potential (E_{rev}) of about 0 mV (n = 60) under symmetrical Cl^- solutions (Fig. 6). Replacement of Cl^- in the bath by gluconate ('Na-gluconate bath solution') in paired experiments resulted in a strong reduction of the outward current and a shift of E_{rev} to about +40 mV (n = 22, Fig. 6), demonstrating the Cl^- selectivity of the activated current. The activated current was sensitive to a panel of Cl^- channel inhibitors of a broad spectrum, such as tannic acid (10 µM) and digallic acid (100 µM) and specific inhibitors of Ca^{2+}-activated Cl^- channels (CaCCs) (132): AO1 (20 µM) and niflumic acid (300 µM) (Fig. 6). We then removed Ca^{2+} from the bath solution in order to test whether Ca^{2+} released from internal stores was sufficient to induce CaCC currents when no extracellular Ca^{2+} entered the cells. The outwardly rectifying current was induced within 4-5 min following achievement of the whole cell configuration (Fig. 6), however the slope outward conductance was only 0.10 ± 0.03nS (n = 8), which was significantly lower (P = 0.0028) than in Ca^{2+}- containing bath. The current was inhibited by niflumic acid (300 µM, Fig. 6F).

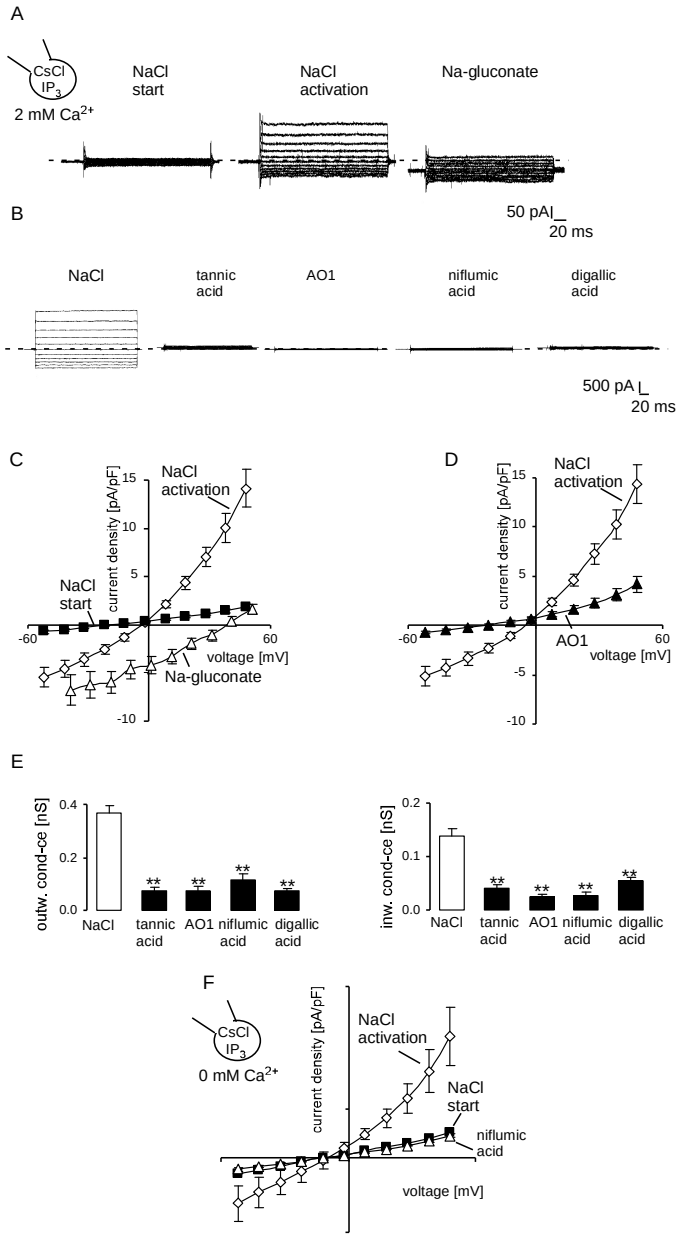

Fig. 6: Cl^- currents are activated by IP_3 in DCs.

- **A.** Current tracings from a dendritic cell (DC) recorded with inositol-1,4,5-triphosphate (IP_3, 40 µM)-containing CsCl pipette solution immediately after reaching the whole-cell mode (start, left), in 2 min upon full current activation (middle) in NaCl bath solution containing 2 mM/l $CaCl_2$ and then after substitution of bath NaCl with Na-gluconate (right). Currents were obtained in fast whole-cell voltage-clamp mode. The membrane potential was held at -30 mV and currents were elicited by 200-ms square pulses to test potentials between -50 and +50 mV in 10 mV steps; zero current is indicated by a dashed line.
- **B.** Representative current tracings recorded from DCs with IP_3-containing CsCl pipette and NaCl bath solutions upon full current activation (left) and after application of Cl^- channel blockers: tannic acid (10 µM), AO1 (20 µM), niflumic acid (300 µM) and digallic acid (100 µM). Currents were recorded as in A.
- **C.** Mean current-voltage (I-V) relations (± SE, n = 22-26) of DCs (recorded as in A) immediately after reaching the whole-cell mode (NaCl start, closed squares), in 1-2 min upon full current activation in NaCl (NaCl activation, open almonds) and in Na-gluconate (open triangles) bath solutions.
- **D.** Mean I-V relations (± SE, n = 26) of DCs recorded as in B upon full current activation (open almonds) and after application of the Cl^- channel blocker AO1 (20 µM).
- **E.** Mean outward (left) and inward (right) conductances (± SE) calculated from the individual I-V relations (as in D) by linear regression of outward current between +10 and +50 mV and of inward current between -10 and -50 mV, respectively, in DCs upon full current activation (NaCl) and after application of Cl^- channel blockers: tannic acid (10 µM, n = 15), AO1 (20 µM, n = 26), niflumic acid (300 µM, n = 7) and digallic acid (100 µM, n = 12). ** ($p<0.01$), ANOVA, Dunnett test.
- **F.** Mean current-voltage (I-V) relations (± SE, n = 6-8) of DCs recorded with IP_3-containing CsCl pipette solution and Ca^{2+}-free NaCl bath solution immediately after reaching the whole-cell mode (NaCl start, closed squares), in 4 min upon full current activation (NaCl activation, open almonds) and then upon inhibition of the current with niflumic acid (300 µM, open triangles).

To further explore the Ca^{2+} dependence of detected currents we exposed DCs to the Ca^{2+} ionophore ionomycin in Ca^{2+} containing and Ca^{2+} free extracellular solutions (Fig. 7). These and following patch-clamp experiments, to study CaCCs, were performed using pipette and bath solutions containing NMDG as a Na^+ and K^+ replacement, and Cl^- as the major permeable ion ('NMDG-Cl pipette and bath solutions'). In the presence of extracellular Ca^{2+}, ionomycin (1 µM) induced fast outwardly rectifying current activation (Fig. 7A). After full current activation was reached, the Ca^{2+} containing extracellular solution was replaced in paired experiments with a nominally Ca^{2+} free solution (0 Ca^{2+}, 10 mM EGTA, Fig. 7A). The Ca^{2+} removal was followed by a significant decline, in both, outward and inward currents (Fig. 7A), indicating that elevated intracellular Ca^{2+} via the Ca^{2+} ionophore was responsible for the Cl^- current activation. Readdition of Ca^{2+} into the bath solution led to reactivation of the current, which was subsequently inhibited, with niflumic acid (300 µM, Fig. 7A, C). Therefore, mouse DCs express functional CaCCs.

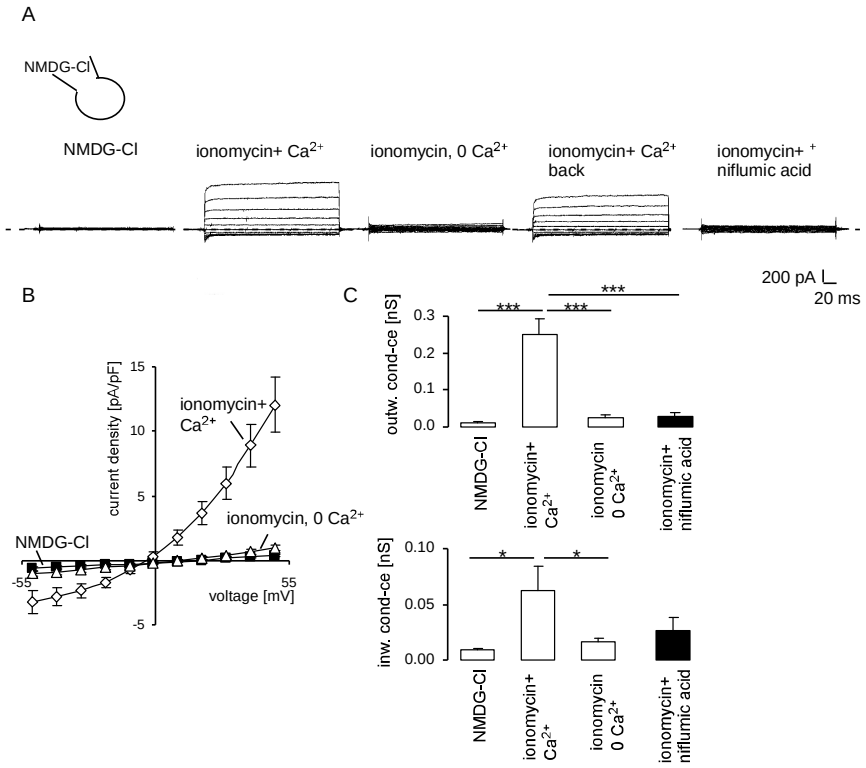

Fig. 7: Cl^- currents are activated by ionomycin-induced Ca^{2+} increase in DCs.

A. Current tracings from a DC recorded with NMDG-Cl pipette solution before (1st trace) and after application of ionomycin (1 µM) in Ca^{2+}-containing (2 mM $CaCl_2$, 2nd and 4th traces), in Ca^{2+}-free (10 mM EGTA, 3rd trace) and in Ca^{2+}- and niflumic acid (300 µM)-containing (last trace) NMDG-Cl bath solution.

B. Mean I-V relations (± SE, n = 11-18) of DCs recorded as in A before (NMDG-Cl, closed squares) and after application of ionomycin (1 µM) in Ca^{2+}-containing (ionomycin + Ca^{2+}, open almonds) and then in Ca^{2+}-free (ionomycin, 0 Ca^{2+}, open triangles) NMDG-Cl bath solution.
Mean outward (upper panel) and inward (lower panel) conductances (± SE, n = 11-18) calculated from the individual I-V relations (as in B) by linear regression of outward current between +10 and +50 mV and of inward current between -10 and -50 mV, respectively, in DCs before (NMDG-Cl) and after application of ionomycin (1 µM) in Ca^{2+}-containing (ionomycin + Ca^{2+}), in Ca^{2+}-free (ionomycin, 0 Ca^{2+}) and in Ca^{2+}- and niflumic acid (300 µM)-containing (ionomycin+niflumic acid) NMDG-Cl bath solution. * ($p<0.05$) and *** ($p<0.001$), ANOVA, Bonferroni test.

To explore whether CaCCs are activated by physiological stimuli, additional experiments were performed with the chemokine CCL21, a ligand of CCR7 chemokine receptor expressed on DC cell membrane, which triggers chemotactic responses and guides mature DCs to the T zones of secondary lymphoid organs (75). It has been shown that CCR7 stimulation leads to an increase of $[Ca^{2+}]_i$ in DCs (9). According to patch clamp experiments, CCL21 applied to the bath solution in the concentration of 75 ng/ml, which is known to activate Ca^{2+} entry in DCs (9) activated CaCCs in 75% of measured cells. The currents were rapidly activated by CCL21, showed a very strong outward rectification and a fast rundown (Fig. 8A). Upon stabilization of currents after primary activation, Cl^- in the bath was substituted by gluconate, which resulted in a strong decrease of the outward currents and a shift of E_{rev} towards positive potentials, indicating Cl^- selectivity of CCL21-activated current (Fig. 8A). The outward currents were restored on return to Cl^- bath solution to the levels at which they stabilized after primary activation (Fig. 8A).

III.I.II Store-operated Ca^{2+} entry is suppressed by Cl^- channel inhibitors in DCs

The outwardly rectifying CaCC currents in DCs may provide a positive feedback for the Ca^{2+} entry by maintaining the negative membrane potential and providing the necessary electrical driving force. Since the principal Ca^{2+} entry mechanism in DCs is the store-operated Ca^{2+} (SOC) channels (8, 50, 82), membrane hyperpolarization would enhance the Ca^{2+} signal. Utilizing the Ca^{2+} ratiometric dye Fura-2/AM we tested whether the increase of cytosolic Ca^{2+} concentrations ($[Ca^{2+}]_i$) upon intracellular store depletion in DCs was sensitive to inhibition of CaCCs by AO1 (20 µM) and niflumic acid (300 µM). To this end the intracellular stores were emptied by removal of Ca^{2+} from the extracellular environment in the presence of the sarco-endoplasmic reticulum Ca^{2+}-ATPase (SERCA) inhibitor thapsigargin. As a result, AO1 and niflumic acid did not significantly modify the Ca^{2+} release from the stores (Fig. 9), but significantly blunted the $[Ca^{2+}]_i$ increase upon readdition of Ca^{2+} to the extracellular solution, reflecting Ca^{2+} influx through SOC channels. Both, the amplitude (analyzed as peak, (Fig. 9B) and the velocity (analyzed as slope, Fig. 9B) of the $[Ca^{2+}]_i$ increase were significantly decreased by the inhibitors.

Similarly, when SOC activation in DCs was induced through a physiological stimulus, the chemokine CCL21 (9), CCL21-induced $[Ca^{2+}]_i$ increase was strongly impaired in DCs treated with AO1 (20 µM) or niflumic acid (300 µM) (Fig. 9C, D).

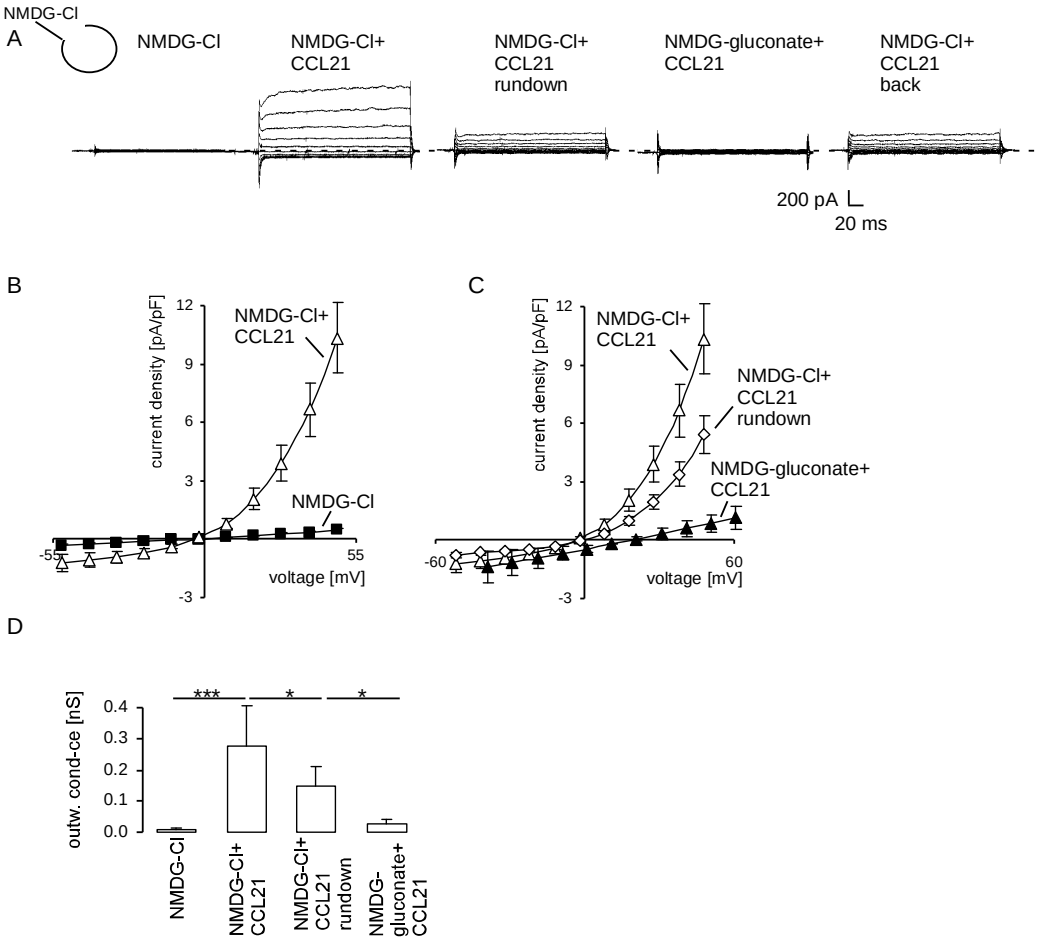

Fig. 8: Cl^- currents are activated by CCL21 in DCs.

- **A.** Current tracings from a DC recorded with NMDG-Cl pipette solution before (1st trace) and after application of CCL21 (75 ng/ml, 2nd,3rd and 5th traces) 30 s (2nd trace) and 4 min (3rd trace, showing current rundown) after CCL21 application in NMDG-Cl bath solution, after substitution of bath NMDG-Cl with NMDG-gluconate (4th trace) and after a wash-out of Na-gluconate with NMDG-Cl (5th trace).
- **B.** Mean I-V relations (± SE, n = 9) of DCs (recorded as in A) before (NMDG-Cl, closed squares) and 30 s after (NMDG-Cl+CCL21, open triangles) application of CCL21 (75 ng/ml) in NMDG-Cl bath solution.
- **C.** Mean I-V relations (± SE, n = 2-9) of DCs (recorded as in A) 30 s (NMDG-Cl+CCL21, open triangles) and 4 min (NMDG-Cl+CCL21 rundown, open almonds) after application of CCL21 (75 ng/ml) in NMDG-Cl bath solution and after substitution of bath NMDG-Cl with NMDG-gluconate (NMDG-gluconate+CCL21, closed triangles).
  Mean outward conductances (± SE, n = 2-9) calculated from the individual I-V relations (as in B and C) by linear regression of the current between +10 and +50 mV in DCs before (NMDG-Cl) and after application of CCL21 (75 ng/ml) 30 s (NMDG-Cl+CCL21) and 4 min (NMDG-Cl+CCL21 rundown) after CCL21 application in NMDG-Cl bath solution and after substitution of bath NMDG-Cl with NMDG-gluconate (NMDG-gluconate+CCL21). * ($p<0.05$) and *** ($p<0.001$), ANOVA, Bonferroni test.

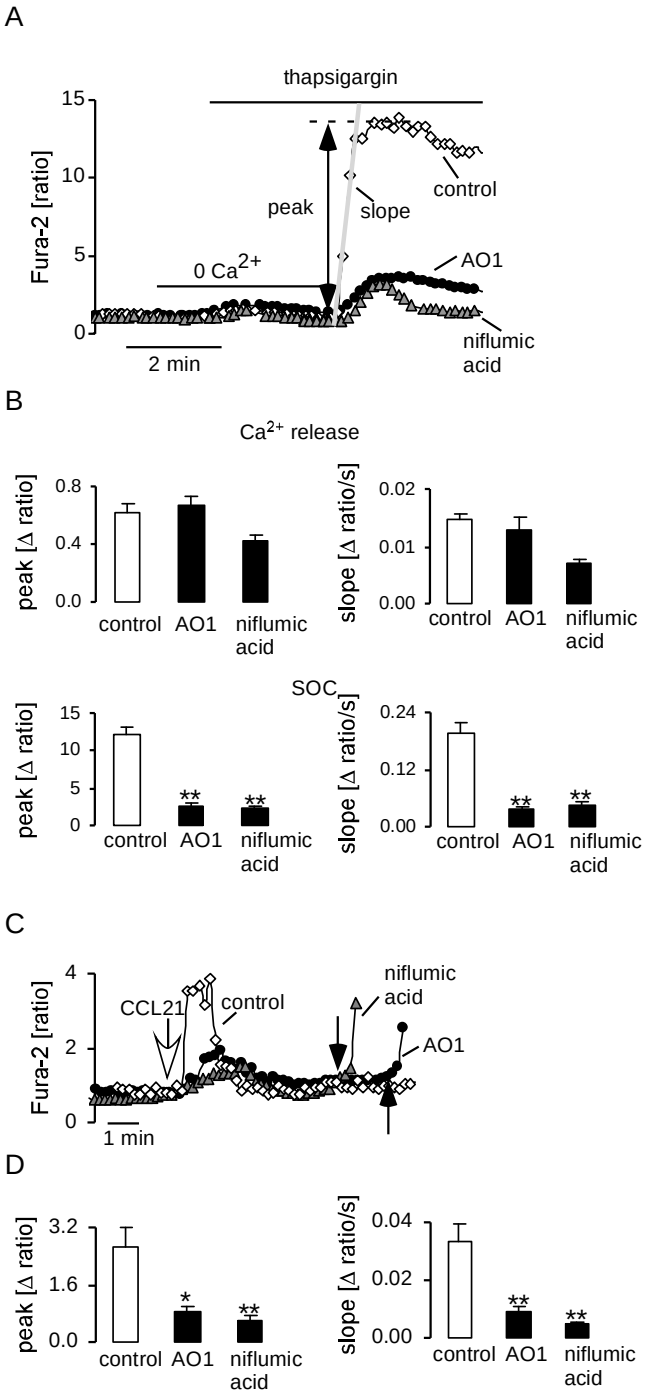

Fig. 9: Inhibition of Ca^{2+}-activated Cl^- channels attenuates the store-operated Ca^{2+} entry in DCs.

- **A.** Time course of the mean ratio between the 340 nm- and the 380 nm-excited Fura-2 fluorescence as a measure of the cytosolic free Ca^{2+} concentration. Ratios were recorded in control and AO1 (20 µM, 30 min)- or niflumic acid (300 µM, 30 min)- pretreated DCs during removal and re-addition of external Ca^{2+} upon Ca^{2+} store depletion induced by the SERCA pump inhibitor thapsigargin (1 µM). For quantification of Ca^{2+} entry the slope (Δ ratio/s) and peak (Δ ratio) of $[Ca^{2+}]_i$ increase were calculated. At the end of each experiment ionomycin (10 µM) was added for calibration purposes.
- **B.** Mean (± SE) of the peak value (left) and slope (right) of the change in Fura-2 fluorescence following addition of thapsigargin to the bath solution in the absence (Ca^{2+} release, upper bars) and presence (SOC, lower bars) of Ca^{2+} in control (open bar) and AO1 (20 µM, 30 min)- or niflumic acid (300 µM, 30 min)-pretreated DCs. ** ($p<0.01$), ANOVA, Dunnett test.
- **C.** Representative original tracings showing the Fura-2 fluorescence ratios (340/380 nm) in Fura-2/AM loaded control and AO1 (20 µM, 30 min)- or niflumic acid (300 µM, 30 min)- pretreated DCs prior to and following acute addition of CCL21 (75 ng/ml; white arrow). At the end of each experiment ionomycin (10 µM; black arrows) was added for calibration purposes.
- **D.** Mean (± SE) of the peak value (left) and slope (right) of the change in Fura-2 fluorescence following addition of CCL21 to the bath solution in control (open bar) and AO1 (20 µM, 30 min)- or niflumic acid (300 µM, 30 min)-pre-treated DCs. * ($p<0.05$) and ** ($p<0.01$), ANOVA, Dunnett test.

III.I.III Migration of DCs is highly dependent on CaCC activity

It is well established that both immigration of immature DCs into the peripheral tissues as well as emigration to secondary lymphoid sites following microbial challenge are Ca^{2+}-dependent processes (109, 121), which require activity of SOC channels (82, 141). Since CaCCs seem to be involved in Ca^{2+} homeostasis in DCs, we further analyzed the influence of CaCC-specific inhibitors AO1 and niflumic acid on migration of immature and mature DCs. To induce DC maturation, cells were incubated with LPS (1 µg/ml) for 24h prior to assay performance. Migration was tested in both, the absence and presence of the chemokines CXCL12 (50 ng/ml) in immature DCs and CCL21 (25 ng/ml) in LPS-matured cells. In a transwell migration assay both, spontaneous and chemokine-induced, migration of immature and mature DCs was strongly impaired by the CaCC-specific blockers AO1 (20 µM) and niflumic acid (300 µM) (Fig. 10).

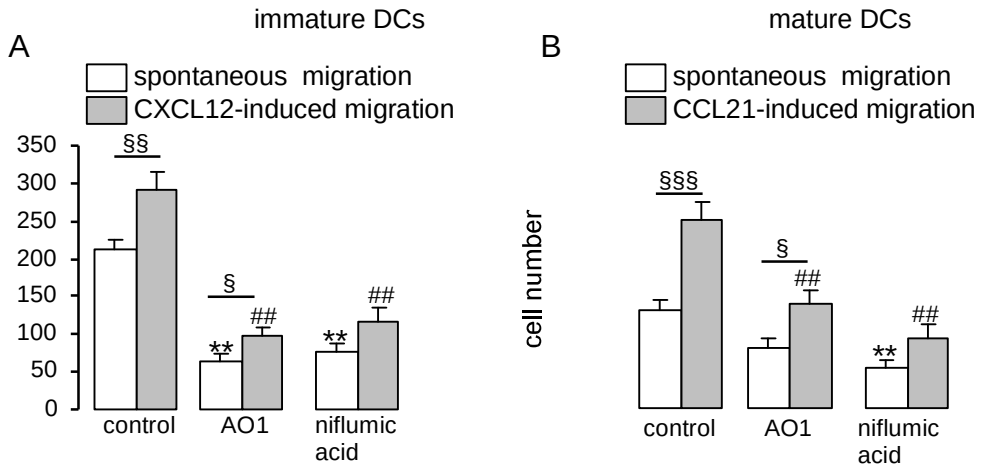

Fig. 10: Dendritic cells migration was strongly inhibited by treatment with CaCC channels blockers.

A.Number (± SE, n = 15-65) of spontaneously migrating DCs (open bars) and DCs migrating towards the chemokine CXCL12 (50 ng/ml, grey bars) measured in transwell migration assay with and without Cl^- channel inhibitors: AO1 (20 µM) and niflumic acid (300 µM) DCs were preincubated with channel inhibitors for 24 h. ** ($p<0.01$) shows difference from control spontaneously migrated DCs, ## ($p<0.01$) shows difference from control DCs migrated towards CXCL12, § ($p<0.05$) and §§ ($p<0.01$) show difference between indicated groups, ANOVA.
B.Number (± SE, n = 15-65) of spontaneously migrating mature DCs (open bars) and mature DCs migrating towards the chemokine CCL21 (25 ng/ml, grey bars) measured in transwell migration assay with and without Cl^- channel inhibitors: AO1 (20 µM) and niflumic acid (300 µM). Maturation of DCs was induced by LPS (1 µg/ml, 24 h). DCs were preincubated with channel inhibitors for 24 h. ** ($p<0.01$) show difference from control spontaneously migrated DCs, ## ($p<0.01$) shows difference from control DCs migrated towards CCL21, § ($p<0.05$) and §§§ ($p<0.001$) show difference between indicated groups, ANOVA.

III.I.IV CaCCs control cytokine secretion of DCs

Release of several cytokines in DCs has been demonstrated to be a Ca^{2+} dependent process (82, 87, 141, 144). Therefore the possibility was explored that cytokine secretion in DCs also fell under CaCC control. We analyzed Ca^{2+}-dependent cytokines IL-2 (144) and IL-6 (130) in supernatants collected from DCs treated with LPS (1 µg/ml, 24 h for IL-6 assay) or LPS (1 µg/ml) with thapsigargin (50 nM, 18 h for IL-2 assay), which is a strong stimulus for IL-2 production (144), in the presence or absence of AO1 (20 µM) or niflumic acid (300 µM). Secretion of IL-2 and IL-6 was significantly decreased by treatment with AO1 or niflumic acid (Fig. 11). We also checked levels of others cytokines, IL-12, IL-10 and TNFα, but no significant difference between AO1- or niflumic acid- treated and untreated cells was detected (data not shown).

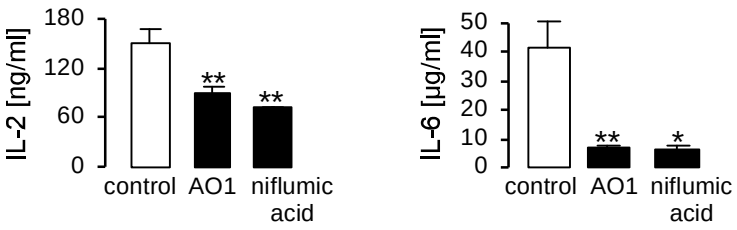

Fig. 11: Production of cytokines showes sensitivity to Cl^- channels blockers

Production of IL-2 (left) and IL-6 (right) (± SE, n = 7-10) as induced by DC incubation with LPS (1 µg/ml) + thapsigargin (50 nM) for 18 h (IL-2) or LPS (1 µg/ml) for 24 h (IL-6) in the absence (control, open bars) or presence of AO1 (20 µM, closed bars) or niflumic acid (300 µM, closed bars). * ($p<0.05$), ANOVA.

III.I.V Expression of mRNA of Anoctamin family of proteins in dendritic cells

Some of the members of the Anoctamin (ANO) protein family have been identified as Ca^{2+}-activated Cl^- channels (21, 117, 126, 128, 142). To explore whether ANO channels are expressed in DCs and could contribute to or account for the detected CaCC conductances, we performed RT-PCR analysis with primers specific for all ten members of the ANO family. RT-PCR revealed mRNA expression of ANO6, ANO8 and ANO10 in mouse DCs (Fig. 12A) with ANO6 having the highest expression level (Fig. 12B). Among these ANO members only ANO6 has been shown to generate a Ca^{2+}-activated Cl^- channel (115). Accordingly, western bloting was performed with ANO6 antibodies and demonstrated that ANO6 protein was indeed expressed in mouse DCs (Fig. 12C).

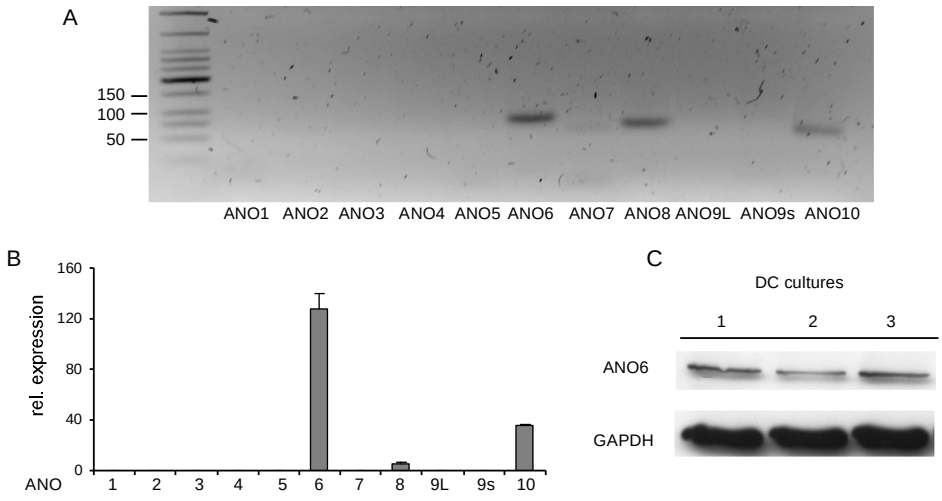

Fig. 12: Expression of Anoctamins in mouse DCs.

A. Agarose gel with PCR products specific for Anoctamins 1-10 amplified from cDNA isolated from mouse DCs.
B. ANO1-10 mRNA levels (± SE, n = 3) determined after isolation from mouse DCs and assessed by real-time PCR using TBP mRNA as a reference gene.
C. Western Blot analysis of ANO6 expression in whole cell protein lysates extracted from mouse DCs

III.I.VI Knock-down of ANO6 reveals that it accounts for CaCC conductances in DCs

Next we performed whole-cell patch clamp experiments in DCs in which ANO6 was silenced with ANO6-siRNA. Knock-down efficiency was about 61% as tested with real-time RT-PCR. Within 1-2 min following membrane disruption in experiments using IP_3 -containing pipette solution, about 80% of control cells demonstrated outwardly rectifying currents sensitive to AO1 (Fig. 13). In contrast about 70% of DCs (15 out of 22 cells) with silenced ANO6 showed no development of AO1-sensitive outwardly rectifying currents within 5-10 min of recording (Fig. 13). In 7 out of 22 measured DCs with silenced ANO6 normal CaCC currents indistinguishable from control DCs were observed.

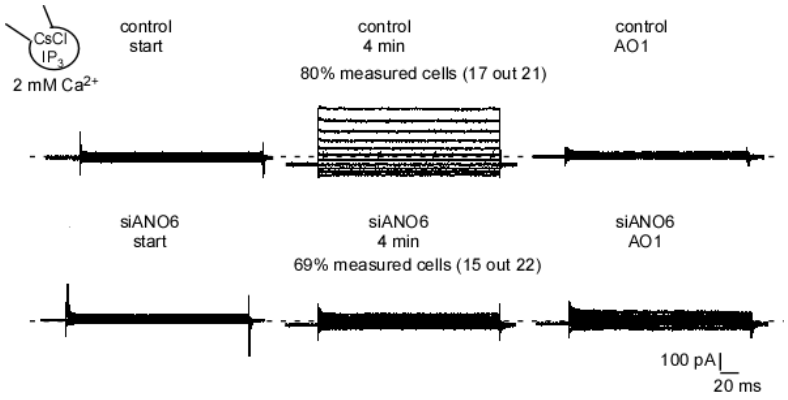

Fig. 13 : Knockdown of ANO6 inhibits CaCC currents in DCs.

Current tracings recorded with IP_3-containing CsCl pipette and NaCl bath solutions immediately after reaching the whole-cell mode (start, left), upon full current activation (activation, middle) and after application of CaCC blocker AO1 (20 µM) in control DCs (upper panel, representative for 80% (17 out of 21) measured cells) and in siANO6-DCs (lower panel, representative for 69% (15 out of 22) measured cells). The efficiency of knockdown was 61%. A dashed line indicates zero current.

III.I.VII Migration of DCs is dependent on ANO6 activity

Since DC migration was extremely sensitive to CaCC blockers, we further analyzed migration of immature and mature DCs upon silencing of ANO6. To induce DC maturation, cells were incubated with LPS (1 µg/ml) for 24h prior to assay performance. Migration was tested in both, the absence and presence of the chemokines CXCL12 (50 ng/ml) in immature DCs and CCL21 (25 ng/ml) in LPS-matured cells. In a transwell migration assay chemokine-induced migration of both immature and mature DCs was strongly impaired by siRNA for ANO6 (Fig. 14).

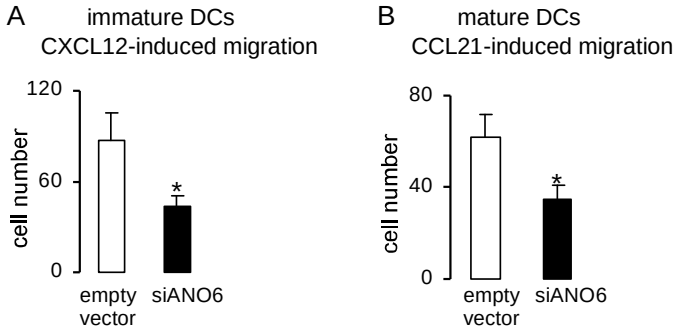

Fig. 14: Chemokine-induced DC migration is inhibited by knock-down of ANO6.

A. Number (± SE, n = 17-26) of immature (A) or mature (B) DCs migrating towards the chemokine CXCL12 (50 ng/ml, A) or CCL21 (25 ng/ml, B), respectively, measured in transwell migration assay with control (empty vector-transfected, open bars) and siANO6-DCs (closed bars). Maturation of DCs was induced by LPS (1 µg/ml, 24 h). The data are corrected for spontaneous migration. * ($p<0.05$), unpaired two-tailed *t*-test.

III.II Proton channels

III.II.I Proton currents in DCs

In order to determine whether mouse bone marrow-derived DCs express functional H^+ channels, patch clamp whole-cell experiments were performed with TMA^+-based pipette and bath solutions containing 100mM buffer. Depolarizing pulses lasting 4s between -80 and + 80 mV were applied from the holding potential of -80 mV in 20 mV steps at 40s intervals. Fig. 15 shows typical slowly activating outward currents and the mean current-voltage (I/V) relationships obtained at the end of 4s pulses measured with intracellular pH (pH_i) of 6.0 (Fig. 15 A, C) and pH_i of 7.0 (Fig. 15B) and extracellular pH (pH_o) of 6.0, 7.0, and 8.0. The current amplitude increased with increasing pH gradient between pH_o and pH_i (ΔpH). The threshold voltage for the current activation ($V_{treshold}$) shifted in general 40mV per unit pH, towards more negative potentials, and was close to the threshold voltage predicted by the formula $V_{Threshold}$= 20 – 40 x ΔpH with ΔpH= pH_o - pH_i . The currents were sensitive to 50 µM Zn^{2+}, a known inhibitor of H^+ channels (Fig. 15C).

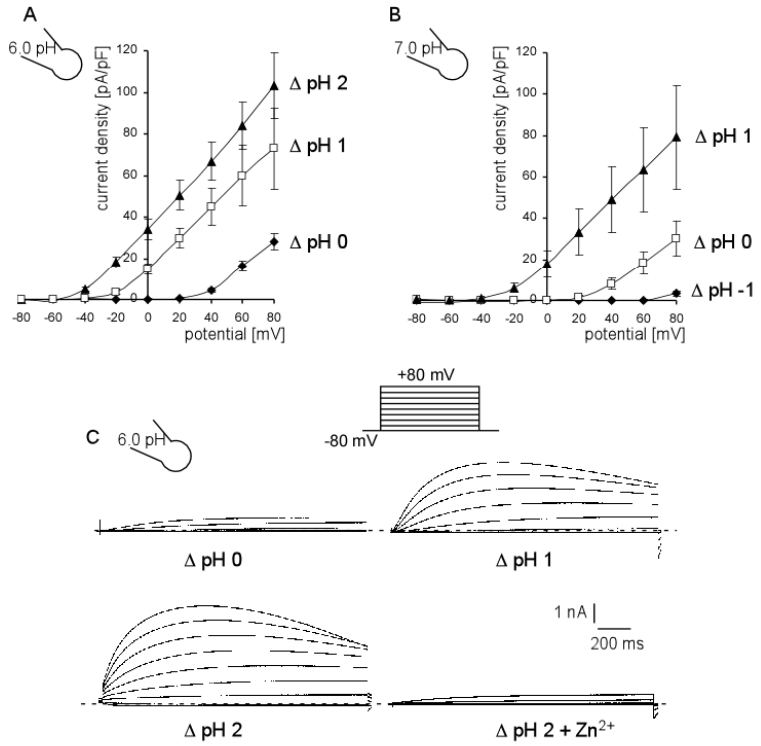

Fig. 15: Proton currents in DCs.

Mean I/V curves (± SE, n = 7-28) from mouse DCs recorded at pH_i 6.0 (**A**) or pH_i 7.0 (**B**) in the pipette solution and various bath pH_o values (6.0, 7.0, 8.0) and original current tracings obtained at pipette pH_i 6.0 and bath pH_o 6.0, 7.0, and 8.0 and finally after application of Zn^2 (50 µM) to the bath solution (C). The voltage protocol is shown (not to scale), whereby cells were held at -80 mV and voltage steps were applied in 20 mV increments for 4 s from -80 mV to +80 mV at 40 s intervals. A dashed line indicates zero current

The corresponding conductance-voltage (G/V) curves are shown in Fig. 16 A and B. The chord conductance reached a limiting maximum when ΔpH was ≥ 1. The activation threshold $V_{treshold}$ was similar at the same ΔpH when measured with pH_i 6.0 and pH_i 7.0. Fig. 16C shows the analysis of time-dependent activation of the H^+ currents in DCs. The mean activation time constant (τ_{act}) was calculated from the fitting of the current tracings measured at pH_i of 6.0 and pH_o of 6.0, 7.0, and 8.0 with a monoexponential growth function. The τ act decreased (i.e. the faster activation) with stronger depolarization and increasing ΔpH (Fig. 16C).

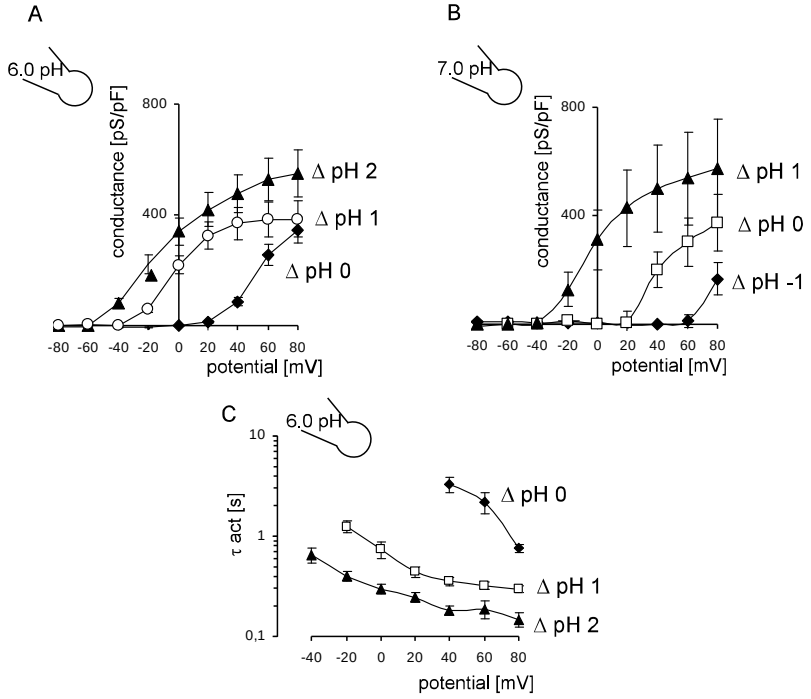

Fig 16: Analysis of G/V relationship and τ of activation of proton currents in DCs.

A,B. Mean conductance/voltage (G/V) relations (± SE, n = 7-28) at pipette pH_i 6.0 (A) and pH_i 7.0 (B) and various bath pH_o (6.0, 7.0, 8.0) values as calculated from the data in Fig. 15A and Fig. 15B, respectively, assuming reversal potential at E_H.
C. Mean time constant of activation (τ_{act}± SE, n = 12-24) determined by fitting monoexponential growth functions to the current tracings recorded at pH_i 6.0 and pH_o 6.0, 7.0, 8.0 upon cell depolarization to potentials between -40 mV and +80 mV as a function of membrane potential

In order to estimate the reversal potential (E_{rev}), tail currents were measured at pH i 6.0 and various pH_o (6.0, 7.0, 7.5 and 8.0) (Fig. 17A, B). Plotting E_{rev} against ΔpH and fitting the data by linear regression yielded a slope of -38 mV/ΔpH, indicating a 38 mV shift in E_{rev} per pH unit, which differs from the theoretical equilibrium potential calculated with the use of the Nernst equation of -58 mV. However, the measured channels were highly selective for H^+ with a permeability ratio P_{H+}/P_{TMA+} of 1.94 x 10^6 at ΔpH = 2.0, calculated with the Goldman-Hodgkin-Katz equation.

The time constant of deactivation (τ_{tail}) obtained by fitting the tail currents with a monoexponential decay function showed an exponential dependence on the voltages and changed e-fold every 22.5 ± 0.6 mV (Fig. 17C). Finally, Hv1 mRNA and protein are expressed in bone marrow derived DCs, as demonstrated by RT-PCR and western blott analysis (Fig. 17D). All together these data allow concluding that DCs express functional H^+ channels.

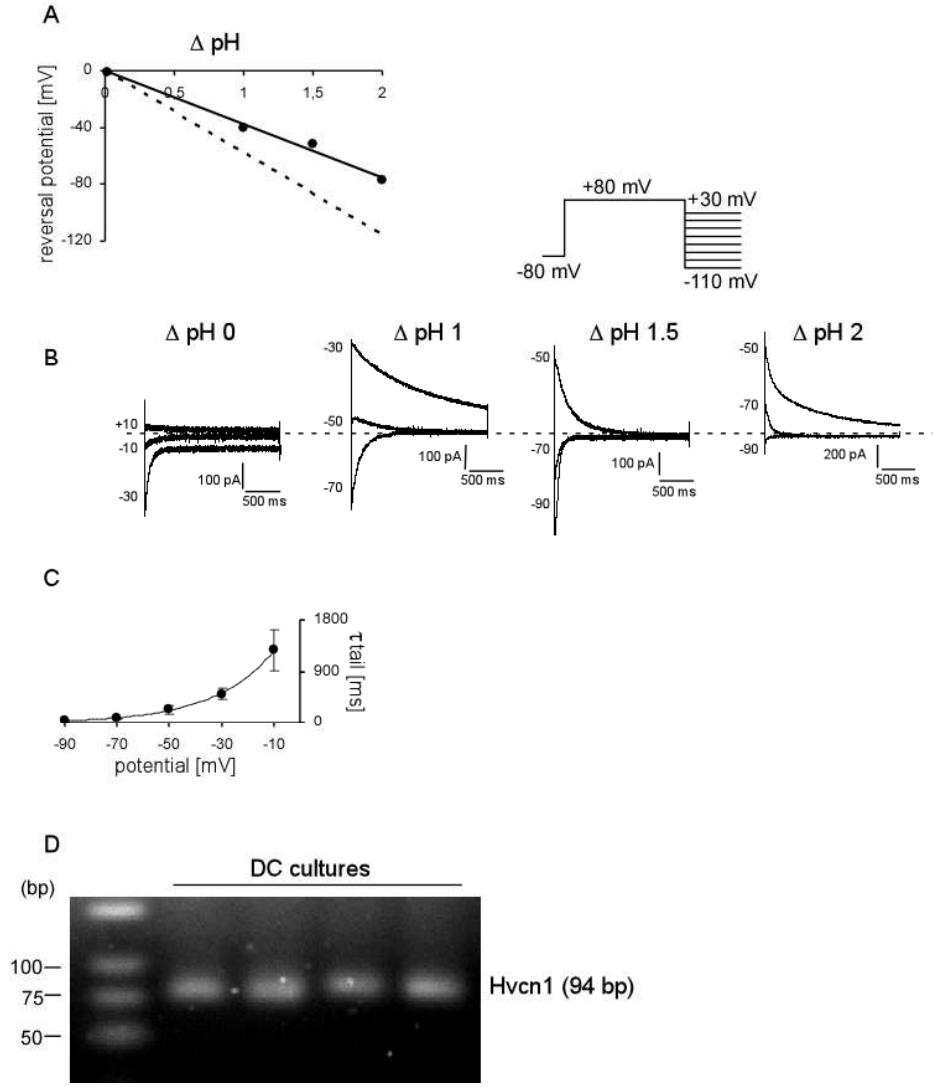

Fig 17: Analysis of Hv1 channel tail currents.

A,B. Mean values of the reversal potential (± SE, n = 4-6) as a function of ΔpH determined by tail currents at pH_i 6.0 in the pipette solution and bath pH_o values of 6.0, 7.0, 7.5, 8.0. Data were fitted by linear regression with a slope of -38 mV/pH unit. The equilibrium Nernst potential for H^+ with a slope of -58 mV/pH unit is shown by the dashed line. To record tail currents, depolarizing prepulse was given to +80 mV for 2 s, after which the membrane potential was clamped to -110 mV - +30 mV. Original tail currents at ΔpH 0, 1, 1.5 and 2.0 (B).
C. Mean time constant of deactivation (τ_{tail} ± SE, n = 6-9) determined by fitting the tail currents measured at -10 mV to -90 mV by a monoexponential decay function.
D. Agarose gel with PCR products specific for Hvcn1 amplified from cDNA isolated from 4 different cultures of mouse DCs. Specificity of the PCR product was confirmed by analysis of melting curves, and the right size of the products was confirmed by the agarose gel.

III.II.II Lipopolisaccharide regulation of proton currents in DCs

H^+ currents in DCs were extremely sensitive to the maturation stimulus, such as lipopolysaccharides (LPS), ligands of toll like receptors 4 (TLR4). When the full-blown maturation was induced by 24 h treatment with LPS (1 µg/ml), the amplitude of H^+ currents in DCs was strongly decreased (Fig. 18A, B). At the same time LPS-matured DCs significantly decreased the production of reactive oxygen species (ROS) as measured by FACS with ROS - sensitive dye DCFDA (10µM) (Fig. 18 C). The decline of the H^+ currents was paralleled with a decrease in the transcript abundance of Hv1, as assessed by quantitative RT-PCR (Fig. 18D). However, no change in Hv1 protein level was observed (Fig. 18E). Expression of NOX2 was not significantly different in LPS-matured DCs if compared to immature cells (Fig. 18D, E).

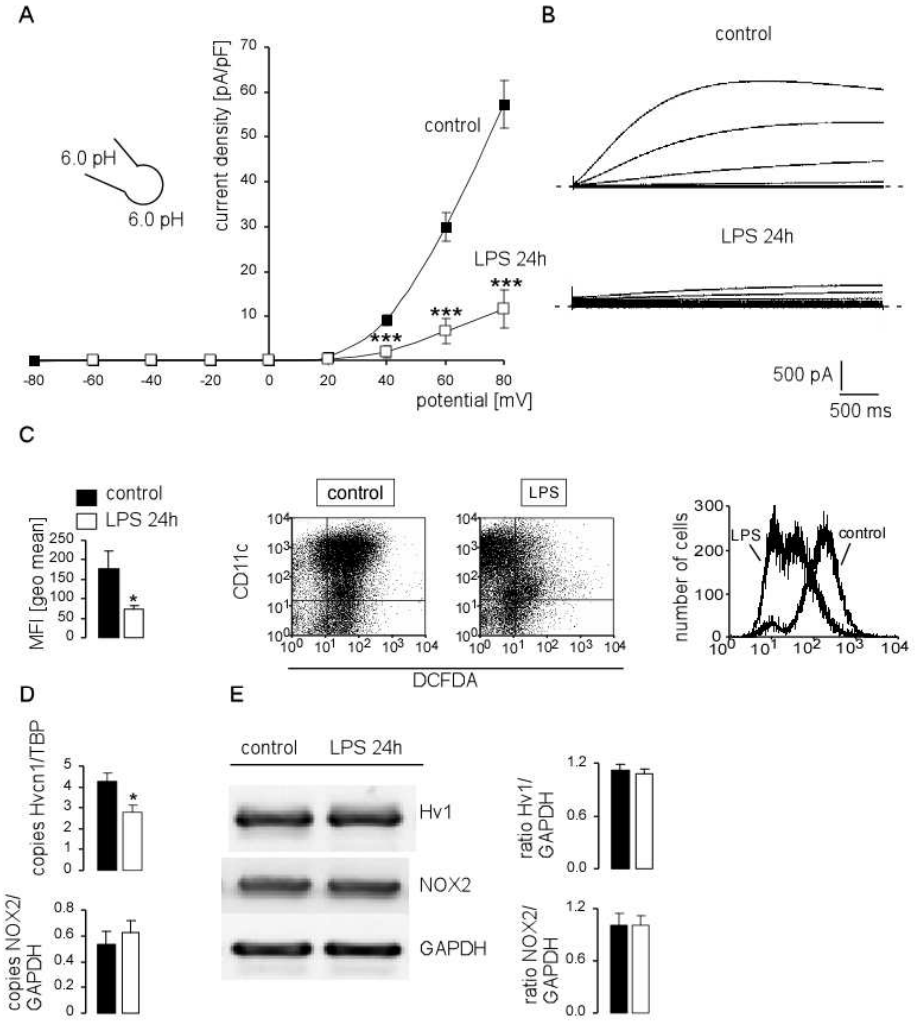

Fig. 18: LPS matured DCs show proton currents inhibition and decreased ROS production.

A,B. Mean I/V curves (± SE, A) and original current tracings (B) of immature (control, n=20) and LPS (1 µg/ml, 24 h, n=12)-matured DCs measured at pH 6.0 in pipette and bath solution. *** (p<0.001), two-tailed unpaired *t*-test. Zero current is indicated by dashed line.
C. Reactive oxygen species (ROS) production, analyzed as mean fluorescent intensity (MFI ± SE, n = 17, left) in immature (control) and LPS (1 µg/ml, 24 h) –matured DCs measured from ROS-dependent DCFDA fluorescence by FACS. * (p<0.05), Welch-corrected two-tailed unpaired *t*-test. Original dot plots of $CD11c^+$ DCFDA (middle) and histograms of DCFDA fluorescence on $CD11c^+$ cells (right) in a representative experiment.
D. Hvcn1 (top) and NOX2 (bottom) mRNA levels (± SE, n = 3-7) determined after isolation from immature (control) and LPS (1 µg/ml, 24 h) –matured DCs and assessed by real-time PCR using TBP or GAPDH mRNA as a reference gene. * (p<0.05), two-tailed unpaired *t*-test.
E. Representative western blot showing Hv1, NOX2 and GAPDH as a loading control (left) and mean Hv1/GAPDH and NOX2/GAPDH protein ratio (± SE, n = 7, right) in immature (control) and LPS (1 µg/ml, 24 h) –matured DCs.

However, an early triggering of TLR4 with LPS is known to transiently increase the phagocytic abilities of DCs (139). Consistently, we analyzed the H^+ currents upon acute application of LPS under more "physiological" conditions: with CsCl in the pipette and NaCl in the bath and ΔpH = 0.2. Under these conditions the threshold voltage of activation $V_{threshold}$ was about +20 mV in the absence of LPS, which was slightly more positive than the $V_{treshold}$ predicted by the formula (+12 mV) (Fig. 19A). Addition of LPS (1µg/ml) to the bath solution caused a significant increase of the

outward Zn^{2+} (50µM)-inhibited conductance and a shift of the $V_{threshold}$ towards more negative potentials (Fig. 19A,B). Stimulation of H^+ currents by LPS required functional PKC, since inhibiting PKC with GFX (10nM) abolished this effect (Fig. 19C).

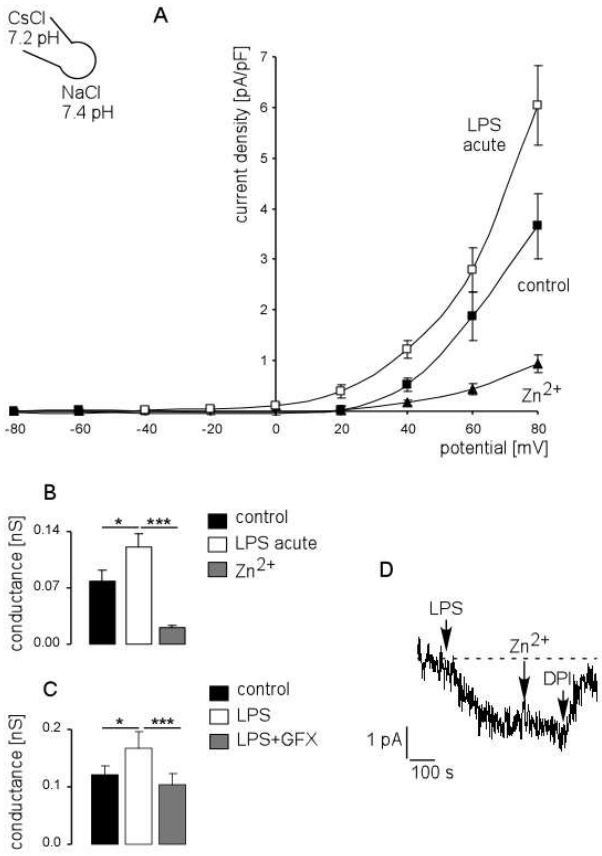

Fig. 19: Acute LPS treatment stimulated enhanced Hv1 gating and NOX2 electron currents.

A. Mean I/V curves (± SE, n = 19) of immature DCs measured with CsCl pipette (pH 7.2) and NaCl bath (pH 7.4) solutions before (control) and after application of LPS (1 µg/ml) first in the absence (LPS acute) and then in the presence of Zn^{2+} (50 µM).
B. Mean current conductance (± SE, n = 19) calculated from individual I/V curves as in A by linear regression of the current between +40 and +80 mV. * ($p<0.05$) and *** ($p<0.001$), ANOVA.
C. Mean conductance (± SE, n = 11) calculated from individual I/V curves by linear regression of the current between +40 and +80 mV obtained in paired experiments before (control) and after application of LPS (1 µg/ml) in the absence (LPS) and in the presence (LPS+GFX) of PKC inhibitor GFX (10 nM). * ($p<0.05$) and *** ($p<0.001$), repeated measures ANOVA.
D. Original whole-cell inward currents generated by NADPH oxidase upon application of LPS (1 µg/ml) in DCs. The measurements were performed in the presence of 300 µM niflumic acid and with the 'reversed' pH gradient (pH_i of 7.6 and pH_o of 7.1). Where indicated, Zn^{2+} (50 µM, to exclude the contribution of H^+ channels) and NADPH oxidase inhibitor DPI (20 µM) was added to the bath solution. CsCl-based bath and CsCl-based pipette solution, containing 8 mM NADPH, were used, the holding potential was 0 mV. Zero current is indicated by dashed line.

III.II.III Lipopolisaccharide regulation of NOX2 electron currents in DCs

At the same time NOX2 activation could be observed by the appearance of LPS-induced electron currents. In order to measure electron currents, the experimental conditions were designed to minimize the currents through other channels and transporters (116). The measurements were performed in the presence

of 300µM niflumic acid, to avoid the contribution of Cl^- currents. Furthermore, the 'reversed' pH gradient (ph_i of 7.6 and pH_o of 7.1) and the 0mV holding potential allowed to exclude H^+ currents. The measured currents were indeed not modified by addition of 50µM Zn^{2+} to the bath solutions (Fig. 19D). The mean electron current density at 0mV was 0.16 ± 0.03 pA/pF, (n=9), measured with the pipette solution containing NADPH (8mM) (Fig. 19D). These currents were inhibited by the NOX2 blocker diphenylene iodonium (DPI, 10µM, Fig. 19D). Immature human DCs under phorbol-12-myristate-13-acetate (PMA) stimulation generate superoxide anions ($O_2\cdot^-$) in approximate amounts of 2nM $O_2\cdot^-$ per min per 10^6 cells (116). When translated into electron currents, NADPH oxidase should transport ~2 x 10^7 electrons per second per cell, giving the rough estimate of the expected inward currents with the amplitude of 2-4pA (116), which is in agreement with our measurements (Fig. 19D).

IV. DISCUSSION

IV.I Calcium activated chloride channels

Our study is the first one to identify Ca^{2+}-activated Cl^- channel (CaCC) ANO6 in DCs and to examine its role in DC function. In whole-cell patch clamp experiments performed on mouse DCs, we demonstrated outwardly rectifying Cl^- conductance activated by elevation of cytosolic Ca^{2+}, triggered either by the ionophore ionomycin in the presence of extracellular Ca^{2+}, or by IP_3-dependent Ca^{2+} mobilization. Moreover, we detected a physiological mechanism of CaCC activation in DCs upon stimulation of the chemokine receptor CCR7. Recorded currents show all the hallmarks of endogenous CaCCs. Like in neurons (56), cardiomyocytes (47) and *Xenopus laevis* oocytes (66, 67) both, Ca^{2+} entry from extracellular environment and Ca^{2+} release from intracellular stores, were able to activate CaCCs in DCs.

When Ca^{2+}-activated Cl^- currents were induced by the chemokine CCL21, the current-voltage (I-V) relationship showed stronger outward rectification, if compared to more linear I-V curves when the trigger was the Ca^{2+} ionophore ionomycin or IP_3 in the pipette solution. This was consistent with previously described features of CaCCs, that the outward rectification is lost with higher $[Ca^{2+}]_i$ (22, 45, 66, 67), as extracellular ionomycin or IP_3 in the pipette would induce much higher and/or more prolonged increase of $[Ca^{2+}]_i$ than CCL21. Even though specificity of CaCC inhibitors is limited, the currents detected in DCs showed sensitivity to most commonly used Cl^- channel blockers, including AO1, a specific inhibitor of the anoctamin CaCC family (132).

The molecular identity of CaCCs stirred up, over the years, a lot of controversy but since identification of ANO1 as Ca^{2+}-activated Cl^- channel by three independent groups in 2008 (21, 117, 142) the mystery seems to be, at least partly, solved. We detected expression of three members of the Anoctamin family ANO6, ANO8, ANO10 in mouse DCs. Among those, only ANO6 has previously been shown to generate Ca^{2+}-activated Cl^- currents whereas ANO8 has not produced any detectable current when expressed in FTR cells and ANO10 has even suppressed baseline Cl^- conductance and its co-expression with ANO1 caused decrease of the ANO1-

generated currents (115). In the present study by knockdown of ANO6 with siRNA, we showed that CaCC currents could not be detected in almost 70% of measured cells, which was consistent with the efficiency of knockdown, that was about 61% in our experiments. In the light of those observations we suggest that ANO6 is responsible for Ca^{2+}-activated Cl^- currents detected in DCs.

Even though the molecular identity of representatives of CaCCs has been defined only recently (21, 117, 142), their functions in many cells and tissue models have been investigated for almost three decades. In cells of hematopoetic origin, CaCC currents have been characterized in neutropils (61), macrophages (49), Jurkat lymphocytes (93) and human mast cell line HMC-1 (30). In these studies CaCCs were activated by Ca^{2+} ionophore or by dialyzing the cell with high concentrations of Ca^{2+} in the patch pipette. Martins et al. have recently shown an important function of ANO6 as an essential component of the outwardly rectifying chloride channel (ORCC) in airway epithelial cells and Jurkat T lymphocytes (79). ANO6/ORCC is activated upon membrane depolarization and apoptosis. In addition the cystic fibrosis transmembrane conductance regulator (CFTR) in presence of cAMP augments ANO6/ORCC currents (79). Our present study provides another physiological mechanism of ANO6 activation in DCs, through the stimulation of the chemokine receptor CCR7.

In contrast to our present investigation on DCs, ANO6/ORCC in airway epithelial cells and Jurkat T lymphocytes is not Ca^{2+}-dependent (79). This discrepancy may result from ANO6 forming variable oligomeric complexes and/or associating with variable accessory proteins in different cell types. As Schreiber et al. have previously shown, ANO6 is able to generate the Ca^{2+} activated Cl^- currents in ANO6-overexpressing FRT cells (114).

One of the crucial function of DCs is production and secretion of cytokines that play a critical role in the regulation of T cell responses (124). We were able to determine that AO1 and niflumic acid, specific CaCC inhibitors, significantly suppressed secretion of Ca^{2+}-dependent cytokines (53, 130), IL-2 and IL-6 in DCs. IL-2 is a unique cytokine controlling T cell proliferation and development with a substantial role in activation-induced cell death, maintenance of peripheral $CD4^+$

$CD25^+$ regulatory T cells and elimination of self-reactive T cells (137). IL-6, on the other hand, determines the fate of naïve $CD4^+$ helper T cells (29). Results of present investigation would suggest that manipulation of CaCC activity might have a major impact on immune responses orchestrated by DCs.

Migration is another of the essential functions of DCs. The process is induced by chemoattractants present at infection/inflammation sites as well as expressed by secondary lymphoid organs (75). The pilot experiments, with use of CaCC blockers showed that DC migration was highly sensitive to the activity of Cl^- channels. However, our concern was that CaCC inhibitors might influence the Ca^{2+} entry directly, not by the feedback mechanism. Therefore, we knocked down ANO6 and examined migration efficiency of ANO6-deficient DCs. Our results show that the chemokine-induced migration of both immature (towards the chemokine CXCL12) and mature (towards the chemokine CCL21) DCs requires activity of ANO6.

A possible mechanism of ANO6-regulated DC migration and may include ANO6-mediated local volume changes required for lamellipodium growth and/or cell rear end retraction by uptake and/or efflux of osmotically active Cl^-. Another mechanism shown in the present study is CaCC-mediated positive feedback provided by CaCCs to store-operated Ca^{2+} influx. The resting membrane potential of mouse DCs has been estimated as ~ -20 mV (82) that is most probably more positive than the equilibrium Cl^- potential. Thus opening of ANO6 channels would lead to hyperpolarization of the cell membrane, providing electrical driving force for Ca^{2+} entry through the store-operated Ca^{2+} channels, which are steeply inwardly rectifying (99). CaCCs supporting Ca^{2+} influx have been also demonstrated in pulmonary arterial smooth muscle (76) and Cajal (53) cells.

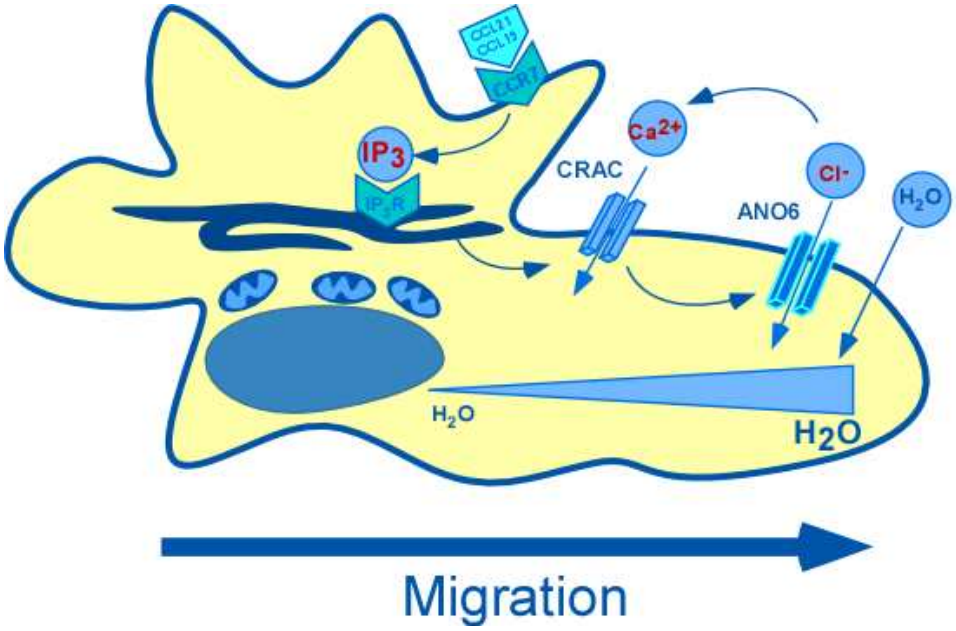

Fig. 20: Graphic representation of possible mechanisms by which activity of ANO6 regulate migration of DCs.

In summary, we identified novel Ca^{2+}-activated Cl^- channels in bone marrow derived murine DCs. We demonstrated that these channels are activated upon ligation of the chemokine receptor CCR7. By the siRNA knockdown approach we could show that ANO6 isoform of the anoctamin protein family accounts for the measured currents. Moreover, ANO6 played an important role in the store-operated Ca^{2+} entry and chemokine-induced migration of both immature and mature DCs.

IV.II Proton channels in dendritic cells

The present study reports the functional expression of H^+ channels in mouse DCs by direct patch clamp studies. Measured currents exhibited typical properties of H^+ currents observed in other cells (24), such as strongly outwardly rectifying I/V relationship, high selectivity for H^+, dependence of the threshold voltage of activation on the pH gradient, slow time-dependent activation kinetics upon depolarization, and sensitivity to Zn^{2+}. The reversal potential of -38mV at ΔpH=1 obtained in this study differs from the theoretical equilibrium potential calculated with the use of the Nernst equation of -58 mV. The reason for that discrepancy could be that cells with large H^+ currents could accumulate protons on the extracellular side of the membrane before all protons can be buffered. The local extracellular pH could become more acidic than the overall pH of the bath solution. This would lower the local pH gradient so that the reversal potential does not follow the predicted values. The selectivity of the H^+ channel measured in the present study was extremely high, the channel was more than 10^6 times more permeable for H^+ than for TMA^+.

The H^+ current amplitude in mouse DCs reached 56 pA/pF (when analyzed at +60 mV at pH_i of 6.0 and pH_o 7.5, which is about 150mV positive to the reversal potential). The amplitude was similar to the H^+ current amplitude in mouse neutrophils (~50 pA/pF at pHi 7.0 (34)) but higher than in mouse macrophages (30 pA/pF at pHi 6.0, (57)) and mast cells (9.6 pA/pF at pHi 5.5, (62)). Among all cells in which the expression of H^+ channels has been established directly by patch clamp studies, only human B lymphocytes (94.7 pA/pF at pHi 6.0, (27)), human eosinophils (~200 pA/pF at pHi 6.0, (41)) and human basophils (~100 pA/pF at pHi 5.5, (91)) have shown higher H^+ current density than the current density observed here in DCs.

The main established function of Hv1 channels is to mediate H^+ efflux upon respiratory burst during phagocytosis (25). In granulocytes and macrophages phagocytosis starts with the so called respiratory burst characterized by an extremely high activity of NADPH oxidase (NOX2) and $O_2^{\cdot-}$ production (25). Activation of even a fraction of available NADPH oxidase may result in a depolarization sufficient to activate H^+ channels in phagocytes (89, 103). Hv1 activity supports the function of NOX2 by charge compensation and by H^+ extrusion (25). Accordingly, $O_2^{\cdot-}$ production within the first few minutes after PMA (phorbol myristate acetate)- induced activation of NOX2 is decreased by 75% in granulocytes from $Hv1^{-/-}$ mice (104).

While in neutrophils and macrophages phagocytosis is followed by complete degradation of captured dangerous particles (111), in DCs phagocytosis progresses more gently allowing to preserve peptide fragments for the presentation on MHCII (7). The reduced proteolytic efficiency in DCs strongly depends on NOX2 activity (108, 112), although DCs express only 5% of NOX2 in comparison to neutrophils (33). However, unlike the pattern observed in neutrophils and macrophages, NOX2 in DCs demonstrates prolonged association with the phagosomes and the NOX2 activity is sustained beyond 1 h after internalization of the particles (77, 108, 112). NOX2-mediated ROS production in DCs has been proposed to result in proton consumption in the phagosome lumen, causing phagosomal alkalinization (112). However, in a recent study, in which real-time fluorometry of DC phagosomes has been performed, DCs have been able to fully acidify their phagosomes to a pH below 5.0 within 30 min and the mechanism of NOX2-dependent control of phagosomal proteolysis has been shown to be pH-independent involving redox modulation of local cycteine cathepsines (108). In any case NOX2 activity requires charge compensation and proton translocation into the phagosomes. The Hv1 channel is perfectly suited to perform both functions simultaneously. As shown recently, phagosomal NOX2 activity is indeed moderately attenuated in Hv1-deficient mouse DCs (108).

In the present study, the classical agent inducing DC maturation, LPS, a ligand of TLR4, stimulated H^+ currents when applied acutely but reduced Hv1 channel mRNA abundance and H^+ currents after 24 h incubation. The Hv1 protein abundance was however not changed by 24 h incubation with LPS. Stimulation of H^+ currents by

acute LPS treatment was accompanied by a fast activation of NOX2 and generation of NOX2 electron currents. The activation of H^+ channels by acute LPS application seems to result from the LPS-dependent stimulation of PKC, since the stimulating effect of LPS was abolished by inhibition of PKC with GFX. PKC is known to be involved in signaling downstream from TLRs (74). On the other hand, PKC phosphorylates Hv1 channel on the threonine 29 (90) resulting in enhanced gating mode of Hv1 (86) with increased maximal H^+ conductance and a 40 mV shift in the threshold voltage of activation towards more negative potentials (86, 90), which is close to the observed alterations of H^+ currents upon acute stimulation of DCs with LPS in the present study.

Activation of Hv1 channel by LPS could support NOX2 activity and promote antigen uptake and ROS production in DCs. Upon LPS stimulation a transient increase in the ability of DCs to uptake soluble antigens, immune and phagocytable complex antigens was observed (18, 40, 139). LPS in RAW264.7 cells enhance ROS production, HEK293T cells over expressing TLR4 and bone marrow derived DCs (80, 100, 105). Moreover, direct interaction between TLR4 and NADPH oxidase has been shown in HEK293T cells (100). It is tempting to speculate that PKC dependent Hv1 channel regulation might underlie the previously reported decrease in LPS-induced phagocytosis in murine microglia upon inhibition of PKCδ (60), the isoform that phosphorylates Hv1 (90).

Inhibition of H^+ currents after 24 h stimulation of DCs with LPS may reflect the loss of endocytic capacity in mature DCs (143). It has been shown that the early increase in endocytic capacity upon LPS stimulation in DCs peaks 2 hours after ligation of the TLR4 receptor (139) and then the ability for endocytosis is gradually lost becoming strongly reduced after 18 hours stimulation with LPS (42). Moreover, as observed in the present study, ROS production was also diminished in LPS-matured DCs.

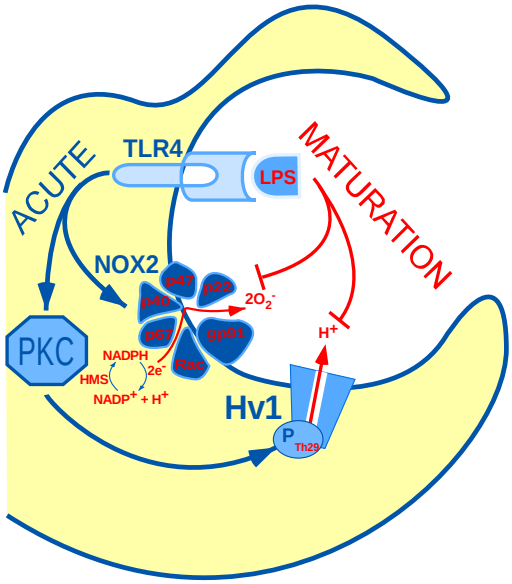

Fig. 21: Acute and long term LPS regulation of Hv1 and NOX2 in DCs.

In conclusion, our study demonstrated the functional expression of LPS-regulated Hv1 channels in mouse DCs. LPS regulated Hv1 in a bimodal way: acutely by PKC-dependent phosphorylation that turns on the enhanced gating mode of Hv1, whereas, LPS induced maturation caused strong reduction of H^+ currents in fully matured DCs.

REFERENCES

1. **Affaticati P, Mignen O, Jambou F, Potier MC, Klingel-Schmitt I, Degrouard J, Peineau S, Gouadon E, Collingridge GL, Liblau R, Capiod T, and Cohen-Kaminsky S**. Sustained calcium signalling and caspase-3 activation involve NMDA receptors in thymocytes in contact with dendritic cells. *Cell Death Differ* 18: 99-108, 2011.
2. **Aki D, Minoda Y, Yoshida H, Watanabe S, Yoshida R, Takaesu G, Chinen T, Inaba T, Hikida M, Kurosaki T, Saeki K, and Yoshimura A**. Peptidoglycan and lipopolysaccharide activate PLCgamma2, leading to enhanced cytokine production in macrophages and dendritic cells. *Genes Cells* 13: 199-208, 2008.
3. **Alvarez D, Vollmann EH, and von Andrian UH**. Mechanisms and consequences of dendritic cell migration. *Immunity* 29: 325-342, 2008.
4. **Andre S, Boukhaddaoui H, Campo B, Al-Jumaily M, Mayeux V, Greuet D, Valmier J, and Scamps F**. Axotomy-induced expression of calcium-activated chloride current in subpopulations of mouse dorsal root ganglion neurons. *J Neurophysiol* 90: 3764-3773, 2003.
5. **Angermann JE, Sanguinetti AR, Kenyon JL, Leblanc N, and Greenwood IA**. Mechanism of the inhibition of Ca2+-activated Cl- currents by phosphorylation in pulmonary arterial smooth muscle cells. *J Gen Physiol* 128: 73-87, 2006.
6. **Ardavin C**. Origin, precursors and differentiation of mouse dendritic cells. *Nat Rev Immunol* 3: 582-590, 2003.
7. **Banchereau J, Briere F, Caux C, Davoust J, Lebecque S, Liu YJ, Pulendran B, and Palucka K**. Immunobiology of dendritic cells. *Annu Rev Immunol* 18: 767-811, 2000.
8. **Bandyopadhyay BC, Pingle SC, and Ahern GP**. Store-operated Ca(2)+ signaling in dendritic cells occurs independently of STIM1. *J Leukoc Biol* 89: 57-62, 2011.
9. **Barbet G, Demion M, Moura IC, Serafini N, Leger T, Vrtovsnik F, Monteiro RC, Guinamard R, Kinet JP, and Launay P**. The calcium-activated nonselective cation channel TRPM4 is essential for the migration but not the maturation of dendritic cells. *Nat Immunol* 9: 1148-1156, 2008.
10. **Barro-Soria R, Aldehni F, Almaca J, Witzgall R, Schreiber R, and Kunzelmann K**. ER-localized bestrophin 1 activates Ca2+-dependent ion channels TMEM16A and SK4 possibly by acting as a counterion channel. *Pflugers Arch* 459: 485-497, 2010.
11. **Barry PH, and Lynch JW**. Liquid junction potentials and small cell effects in patch-clamp analysis. *J Membr Biol* 121: 101-117, 1991.
12. **Basu S, and Srivastava P**. Immunological role of neuronal receptor vanilloid receptor 1 expressed on dendritic cells. *Proc Natl Acad Sci U S A* 102: 5120-5125, 2005.
13. **Becker SM, Delamarre L, Mellman I, and Andrews NW**. Differential role of the Ca(2+) sensor synaptotagmin VII in macrophages and dendritic cells. *Immunobiology* 214: 495-505, 2009.
14. **Bekar LK, Loewen ME, Cao K, Sun X, Leis J, Wang R, Forsyth GW, and Walz W**. Complex expression and localization of inactivating Kv channels in cultured hippocampal astrocytes. *J Neurophysiol* 93: 1699-1709, 2005.
15. **Berridge MJ, Bootman MD, and Roderick HL**. Calcium signalling: dynamics, homeostasis and remodelling. *Nat Rev Mol Cell Biol* 4: 517-529, 2003.
16. **Blander JM**. Coupling Toll-like receptor signaling with phagocytosis: potentiation of antigen presentation. *Trends Immunol* 28: 19-25, 2007.
17. **Blander JM, and Medzhitov R**. On regulation of phagosome maturation and antigen presentation. *Nat Immunol* 7: 1029-1035, 2006.
18. **Blander JM, and Medzhitov R**. Regulation of phagosome maturation by signals from toll-like receptors. *Science* 304: 1014-1018, 2004.
19. **Boldyrev AA, Carpenter DO, and Johnson P**. Emerging evidence for a similar role of glutamate receptors in the nervous and immune systems. *J Neurochem* 95: 913-918, 2005.
20. **Calle Y, Carragher NO, Thrasher AJ, and Jones GE**. Inhibition of calpain stabilises podosomes and impairs dendritic cell motility. *J Cell Sci* 119: 2375-2385, 2006.
21. **Caputo A, Caci E, Ferrera L, Pedemonte N, Barsanti C, Sondo E, Pfeffer U, Ravazzolo R, Zegarra-Moran O, and Galietta LJ**. TMEM16A, a membrane protein associated with calcium-dependent chloride channel activity. *Science* 322: 590-594, 2008.
22. **Chen Y, An H, Li T, Liu Y, Gao C, Guo P, Zhang H, and Zhan Y**. Direct or indirect regulation of calcium-activated chloride channel by calcium. *J Membr Biol* 240: 121-129, 2011.
23. **Claus V, Jahraus A, Tjelle T, Berg T, Kirschke H, Faulstich H, and Griffiths G**. Lysosomal enzyme trafficking between phagosomes, endosomes, and lysosomes in J774 macrophages. Enrichment of cathepsin H in early endosomes. *J Biol Chem* 273: 9842-9851, 1998.
24. **DeCoursey TE**. Voltage-gated proton channels. *Cell Mol Life Sci* 65: 2554-2573, 2008.

25. **DeCoursey TE**. Voltage-gated proton channels find their dream job managing the respiratory burst in phagocytes. *Physiology (Bethesda)* 25: 27-40, 2010.
26. **DeCoursey TE, and Cherny VV**. Temperature dependence of voltage-gated H+ currents in human neutrophils, rat alveolar epithelial cells, and mammalian phagocytes. *J Gen Physiol* 112: 503-522, 1998.
27. **Demaurex N, and El Chemaly A**. Physiological roles of voltage-gated proton channels in leukocytes. *J Physiol* 588: 4659-4665, 2010.
28. **Di Virgilio F**. Purinergic mechanism in the immune system: A signal of danger for dendritic cells. *Purinergic Signal* 1: 205-209, 2005.
29. **Diehl S, and Rincon M**. The two faces of IL-6 on Th1/Th2 differentiation. *Mol Immunol* 39: 531-536, 2002.
30. **Duffy SM, Lawley WJ, Conley EC, and Bradding P**. Resting and activation-dependent ion channels in human mast cells. *J Immunol* 167: 4261-4270, 2001.
31. **Duran C, Qu Z, Osunkoya AO, Cui Y, and Hartzell HC**. ANOs 3-7 in the anoctamin/Tmem16 Cl- channel family are intracellular proteins. *Am J Physiol Cell Physiol* 302: C482-493, 2012.
32. **Dustin ML, and Colman DR**. Neural and immunological synaptic relations. *Science* 298: 785-789, 2002.
33. **Elsen S, Doussiere J, Villiers CL, Faure M, Berthier R, Papaioannou A, Grandvaux N, Marche PN, and Vignais PV**. Cryptic O2- -generating NADPH oxidase in dendritic cells. *J Cell Sci* 117: 2215-2226, 2004.
34. **Essin K, Salanova B, Kettritz R, Sausbier M, Luft FC, Kraus D, Bohn E, Autenrieth IB, Peschel A, Ruth P, and Gollasch M**. Large-conductance calcium-activated potassium channel activity is absent in human and mouse neutrophils and is not required for innate immunity. *Am J Physiol Cell Physiol* 293: C45-54, 2007.
35. **Fordyce CB, Jagasia R, Zhu X, and Schlichter LC**. Microglia Kv1.3 channels contribute to their ability to kill neurons. *J Neurosci* 25: 7139-7149, 2005.
36. **Gardella S, Andrei C, Costigliolo S, Olcese L, Zocchi MR, and Rubartelli A**. Secretion of bioactive interleukin-1beta by dendritic cells is modulated by interaction with antigen specific T cells. *Blood* 95: 3809-3815, 2000.
37. **Gardella S, Andrei C, Lotti LV, Poggi A, Torrisi MR, Zocchi MR, and Rubartelli A**. CD8(+) T lymphocytes induce polarized exocytosis of secretory lysosomes by dendritic cells with release of interleukin-1beta and cathepsin D. *Blood* 98: 2152-2159, 2001.
38. **Gardella S, Andrei C, Poggi A, Zocchi MR, and Rubartelli A**. Control of interleukin-18 secretion by dendritic cells: role of calcium influxes. *FEBS Lett* 481: 245-248, 2000.
39. **Geissmann F, Manz MG, Jung S, Sieweke MH, Merad M, and Ley K**. Development of monocytes, macrophages, and dendritic cells. *Science* 327: 656-661, 2010.
40. **Gil-Torregrosa BC, Lennon-Dumenil AM, Kessler B, Guermonprez P, Ploegh HL, Fruci D, van Endert P, and Amigorena S**. Control of cross-presentation during dendritic cell maturation. *Eur J Immunol* 34: 398-407, 2004.
41. **Gordienko DV, Tare M, Parveen S, Fenech CJ, Robinson C, and Bolton TB**. Voltage-activated proton current in eosinophils from human blood. *J Physiol* 496 (Pt 2): 299-316, 1996.
42. **Granucci F, Ferrero E, Foti M, Aggujaro D, Vettoretto K, and Ricciardi-Castagnoli P**. Early events in dendritic cell maturation induced by LPS. *Microbes Infect* 1: 1079-1084, 1999.
43. **Guo D, Young L, Patel C, Jiao Z, Wu Y, Liu T, Kowey PR, and Yan GX**. Calcium-activated chloride current contributes to action potential alternations in left ventricular hypertrophy rabbit. *Am J Physiol Heart Circ Physiol* 295: H97-H104, 2008.
44. **Hamill OP, Marty A, Neher E, Sakmann B, and Sigworth FJ**. Improved patch-clamp techniques for high-resolution current recording from cells and cell-free membrane patches. *Pflugers Arch* 391: 85-100, 1981.
45. **Hartzell C, Putzier I, and Arreola J**. Calcium-activated chloride channels. *Annual review of physiology* 67: 719-758, 2005.
46. **Hartzell HC, Yu K, Xiao Q, Chien LT, and Qu Z**. Anoctamin/TMEM16 family members are Ca2+-activated Cl- channels. *J Physiol* 587: 2127-2139, 2009.
47. **Hiraoka M, Kawano S, Hirano Y, and Furukawa T**. Role of cardiac chloride currents in changes in action potential characteristics and arrhythmias. *Cardiovasc Res* 40: 23-33, 1998.
48. **Hogan PG, and Rao A**. Dissecting ICRAC, a store-operated calcium current. *Trends Biochem Sci* 32: 235-245, 2007.
49. **Holevinsky KO, Jow F, and Nelson DJ**. Elevation in intracellular calcium activates both chloride and proton currents in human macrophages. *J Membr Biol* 140: 13-30, 1994.
50. **Hsu CY, Leu SJ, Chiang BL, Liu HE, Su HC, and Lee YL**. Cytokine gene-modulated dendritic cells protect against allergic airway inflammation by inducing IL-10(+)IFN-gamma(+)CD4(+) T cells. *Gene Ther* 17: 1011-1021, 2010.

51. **Huggins A, Paschalidis N, Flower RJ, Perretti M, and D'Acquisto F**. Annexin-1-deficient dendritic cells acquire a mature phenotype during differentiation. *FASEB journal : official publication of the Federation of American Societies for Experimental Biology* 23: 985-996, 2009.
52. **Huppa JB, and Davis MM**. T-cell-antigen recognition and the immunological synapse. *Nat Rev Immunol* 3: 973-983, 2003.
53. **Hwang SJ, Blair PJ, Britton FC, O'Driscoll KE, Hennig G, Bayguinov YR, Rock JR, Harfe BD, Sanders KM, and Ward SM**. Expression of anoctamin 1/TMEM16A by interstitial cells of Cajal is fundamental for slow wave activity in gastrointestinal muscles. *J Physiol* 587: 4887-4904, 2009.
54. **Idzko M, Dichmann S, Ferrari D, Di Virgilio F, la Sala A, Girolomoni G, Panther E, and Norgauer J**. Nucleotides induce chemotaxis and actin polymerization in immature but not mature human dendritic cells via activation of pertussis toxin-sensitive P2y receptors. *Blood* 100: 925-932, 2002.
55. **Inaba K, Inaba M, Romani N, Aya H, Deguchi M, Ikehara S, Muramatsu S, and Steinman RM**. Generation of large numbers of dendritic cells from mouse bone marrow cultures supplemented with granulocyte/macrophage colony-stimulating factor. *J Exp Med* 176: 1693-1702, 1992.
56. **Ivanenko A, Baring MD, Airey JA, Sutko JL, and Kenyon JL**. A caffeine- and ryanodine-sensitive Ca2+ store in avian sensory neurons. *J Neurophysiol* 70: 710-722, 1993.
57. **Kapus A, Romanek R, Qu AY, Rotstein OD, and Grinstein S**. A pH-sensitive and voltage-dependent proton conductance in the plasma membrane of macrophages. *J Gen Physiol* 102: 729-760, 1993.
58. **Kawai T, and Akira S**. The role of pattern-recognition receptors in innate immunity: update on Toll-like receptors. *Nat Immunol* 11: 373-384, 2010.
59. **Khanna R, Roy L, Zhu X, and Schlichter LC**. K+ channels and the microglial respiratory burst. *Am J Physiol Cell Physiol* 280: C796-806, 2001.
60. **Kim DC, Kim SH, Jeong MW, Baek NI, and Kim KT**. Effect of rottlerin, a PKC-delta inhibitor, on TLR-4-dependent activation of murine microglia. *Biochem Biophys Res Commun* 337: 110-115, 2005.
61. **Krause KH, and Welsh MJ**. Voltage-dependent and Ca2(+)-activated ion channels in human neutrophils. *J Clin Invest* 85: 491-498, 1990.
62. **Kuno M, Kawawaki J, and Nakamura F**. A highly temperature-sensitive proton current in mouse bone marrow-derived mast cells. *J Gen Physiol* 109: 731-740, 1997.
63. **Kunzelmann K, Kongsuphol P, Chootip K, Toledo C, Martins JR, Almaca J, Tian Y, Witzgall R, Ousingsawat J, and Schreiber R**. Role of the Ca2+ -activated Cl- channels bestrophin and anoctamin in epithelial cells. *Biol Chem* 392: 125-134, 2011.
64. **Kunzelmann K, Milenkovic VM, Spitzner M, Soria RB, and Schreiber R**. Calcium-dependent chloride conductance in epithelia: is there a contribution by Bestrophin? *Pflugers Arch* 454: 879-889, 2007.
65. **Kunzelmann K, Tian Y, Martins JR, Faria D, Kongsuphol P, Ousingsawat J, Thevenod F, Roussa E, Rock J, and Schreiber R**. Anoctamins. *Pflugers Arch* 462: 195-208, 2011.
66. **Kuruma A, and Hartzell HC**. Bimodal control of a Ca(2+)-activated Cl(-) channel by different Ca(2+) signals. *J Gen Physiol* 115: 59-80, 2000.
67. **Kuruma A, and Hartzell HC**. Dynamics of calcium regulation of chloride currents in Xenopus oocytes. *Am J Physiol* 276: C161-175, 1999.
68. **Lalonde MR, Kelly ME, and Barnes S**. Calcium-activated chloride channels in the retina. *Channels (Austin)* 2: 252-260, 2008.
69. **Lamb FS, Moreland JG, and Miller FJ, Jr.** Electrophysiology of reactive oxygen production in signaling endosomes. *Antioxid Redox Signal* 11: 1335-1347, 2009.
70. **Lee HC**. Multiplicity of Ca2+ messengers and Ca2+ stores: a perspective from cyclic ADP-ribose and NAADP. *Curr Mol Med* 4: 227-237, 2004.
71. **Lewis RS, and Cahalan MD**. Potassium and calcium channels in lymphocytes. *Annu Rev Immunol* 13: 623-653, 1995.
72. **Li Q, and Verma IM**. NF-kappaB regulation in the immune system. *Nat Rev Immunol* 2: 725-734, 2002.
73. **Lioudyno MI, Kozak JA, Penna A, Safrina O, Zhang SL, Sen D, Roos J, Stauderman KA, and Cahalan MD**. Orai1 and STIM1 move to the immunological synapse and are up-regulated during T cell activation. *Proc Natl Acad Sci U S A* 105: 2011-2016, 2008.
74. **Loegering DJ, and Lennartz MR**. Protein kinase C and toll-like receptor signaling. *Enzyme Res* 2011: 537821, 2011.
75. **Luther SA, Bidgol A, Hargreaves DC, Schmidt A, Xu Y, Paniyadi J, Matloubian M, and Cyster JG**. Differing activities of homeostatic chemokines CCL19, CCL21, and CXCL12 in lymphocyte and dendritic cell recruitment and lymphoid neogenesis. *J Immunol* 169: 424-433, 2002.

76. **Manoury B, Tamuleviciute A, and Tammaro P**. TMEM16A/anoctamin 1 protein mediates calcium-activated chloride currents in pulmonary arterial smooth muscle cells. *J Physiol* 588: 2305-2314, 2010.
77. **Mantegazza AR, Savina A, Vermeulen M, Perez L, Geffner J, Hermine O, Rosenzweig SD, Faure F, and Amigorena S**. NADPH oxidase controls phagosomal pH and antigen cross-presentation in human dendritic cells. *Blood* 112: 4712-4722, 2008.
78. **Marmorstein AD, and Kinnick TR**. Focus on molecules: bestrophin (best-1). *Exp Eye Res* 85: 423-424, 2007.
79. **Martins JR, Faria D, Kongsuphol P, Reisch B, Schreiber R, and Kunzelmann K**. Anoctamin 6 is an essential component of the outwardly rectifying chloride channel. *Proc Natl Acad Sci U S A* 108: 18168-18172, 2011.
80. **Matsuzawa A, Saegusa K, Noguchi T, Sadamitsu C, Nishitoh H, Nagai S, Koyasu S, Matsumoto K, Takeda K, and Ichijo H**. ROS-dependent activation of the TRAF6-ASK1-p38 pathway is selectively required for TLR4-mediated innate immunity. *Nat Immunol* 6: 587-592, 2005.
81. **Matthews HR, and Reisert J**. Calcium, the two-faced messenger of olfactory transduction and adaptation. *Curr Opin Neurobiol* 13: 469-475, 2003.
82. **Matzner N, Zemtsova IM, Nguyen TX, Duszenko M, Shumilina E, and Lang F**. Ion channels modulating mouse dendritic cell functions. *J Immunol* 181: 6803-6809, 2008.
83. **Miledi R**. A calcium-dependent transient outward current in Xenopus laevis oocytes. *Proc R Soc Lond B Biol Sci* 215: 491-497, 1982.
84. **Milton RH, Abeti R, Averaimo S, DeBiasi S, Vitellaro L, Jiang L, Curmi PM, Breit SN, Duchen MR, and Mazzanti M**. CLIC1 function is required for beta-amyloid-induced generation of reactive oxygen species by microglia. *J Neurosci* 28: 11488-11499, 2008.
85. **Montes M, McIlroy D, Hosmalin A, and Trautmann A**. Calcium responses elicited in human T cells and dendritic cells by cell-cell interaction and soluble ligands. *Int Immunol* 11: 561-568, 1999.
86. **Morgan D, Cherny VV, Finnegan A, Bollinger J, Gelb MH, and DeCoursey TE**. Sustained activation of proton channels and NADPH oxidase in human eosinophils and murine granulocytes requires PKC but not cPLA2 alpha activity. *J Physiol* 579: 327-344, 2007.
87. **Mullen KM, Rozycka M, Rus H, Hu L, Cudrici C, Zafranskaia E, Pennington MW, Johns DC, Judge SI, and Calabresi PA**. Potassium channels Kv1.3 and Kv1.5 are expressed on blood-derived dendritic cells in the central nervous system. *Ann Neurol* 60: 118-127, 2006.
88. **Muller T, Robaye B, Vieira RP, Ferrari D, Grimm M, Jakob T, Martin SF, Di Virgilio F, Boeynaems JM, Virchow JC, and Idzko M**. The purinergic receptor P2Y2 receptor mediates chemotaxis of dendritic cells and eosinophils in allergic lung inflammation. *Allergy* 65: 1545-1553, 2010.
89. **Murphy R, and DeCoursey TE**. Charge compensation during the phagocyte respiratory burst. *Biochim Biophys Acta* 1757: 996-1011, 2006.
90. **Musset B, Capasso M, Cherny VV, Morgan D, Bhamrah M, Dyer MJ, and DeCoursey TE**. Identification of Thr29 as a critical phosphorylation site that activates the human proton channel Hvcn1 in leukocytes. *J Biol Chem* 285: 5117-5121, 2010.
91. **Musset B, Morgan D, Cherny VV, MacGlashan DW, Jr., Thomas LL, Rios E, and DeCoursey TE**. A pH-stabilizing role of voltage-gated proton channels in IgE-mediated activation of human basophils. *Proc Natl Acad Sci U S A* 105: 11020-11025, 2008.
92. **Musset B, Smith SM, Rajan S, Morgan D, Cherny VV, and Decoursey TE**. Aspartate 112 is the selectivity filter of the human voltage-gated proton channel. *Nature* 480: 273-277, 2011.
93. **Nishimoto I, Wagner JA, Schulman H, and Gardner P**. Regulation of Cl- channels by multifunctional CaM kinase. *Neuron* 6: 547-555, 1991.
94. **O'Connell PJ, Klyachko VA, and Ahern GP**. Identification of functional type 1 ryanodine receptors in mouse dendritic cells. *FEBS Lett* 512: 67-70, 2002.
95. **O'Connell PJ, Wang X, Leon-Ponte M, Griffiths C, Pingle SC, and Ahern GP**. A novel form of immune signaling revealed by transmission of the inflammatory mediator serotonin between dendritic cells and T cells. *Blood* 107: 1010-1017, 2006.
96. **Pacheco R, Oliva H, Martinez-Navio JM, Climent N, Ciruela F, Gatell JM, Gallart T, Mallol J, Lluis C, and Franco R**. Glutamate released by dendritic cells as a novel modulator of T cell activation. *J Immunol* 177: 6695-6704, 2006.
97. **Palucka K, Ueno H, Roberts L, Fay J, and Banchereau J**. Dendritic cell subsets as vectors and targets for improved cancer therapy. *Curr Top Microbiol Immunol* 344: 173-192, 2011.
98. **Papassotiriou J, Eggermont J, Droogmans G, and Nilius B**. Ca(2+)-activated Cl- channels in Ehrlich ascites tumor cells are distinct from mCLCA1, 2 and 3. *Pflugers Arch* 442: 273-279, 2001.
99. **Parekh AB, and Putney JW, Jr.** Store-operated calcium channels. *Physiol Rev* 85: 757-810, 2005.

100. **Park HS, Jung HY, Park EY, Kim J, Lee WJ, and Bae YS**. Cutting edge: direct interaction of TLR4 with NAD(P)H oxidase 4 isozyme is essential for lipopolysaccharide-induced production of reactive oxygen species and activation of NF-kappa B. *J Immunol* 173: 3589-3593, 2004.
101. **Partida-Sanchez S, Gasser A, Fliegert R, Siebrands CC, Dammermann W, Shi G, Mousseau BJ, Sumoza-Toledo A, Bhagat H, Walseth TF, Guse AH, and Lund FE**. Chemotaxis of mouse bone marrow neutrophils and dendritic cells is controlled by adp-ribose, the major product generated by the CD38 enzyme reaction. *J Immunol* 179: 7827-7839, 2007.
102. **Pfaffl MW**. A new mathematical model for relative quantification in real-time RT-PCR. *Nucleic Acids Res* 29: e45, 2001.
103. **Rada BK, Geiszt M, Kaldi K, Timar C, and Ligeti E**. Dual role of phagocytic NADPH oxidase in bacterial killing. *Blood* 104: 2947-2953, 2004.
104. **Ramsey IS, Ruchti E, Kaczmarek JS, and Clapham DE**. Hv1 proton channels are required for high-level NADPH oxidase-dependent superoxide production during the phagocyte respiratory burst. *Proc Natl Acad Sci U S A* 106: 7642-7647, 2009.
105. **Rotte A, Pasham V, Eichenmuller M, Mahmud H, Xuan NT, Shumilina E, Gotz F, and Lang F**. Effect of bacterial lipopolysaccharide on Na(+)/H(+) exchanger activity in dendritic cells. *Cell Physiol Biochem* 26: 553-562, 2010.
106. **Rotte A, Pasham V, Yang W, Eichenmuller M, Bhandaru M, Shumilina E, and Lang F**. Phosphoinositide 3-kinase-dependent regulation of Na+/H+ exchanger in dendritic cells. *Pflugers Arch* 460: 1087-1096, 2010.
107. **Rybicka JM, Balce DR, Chaudhuri S, Allan ER, and Yates RM**. Phagosomal proteolysis in dendritic cells is modulated by NADPH oxidase in a pH-independent manner. *Embo J* 31: 932-944, 2012.
108. **Rybicka JM, Balce DR, Chaudhuri S, Allan ER, and Yates RM**. Phagosomal proteolysis in dendritic cells is modulated by NADPH oxidase in a pH-independent manner. *Embo J* 2011.
109. **Salter RD, and Watkins SC**. Dendritic cell altered states: what role for calcium? *Immunol Rev* 231: 278-288, 2009.
110. **Sanjuan MA, Milasta S, and Green DR**. Toll-like receptor signaling in the lysosomal pathways. *Immunol Rev* 227: 203-220, 2009.
111. **Savina A, and Amigorena S**. Phagocytosis and antigen presentation in dendritic cells. *Immunol Rev* 219: 143-156, 2007.
112. **Savina A, Jancic C, Hugues S, Guermonprez P, Vargas P, Moura IC, Lennon-Dumenil AM, Seabra MC, Raposo G, and Amigorena S**. NOX2 controls phagosomal pH to regulate antigen processing during crosspresentation by dendritic cells. *Cell* 126: 205-218, 2006.
113. **Schilling T, and Eder C**. Importance of the non-selective cation channel TRPV1 for microglial reactive oxygen species generation. *J Neuroimmunol* 216: 118-121, 2009.
114. **Schreiber R, Uliyakina I, Kongsuphol P, Warth R, Mirza M, Martins JR, and Kunzelmann K**. Expression and function of epithelial anoctamins. *J Biol Chem* 285: 7838-7845, 2010.
115. **Schreiber R, Uliyakina I, Kongsuphol P, Warth R, Mirza M, Martins JR, and Kunzelmann K**. Expression and function of epithelial anoctamins. *J Biol Chem* 285: 7838-7845.
116. **Schrenzel J, Serrander L, Banfi B, Nusse O, Fouyouzi R, Lew DP, Demaurex N, and Krause KH**. Electron currents generated by the human phagocyte NADPH oxidase. *Nature* 392: 734-737, 1998.
117. **Schroeder BC, Cheng T, Jan YN, and Jan LY**. Expression cloning of TMEM16A as a calcium-activated chloride channel subunit. *Cell* 134: 1019-1029, 2008.
118. **Schuber F, and Lund FE**. Structure and enzymology of ADP-ribosyl cyclases: conserved enzymes that produce multiple calcium mobilizing metabolites. *Curr Mol Med* 4: 249-261, 2004.
119. **Segal AW**. How neutrophils kill microbes. *Annu Rev Immunol* 23: 197-223, 2005.
120. **Shortman K, and Naik SH**. Steady-state and inflammatory dendritic-cell development. *Nat Rev Immunol* 7: 19-30, 2007.
121. **Shumilina E, Huber SM, and Lang F**. Ca2+ signaling in the regulation of dendritic cell functions. *Am J Physiol Cell Physiol* 2011.
122. **Shumilina E, Huber SM, and Lang F**. Ca2+ signaling in the regulation of dendritic cell functions. *Am J Physiol Cell Physiol* 300: C1205-1214, 2011.
123. **Shumilina E, Xuan NT, Matzner N, Bhandaru M, Zemtsova IM, and Lang F**. Regulation of calcium signaling in dendritic cells by 1,25-dihydroxyvitamin D3. *FASEB journal : official publication of the Federation of American Societies for Experimental Biology* 24: 1989-1996, 2010.
124. **Steinman RM, and Banchereau J**. Taking dendritic cells into medicine. *Nature* 449: 419-426, 2007.
125. **Steinman RM, and Cohn ZA**. Identification of a novel cell type in peripheral lymphoid organs of mice. I. Morphology, quantitation, tissue distribution. *J Exp Med* 137: 1142-1162, 1973.

126. **Stephan AB, Shum EY, Hirsh S, Cygnar KD, Reisert J, and Zhao H**. ANO2 is the cilial calcium-activated chloride channel that may mediate olfactory amplification. *Proc Natl Acad Sci U S A* 106: 11776-11781, 2009.
127. **Stock C, and Schwab A**. Protons make tumor cells move like clockwork. *Pflugers Arch* 458: 981-992, 2009.
128. **Stohr H, Heisig JB, Benz PM, Schoberl S, Milenkovic VM, Strauss O, Aartsen WM, Wijnholds J, Weber BH, and Schulz HL**. TMEM16B, a novel protein with calcium-dependent chloride channel activity, associates with a presynaptic protein complex in photoreceptor terminals. *J Neurosci* 29: 6809-6818, 2009.
129. **Sumoza-Toledo A, Lange I, Cortado H, Bhagat H, Mori Y, Fleig A, Penner R, and Partida-Sanchez S**. Dendritic cell maturation and chemotaxis is regulated by TRPM2-mediated lysosomal Ca2+ release. *FASEB journal : official publication of the Federation of American Societies for Experimental Biology* 25: 3529-3542, 2011.
130. **Suzuki M, and Mizuno A**. A novel human Cl(-) channel family related to Drosophila flightless locus. *The Journal of biological chemistry* 279: 22461-22468, 2004.
131. **Tian Y, Kongsuphol P, Hug M, Ousingsawat J, Witzgall R, Schreiber R, and Kunzelmann K**. Calmodulin-dependent activation of the epithelial calcium-dependent chloride channel TMEM16A. *FASEB journal : official publication of the Federation of American Societies for Experimental Biology* 25: 1058-1068, 2011.
132. **Tian Y, Kongsuphol P, Hug M, Ousingsawat J, Witzgall R, Schreiber R, and Kunzelmann K**. Calmodulin-dependent activation of the epithelial calcium-dependent chloride channel TMEM16A. *Faseb J* 25: 1058-1068, 2011.
133. **Ueno H, Palucka AK, and Banchereau J**. The expanding family of dendritic cell subsets. *Nat Biotechnol* 28: 813-815, 2010.
134. **Venkatachalam K, and Montell C**. TRP channels. *Annu Rev Biochem* 76: 387-417, 2007.
135. **Vukcevic M, Spagnoli GC, Iezzi G, Zorzato F, and Treves S**. Ryanodine receptor activation by Ca v 1.2 is involved in dendritic cell major histocompatibility complex class II surface expression. *J Biol Chem* 283: 34913-34922, 2008.
136. **Vukcevic M, Zorzato F, Spagnoli G, and Treves S**. Frequent calcium oscillations lead to NFAT activation in human immature dendritic cells. *J Biol Chem* 285: 16003-16011, 2010.
137. **Waldmann TA**. The biology of interleukin-2 and interleukin-15: implications for cancer therapy and vaccine design. *Nat Rev Immunol* 6: 595-601, 2006.
138. **Watts C, West MA, and Zaru R**. TLR signalling regulated antigen presentation in dendritic cells. *Curr Opin Immunol* 22: 124-130, 2010.
139. **West MA, Wallin RP, Matthews SP, Svensson HG, Zaru R, Ljunggren HG, Prescott AR, and Watts C**. Enhanced dendritic cell antigen capture via toll-like receptor-induced actin remodeling. *Science* 305: 1153-1157, 2004.
140. **Williams DA, Fogarty KE, Tsien RY, and Fay FS**. Calcium gradients in single smooth muscle cells revealed by the digital imaging microscope using Fura-2. *Nature* 318: 558-561, 1985.
141. **Xuan NT, Shumilina E, Matzner N, Zemtsova IM, Biedermann T, Goetz F, and Lang F**. Ca2+-dependent functions in peptidoglycan-stimulated mouse dendritic cells. *Cell Physiol Biochem* 24: 167-176, 2009.
142. **Yang YD, Cho H, Koo JY, Tak MH, Cho Y, Shim WS, Park SP, Lee J, Lee B, Kim BM, Raouf R, Shin YK, and Oh U**. TMEM16A confers receptor-activated calcium-dependent chloride conductance. *Nature* 455: 1210-1215, 2008.
143. **Zanoni I, and Granucci F**. Regulation of antigen uptake, migration, and lifespan of dendritic cell by Toll-like receptors. *J Mol Med (Berl)* 88: 873-880, 2010.
144. **Zanoni I, Ostuni R, Capuano G, Collini M, Caccia M, Ronchi AE, Rocchetti M, Mingozzi F, Foti M, Chirico G, Costa B, Zaza A, Ricciardi-Castagnoli P, and Granucci F**. CD14 regulates the dendritic cell life cycle after LPS exposure through NFAT activation. *Nature* 460: 264-268, 2009.
145. **Zhou Z, and Neher E**. Mobile and immobile calcium buffers in bovine adrenal chromaffin cells. *J Physiol* 469: 245-273, 1993.

Curriculum Vitae

Name: Kalina Szteyn

Date of birth: 04.04.1982

Place of birth: Olsztyn, Poland

Nationality: Polish

Education:

BSc Exercise Science

Harding University

Searcy, AR

USA

Awarded: May 2008

Captan of CC and Track Team (Senior Year)

3 times All American (CC and Track)

MSc Molecular Exercise Physiology

University of Aberdeen

Aberdeen, Scotland, UK

Awarded: November 2009 (*With Commendation*)

MSc Research Project:

Institution: MRC Protein Phosphorylation Unit

University of Dundee

Supervisor: Dr Kei Sakamoto

Project: New substrates of AMPK

Dates: April 1st 2009 – August 31st 2009

PhD Biochemistry

University of Tübingen

School of Medicine

Institute of Physiology I

Starting date :October 2009

Work experience:

Title: Computer Imagines and Animation Producer

Employer: BioSERVE

Supervisor: Dr. John Moon

Searcy, AR 72 149

USA

August 2006 to August 2008

Computer Software:

Adobe Illustrator Graphical Software

Adobe Flash Animation Software

MataFluor Ca^{2+} Imaging Software

Plus and PlusFit Patch Clamp Software

Canvas Graphical Software

Languages:

English

Polish

Publications:

1. Ekaterina Shumilina, Nguyen Thi Xuan, Evi Schmid, Shefalee K. Bhavsar, **Kalina Szteyn**, Shuchen Gu, Friedrich Götz and Florian Lang.

Zinc induced apoptotic death of mouse dendritic cells, ***Apoptosis***; Volume 15, Number 10, 1177-1186.

2. Anja Eylenstein, Eva-Maria Gehring, Nicole Heise,Ekaterina Shumilina, Sebastian Schmidt, **Kalina Szteyn**, Patrick Münzer, Meerim K. Nurbaeva, Melanie Eichenmüller, Leonid Tyan,Ivonne Regel, Michael Föller, Dietmar Kuhl, Jonathan Soboloff, Reinhold Penner and Florian Lang.

Stimulation of Ca^{2+}-channel Orai1/STIM1 by serum- and glucocorticoid-inducible kinase 1 (SGK1), ***FASEB Journal****; Volumne 25, 1-10.*

3. Nicole Heise, Ekaterina Shumilina, Meerim K Nurbaeva, Evi Schmid, **Kalina Szteyn**, Wenting Yang, Nguyen Thi Xuan, Kan Wang, Irina M. Zemtsova, Michael Duszenko, and Florian Lang.

Effect of dexamethasone on Na^+/Ca^{2+} exchanger in dendritic cells, ***Am J Physiology Cell Physiology;*** *Volumne 300, C1306-C1313.*

4. Anja Eylenstein , Sebastian Schmidt , Shuchen Gu, Wenting Yang, Evi Schmid 1 , Ioana Alesutan, **Kalina Szteyn**, Ekaterina Shumilina, Ivonne Regel and Florian Lang.

NF-κB dependent expression of the Ca^{2+} channel ORAI1 and ORAI1 stimulating Ca^{2+} sensor STIM1, ***JBC***; *Volume 287, 2719-2730*

5. Kalina Szteyn, Evi Schmid, Meerim K. Nurbaeva, Wenting Yang, Karl Kunzelmann, Florian Lang, Ekaterina Shumilina.
Expression and functional significance of Ca^{2+} activated Cl^- channels in dendritic cells, (submited, ***Jurnal of Cellular Physiology***)

6. Meerim K. Nurbaeva, Evi Schmid, **Kalina Szteyn**, Wenting Yang, Benoit Viollet, Ekaterina Shumilina, Florian Lang

Enhanced Ca^{2+} entry and Na^+/Ca^{2+} exchanger activity in dendritic cells from AMP-activated protein kinase deficient mice, (accepted, ***FASEB***)

7. Evi Schmid, Madhuri Bhandaru, Meerim K. Nurbaeva, Wenting Yang, **Kalina Szteyn**, Christina Leibrock, Leonid Tyan, David Pearce, Ekaterina Shumilina[1], Florian Lang[1]
SGK3 regulates Ca^{2+} entry and migration of dendritic cells, (under revision, ***EJP***)

8. **Kalina Szteyn,** Evi Schmid, Wenting Yang, Florian Lang, Ekaterina Shumilina

Lipopolysaccharide sensitive H^+ current in Dendritic Cells (accepted, ***Am J Physiology Cell Physiology)***

Declaration

I hereby declare that this thesis was created with contribution of other laboratory team members.

Contributions

This project describes two novel ion channels, expressed in dendritic cells, which play a crucial role in regulation of physiological functions in those cells. The majority of the data presented in this thesis was collected from the experiments that I performed personally. I received help in cell culture maintenance from Evi Schmid and Wenting Yang, who also performed RT-PCR experiments.